Multi-element isotope dilution (ID) sector field ICP-MS: a novel technique that leads to new perspectives on the trace element systematics of ocean island basalts

Dissertation
zur Erlangung des Doktorgrades
der Fakultät für Geowissenschaften der
Ludwig-Maximilians-Universität München

vorgelegt von
Matthias Willbold

04. April 2005

1. Berichterstatter: Prof. Dr. E. Hegner
2. Berichterstatter: Prof. Dr. S. Hölzl

Tag der mündlichen Prüfung: 28. September 2005

Zusammenfassung

Spurenelemente (Elemente, deren Anteil an der Gesamtmasse der analysierten Probe weniger als 0.1 Gew.% beträgt) sind wichtige 'Marker' für eine große Vielzahl von prozessgesteuerten Vorgängen in naturwissenschaftlichen Forschungsgebieten, wie etwa Biochemie, Medizin, Halbleiter- und Nanotechnologie und Umwelt- und Geowissenschaften (z. B. Anitha et al. [2002]; Becker et al. [2004]; Barbante et al. [2004]; Tibi and Heumann [2003]). Ein entsprechend hoher wissenschaftlicher und finanzieller Aufwand wird daher für die Entwicklung neuer hochwertiger analytischer Verfahren und Methoden zur Elementspurenanalyse betrieben. In den Geowissenschaften wurden bisher die Möglichkeiten der Spurenelementanalytik noch nicht vollständig ausgeschöpft. Dies liegt zum Einen an der komplexen Zusammensetzung der analysierten Proben (Gesteine), zum Anderen aber auch an den zeitaufwendigen Verfahren, um qualitativ hochwertige Spurenelementdaten mittels Isotopenverdünnung (IV) zu erhalten. Die Zielsetzung dieser Studie ist deshalb, eine neue, leicht anwendbare und schnelle IV-Methode für die Bestimmung einer Vielzahl von Spurenelementkonzentrationen in geologischen Materialien zu entwickeln. Darüber hinaus hat die Anwendung dieses neuen Verfahrens zur Analyse basaltischer Proben von Ozeaninsel-Basalten (OIB) gezeigt, dass die geochemische Entwicklung von Mantelheterogenitäten (HIMU, EM-1, EM-2) sehr viel komplexer ist als bislang angenommen.

Im ersten Teil dieser Arbeit wird ein neues Multielementverfahren vorgestellt, mit dessen Hilfe die Bestimmung der Konzentrationen von 12 Spurenelementen in geologischen Proben mittels der IV und ICP-MS (Inductively Coupled Plasma Mass Spectrometry) direkt an den aufgelösten Proben durchgeführt werden kann. Die Konzentrationsbestimmung von 14 weiteren Elementen erfolgt durch die Verwendung der mittels IV erhalten Elementkonzentrationen als interne Standards. Diese Methode kombiniert die Vorteile von IAV (hohe Präzision und Genauigkeit) und ICP-MS (die Möglichkeit, eine große Anzahl von Elementkonzentrationen gleichzeitig zu bestimmen; hoher Probendurchsatz ohne Separation der Matrix) und schafft Abhilfe für die größten Nachteile von ICP-MS (Matrixeffekte und Drift der Intensität). Für die mittels IV bestimmten Spurenelementkonzentrationen in dem geologischen Referenzmaterial BHVO-1 (n=5) wird eine Reproduzierbarkeit von 1-3% (RSD) und eine Genauigkeit von 1-2% relativ zu den entsprechenden Literaturdaten erreicht. Für alle übrigen Elementkonzentrationen liegt die Genauigkeit bei etwa 2-3%. Um den Leistungsnachweis der Methode zu erbringen, wurden mit dieser Technik 17 gut bestimmte geologische Referenzmaterialien des 'United States Geological Survey' (USGS), des 'Geological Survey of Japan' (GSJ) und der 'International Association of Geoanalyst' (IAG) auf ihre Spurenelementkonzentrationen hin untersucht. Die untersuchten Proben beinhalten sowohl die neuen USGS Referenzgläser BCR-2G, BHVO-2G, BIR1-G, als auch die MPI-DING Referenzgläser KL2-G und ML3B-

G und das 'National Institute of Standards and Technology' (NIST) Referenzglas SRM 612. Zum überwiegenden Teil stimmen die ermittelten Konzentrationen innerhalb von 3-4% mit den entsprechenden Literaturwerten überein. Die Übereinstimmung der Ergebnisse für die USGS Referenzgläser mit den Daten der Ausgangsmaterialien (Gesteinspulver) liegt in den meisten Fällen innerhalb der bestimmten Gesamtunsichertheit der Methode (2-3%). Lediglich die Konzentration von Uran in BIR-1G, relativ zu BIR-1, ist etwa um das Dreifache erhöht.

Im zweiten Teil der vorliegenden Arbeit wird diese neue Methode angewandt, um die Spurenelementkonzentrationen in basaltischen Proben von den Ozeaninseln St. Helena, Gough und Tristan da Cunha zu bestimmen. Ziel dieser Studie ist es, anhand der Daten die bisher gültigen Erkenntnisse über die Spurenelementsystematik von Mantelheterogenitäten zu überprüfen. Seit Anfang der 1990er wurde die Rückführung von alterierter ozeanischer Kruste zusammen mit geringen Anteilen von 'pelagischen' und 'terrigenen' Sedimenten in den Erdmantel und erneutes Aufsteigen derselben (Recycling) zu einem Standardmodell, um die geochemischen und isotopischen Eigenschaften der OIB zu erklären. Die zunehmende Anzahl an geochemischen Daten in der Literatur, zusammen mit den neuen hochpräzisen Daten von Proben von St. Helena, Gough und Tristan da Cunha dieser Studie (zusammengenommen mehr als 300 Analysen von Basalten von 15 Inseln, die für diese Systematik eine Schlüsselstellung einnehmen) führen zu der Erkenntnis, dass die Spurenelementsystematik in 'enriched mantle' (EM)-typischen OIB viel komplexer ist, als bisher angenommen. Im Gegensatz zu den EM Basalten haben die HIMU-Basalte (hohes μ; $\mu = {}^{238}\mathrm{U}/{}^{204}\mathrm{Pb}$) bemerkenswert einheitliche Spurenelementcharakteristika (systematische Verarmung an Cs, Rb, Ba, Th, U, Pb, Sr und eine Anreicherung an Nb und Ta relativ zu La), die nur dadurch erklärt werden kann, dass die Quellen aller HIMU-Basalte eine aus subduktions-modifizieter ozeanischer Kruste bestehende Komponente beinhalten. EM-typische Basalte haben La/Th, Rb/Ba, und Rb/K Verhältnisse, die ähnlich deren von HIMU-Basalten sind. Gleichzeitig haben sie typische Kennzeichen, die sie von den HIMU-Basalten unterscheiden (z. B. hohe Rb/La, Ba/La, Th/U, Rb/Sr und niedrige Nb/La, U/Pb, Th/Pb Verhältnisse). Zusätzlich sind die Gehalte an hochinkompatiblen Spurenelementen (Cs, Rb, Ba, Th, U, Nb, Ta, La) in EM-typische OIB viel variabler, die Konzentrationen an Pb und Sr dagegen weniger verarmt als in den HIMU-Basalten. Darüber hinaus besitzt jede Suite von EM-Basalten eine eigene, spezifische Spurenelementsignatur, die letztendlich unterschiedliche Quellenzusammensetzungen widerspiegeln muss. Daraus folgt, dass, obwohl die EM- und HIMU-typischen OIB ein gemeinsames Ausgangsgestein besitzen (subduzierte ozeanische Kruste), die kompositionellen Unterschiede nur dadurch erklärt werden können, dass die EM-Quellen eine komplexere Evolution durchlaufen haben und/oder, im Gegensatz zu den HIMU-Quellen, eine zusätzliche Komponente beinhalten. Diese zusätzliche Komponente in EM-typischen Basalten entstammt sehr wahrscheinlich

einem gemeinsamen, letztendlich jedoch heterogenen Reservoir. Mögliche Quelle stellen marine Sedimente dar. Allerdings kann die isotopische Bimodalität in den EM-typischen Basalten (EM-1, EM-2) mit dem Zusatz von marinen Sedimenten nicht erklärt werden, da die Mutter/Tochter Verhältnisse in marinen Sedimenten eine unimodale Verteilung aufweisen.

Ähnlich der bimodalen isotopischen Systematik in den EM-Basalten besteht die kontinentale Kruste aus zwei großen geochemischen Reservoirs (obere und untere kontinentale Kruste) mit deutlich unterschiedlichen Zusammensetzungen. Die Anreicherung an inkompatiblen Elementen ist in beiden Reservoirs vergleichbar hoch, jedoch besitzt die untere kontinentale Kruste systematisch niedrigere Rb/Sr, U/Pb, Th/Pb und höhere Th/U Verhältnisse. Über die Zeit gesehen entwickeln sich die obere und untere kontinentale Kruste daher entlang unterschiedlicher isotopischer Pfade, während die komplexen Spurenelementcharakteristika beider Reservoirs unverändert bleiben. Dies ist vergleichbar mit den geochemischen und isotopischen Befunden in den EM-typischen OIB weltweit. Aufgrund dieser Koinzidenz wäre das Recycling von ozeanischer Kruste zusammen mit unterschiedlichen Mengen an Material von unterer kontinentaler Kruste (die während der Subduktion an erosiven Plattenrändern von der darüber liegenden kontinentalen Kruste erodiert wird) und oberer kontinentaler Kruste (in Form von Sedimenten oder erodierter oberer kontinentaler Kruste) eine mögliche Erklärung für die geochemische und isotopische Systematik in EM-typischen Ozeaninsel-Basalten.

Abstract

Trace elements (elements that constitute less than 0.1 wt.% of the analyzed sample) are important tracers for a great variety of processes in many research areas, such as biochemistry, medicine, semi-conductor and nano-technology, environmental science and geosciences (e.g., Anitha et al. [2002]; Becker et al. [2004]; Barbante et al. [2004]; Tibi and Heumann [2003]). Accordingly, much scientific effort and financial resources are raised to develop new high-performance analytical techniques and methods for trace element analysis. In geosciences, the capabilities of trace elements analytics have not been used to its full potential because of the complex matrix of the analyzed samples (rocks) and the time consuming procedure to obtain high-quality trace element data by isotope dilution. Accordingly, the aim of this study is to develop of a new, easy-to-use and fast ID-method for the simultaneous determination of many trace elements in geological materials. In addition, the application of this new technique to the analysis of ocean island basalts (OIB) revealed that evolution of geochemical mantle heterogeneities (HIMU, EM-1, EM-2) is far more complex than perviously thought.

In the first part of this thesis, a multi-element technique for the simultaneous determination of 12 trace element concentrations in geological materials by combined isotope dilution (ID) sector field inductively coupled plasma mass spectrometry (SF-ICP-MS) following simple sample digestion is presented. The concentrations of additional 14 other trace elements have been obtained using the ID determined elements as internal standards. This method combines the advantages of ID (high precision and accuracy) with those of SF-ICP-MS (multi-element capability, fast sample processing without element separation) and overcomes the most prevailing drawbacks of ICP-MS (matrix effects and drift in sensitivity). Trace element concentration data for the geological reference material BHVO-1 (n = 5) reproduce to within 1-3% RSD with an accuracy of 1-2% relative to respective literature data for ID values and 2-3% for all other values. To test the overall performance of the method the technique has been applied to the analysis of 17 well-characterized geological reference materials from the United States Geological Survey (USGS), the Geological Survey of Japan (GSJ) and the International Association of Geoanalysts (IAG). The sample set also includes the new USGS reference glasses BCR-2G, BHVO-2G, and BIR-1G, as well as the MPI-DING reference glasses KL2-G and ML3B-G and the National Institute of Standards and Technology (NIST) SRM 612. Most data agree within 3-4% with respective literature data. The concentration data of USGS reference glasses agree in most cases with respective data of the original rock powder within the combined standard uncertainty of the method (2-3%), except the U concentration of BIR-1G, which shows a three times higher concentration compared to BIR-1.

In the second part of this thesis, this new method is used to determine the trace element concentrations of basaltic samples form the ocean islands St. Helena, Gough and Tristan da Cunha. The results are used to test the validity of established models concerning the trace element systematics of mantle heterogeneities. Since the early 1990's, recycling of altered oceanic crust together with small amounts of 'pelagic' and 'terrigeneous' sediments has become somewhat of a paradigm for explaining the geochemical and isotopic systematics in global OIB. The vastly increased number of data in the literature, in addition to new high-precision trace element data on samples from St. Helena, Gough, and Tristan da Cunha presented here (altogether more than 300 analyses from basalts from 15 key islands), reveals that the trace element systematics in enriched mantle (EM)-type OIB are far more complex than previously thought. In contrast to EM basalts, HIMU (high μ; $\mu = {}^{238}U/{}^{204}Pb$) basalts have remarkably uniform trace element characteristics (systematic depletion in Cs, Rb, Ba, Th, U, Pb, Sr, and enrichment of Nb, Ta relative to La), which are adequately explained by being derived from sources containing subduction-modified oceanic crust. EM-type basalts have La/Th, Rb/Ba, and Rb/K ratios similar to those in HIMU-type OIB, but at the same time, also share some common characteristics that distinguish them from HIMU basalts (e.g., high Rb/La, Ba/La, Th/U, Rb/Sr, low Nb/La, U/Pb, Th/Pb). EM-type OIB also have far more variable very incompatible elements contents (Cs, Rb, Ba, Th, U, Nb, Ta, La) and are less depleted in Pb and Sr than HIMU-type OIB. In addition, each suite of EM-type basalts carries its own specific trace element signature that must ultimately reflect different source compositions. Consequently, although the compositional similarities between HIMU and EM-type basalts suggest that their sources share a common precursor (subducted oceanic crust), their compositional differences can only be explained if EM sources have a more complex evolution and/or contain an additional component compared to HIMU sources. This additional component in EM basalts is likely to originate from a common, although to some degree compositionally heterogeneous, reservoir. Possible candidates are marine sediments; but they do not, at the same time, provide a plausible explanation of the isotopic bimodality in EM-type basalts (EM-1 and EM-2) because the parent/daughter ratios in marine sediments are unimodally distributed. Similar to the bimodal isotopic compositions in EM basalts, the continental crust is composed of two broadly compositionally different parts: the upper and lower continental crust. Relative to the upper continental crust, the lower continental crust is similarly enriched in very incompatible elements, but has systematically lower Rb/Sr, U/Pb, Th/Pb, and higher Th/U ratios. Thus, over time, the upper and lower continental crust evolve along distinct isotopic evolution paths but retain their complex trace element characteristics, similar to what is observed in EM-type basalts worldwide. It is therefore propose here that recycling of oceanic crust together with variable proportions of lower continental crust (scrapped off from the overlying continental crust during subduc-

tion at erosive plate margins) and upper continental crust (either in the form of sediments or eroded continental crust) provides a possible explanation for the trace element and isotope systematics in EM-type ocean island basalts.

Contents

I Multi-element isotope dilution sector field ICP-MS **9**

1 Introduction **10**

2 Theoretical background **11**

2.1 Isotope dilution (ID) 11

2.2 Relative sensitivity factors (RSF) 12

2.3 Mass fractionation 14

3 Experimental **15**

3.1 Composition of multi-element tracer (MET) solutions 15

3.2 Composition of multi-element standard solution 17

3.3 Samples and sample preparation 17

3.4 Instrumentation and data acquisition 19

3.5 Data reduction 21

3.6 Limits of detection 22

4 Combined standard uncertainty **23**

4.1 Sampling/Weighing 23

4.2 Homogeneity/chemical treatment of the sample 25

4.3 Purity of reagents 25

4.4 Purity of tracer solutions 26

4.5 Reference solutions and reference material 26

4.6 Calibration 27

4.7 Drift 27

4.8 Robustness of isotope ratios 28

4.9 Spiking 29

4.10 Instrument effects 30

4.11 Matrix effects 31
4.12 Mass discrimination 32
4.13 Values of constants 32
4.14 Operator bias 33
4.15 Combined standard uncertainty 34

5 Results and discussion **34**
5.1 Accuracy and reproducibility 34
5.2 Data for geological reference materials - special features 37

6 Overall performance of multi-element ID-SF-ICP-MS **39**
6.1 Matrix effects 39
6.2 Instrumental drift 40
6.3 Spectroscopic interferences 40
6.4 Multi-element capability 41
6.5 Time 41
6.6 Reproducibility and accuracy 42
6.7 Combined standard uncertainty 42
6.8 Comparison with other isotope dilution techniques 44

7 Conclusions **44**

II Mantle end-members: the trace element conundrum **45**

8 Introduction **46**

9 Analytical techniques **48**

10 The database **48**

11 Trace element characteristics of OIB and their sources **53**

11.1 Common characteristics to all OIB 53
11.2 HIMU-type OIB 54
11.3 EM-type OIB 56

12 Implications for the origin of OIB source compositions 62
12.1 The nature of the HIMU source 62
12.2 The nature of the EM sources and the trace element conundrum 66
12.3 Sediment recycling 67
12.4 Recycling lower continental crust 71
12.5 Mixing relationships 73
12.6 Mechanisms for recycling lower continental crust 76
12.7 Alternative models: metasomatic processes 77

13 Conclusions 79

14 Acknowledgments 81

A Trace element data for BHVO-1 95

B Trace element data for geological reference materials 97

C Major and trace element data for ocean island basalts 102

D Transition element data for ocean island basalts 109

E Accuracy and reproducibility of ID-LA-ICP-MS 110

F Primitive upper mantle normalized trace element data for OIB 110

G Quantitative modeling of OIB melts 114
G.1 Model parameters 114
G.2 Composition of the recycled continental components 114
G.3 Average lower continental crust 115

G.4 Average upper continental crust 115
G.5 'Mature' lower continental crust 115
G.6 'Young' lower continental crust 116

H Curriculum Vitae **118**

List of Tables

1 Acquisition parameters, composition of multi-element tracer solutions, and composition of stock standard solution 16

2 Analyzed geochemical reference materials and issuing organizations 18

3 Operation parameters of ThermoFinnigan ELEMENT2 21

4 Purity of single spike salts and oxides 24

5 Comparison of three different isotope dilution techniques used at the MPI for Chemistry 43

List of Figures

1 Mass fractionation as a function of mass 15

2 Mass spectrum of the rare-earth element neodymium 19

3 Spectrum of masses 170 to 173 of rare-earth element ytterbium 20

4 Detection modes of secondary electron multiplier 22

5 Limits of detection in solid sample 23

6 Results of long term measurements 28

7 Absolute count rates and isotope ratios determined from analyses of multi-element solutions 29

8 Calculated error magnification factors 30

9 Relative sensitivity factors (RSF) obtained from analyses of a solution of the geological reference material BHVO-1 32

10 Relative sensitivity factors (RSF) obtained from different dilutions of a multi-element solution 33

11 Comparison of trace element data of BHVO-1 with high-precision reference data 35

12 Normalized concentration data of silica-rich geological reference materials . 36

13 Normalized concentration data of basaltic geological reference materials . . 36

14 Normalized concentration data of geological reference glasses 38

15 Comparison of reference glasses with original sample powder 39

16 Mantle end-members as inferred from Sr and Pb isotope systematics 47

17 Averages and standard deviations (1σ) of log(Nb/Rb), log(Nb/U) ratios and of average CI normalized La/Sm, Sm/Yb ratios for individual islands . 49

18 Log-log plots of concentrations of very incompatible trace elements (VICE) 51

19 Data of ocean island basalts in Rb/K versus Rb, Ba/K versus Ba, La/Th versus La, and Nd/Sr versus Nd space 52

20 Data of ocean island basalts in Ba/Nb versus Rb/Nb, and La/Th versus Rb/Th space 54

21 Data of ocean island basalts in Ce/Pb versus U/Pb, Ba/La versus Rb/La, and Rb/Sr versus 1/Sr space 55

22 Modeled source of HIMU-type OIB (St. Helena) 57

23 Averages and standard deviations (1σ) of log (VICE) / log (La) ratios for individual island suites 58

24 Averages and standard deviations (1σ) of log of parent/daughter ratios of Sr, Pb, and Hf isotope decay systems 59

25 $^{87}Sr/^{86}Sr$ and $^{206}Pb/^{204}Pb$ isotopes versus respective parent/daughter ratios in ocean island basalts 60

26 Comparison of trace element ratios of EM-1-type (Pitcairn, Gough) and EM-2-type (Samoa-Malumalu, Society-Tahaa) suites 61

27 Modeled sources of EM-type OIB 63

27 Continued 64

28 Histograms showing the log-normal distribution of parent/daughter ratios of isotope decay systems in presently subducted sediments 69

29 Comparison of ratios of very incompatible trace elements (VICE) in the upper and lower continental crust 72

30 Comparison of average EM-type OIB with modeled trace element patterns . 74

31 Modeling the variation of Ba/Rb versus Th/Rb and Ba/Nb versus Rb/Nb for different OIB suites 75

Parts of this thesis are based on (or directly taken from) published papers, or manuscripts to be published in scientific journals. These papers are (in the order of appearance):

Willbold, M., Jochum, K. P., Raczek, I., Amini, M. A., Stoll, B., Hofmann, A. W., 2003. Validation of multi-element isotope dilution ICPMS for the analysis of basalts. Analytical and Bioanalytical Chemistry 377, 117-125.

Willbold, M., Jochum, K. P., 2005. Multi-element isotope dilution sector field ICP-MS: A precise technique for the analysis of geological materials and its application to geological reference materials. Journal of Geostandards and Geoanalytical Research, in press.

Willbold, M., Jochum, K. P., 2005. Multi-element isotope dilution sector field ICPMS for the analysis of geological materials. In: C. B. Douthitt (Ed.), High Resolution Inductively Coupled Plasma Mass Spectrometry, submitted.

Willbold, M., Stracke, A., Hofmann, A. W., 2005. Mantle end-members: the trace element conundrum. Geochemistry, Geophysics, Geosystems, submitted.

Part I

Multi-element isotope dilution sector field ICP-MS

1 Introduction

Because of its rapid and sensitive multi-element capabilities, inductively coupled plasma mass spectrometry (ICP-MS) has become the leading technique for the determination of a large number of trace element concentrations in geological materials [Brenner and Zander, 1996; Potts, 1997; Roelandts, 1999; Gäbler, 2002]. For a review of the principles of ICP-MS see Hill [1999]. The availability of double focusing instruments using a combination of magnetic and electrostatic fields as a mass filter (also called sector field (SF)-ICP-MS) led to considerable improvements in the performance of ICP-MS instruments by providing enhanced sensitivity, high mass resolution (m $\Delta m^{-1} \geq 10000$), flat-top peak shape, and fast electric scanning. Enhanced sensitivity and high mass resolution have increased the ability to resolve polyatomic interferences, one of the most prevailing problems in ICP-MS [Moens and Jakubowski, 1998; Prohaska et al., 1999; Robinson et al., 1999]. The flat-top peak shape allows the precise determination of isotope ratios, which has heretofore been problematic with quadrupole ICP-MS systems.

Different strategies have been applied for the determination of trace element concentrations in geological materials, using external calibration with one or more internal standards [Longerich et al., 1990; Dulski, 1994; Eggins et al., 1997], and standard addition [Jenner et al., 1990]. In addition to these conventional techniques, isotope dilution (ID) has gained more and more importance [Xie and Kerrich, 1995; Griselin et al., 1999; David et al., 1999; Weyer et al., 2002; Baker et al., 2002; LeFevre and Pin, 2002; Meisel et al., 2003]. The application of ID to ICP-MS has been recognized as a powerful technique for the determination of element concentrations (Longerich [1989] and references therein). This is because the sensitivity of the instrument for the element of interest is determined internally in the sample matrix and at the time of data acquisition by the added tracer. Therefore, ID-ICP-MS is capable to diminish two major drawbacks of conventional ICP-MS: (1) the effect of matrix composition on the signal response and (2) the temporal drift of sensitivity. Previously, ID-ICP-MS techniques in geosciences have been restricted to the simultaneous determination of only a few trace element concentrations [Xie and Kerrich, 1995] or involved chemical separation procedures [David et al., 1999; Griselin et al., 1999; Weyer et al., 2002; Baker et al., 2002; LeFevre and Pin, 2002; Meisel et al., 2003]. Therefore, they have not utilized the capability of ICP-MS for multi-element determination and fast sample processing to its full potential.

Here, a new multi-element ID technique is presented that uses the high and low mass resolution modes (HR, and LR respectively) of a ThermoFinnigan ELEMENT2 SF-ICP mass spectrometer. Twelve elements are simultaneously determined by ID in dissolved and diluted rock samples without chemical separation. In addition, 14 other elements are

determined by relative sensitivity factors using the elements that are determined by ID as internal standards. Thus the method combines the advantages of SF-ICP-MS (multi-element capability, sample processing without matrix removal or element separation) with those of ID (high accuracy, elimination of matrix effects and drift in sensitivity, and optimization of mass spectrometer efficiency). Individual factors of error are investigated to estimate the combined standard uncertainty associated with the results of multi-element ID-SF-ICP-MS. This demonstrates that the trace element data obtained by multi-element ID-SF-ICP-MS yields highly precise and accurate results, opening up new perspectives in basic research geosciences.

A variety of geological reference materials has been analyzed and the results have been compared with published reference values. The samples also include the new USGS reference glasses BHVO-2G, BCR-2G, and BIR-1G, the MPI-DING glasses KL2-G and ML3B-G [Jochum et al., 2000] as well as the NIST SRM 612 which are widely used for in-situ microanalysis (e.g. laser ablation ICP-MS, SIMS). As an additional aim of this study, we want to provide new high-quality trace element concentration data to contribute to the characterization of these reference materials.

2 Theoretical background

2.1 Isotope dilution (ID)

Isotope dilution (ID) is one of the most accurate techniques for the determination of element concentrations (Heumann [1986]; Pin and LeFevre [2002] and references therein). It is based on the addition of a known amount of an artificially enriched isotopic 'tracer', also known as 'spike', to a known amount of sample. By measuring the ion intensity of the artificially enriched isotope in the mixture (sample/tracer) and normalizing this intensity to that of a reference isotope of the same element, the concentration C_E^S of this element (E) in the sample (S) can be calculated according to (modified after Pin and LeFevre [2002])

$$C_E^S\ [\mu g\ g^{-1}] = C_E^T \times \frac{m^T \times M_E^S \times X_k^T}{m^S \times M_E^T \times X_i^S} \times \left[\frac{R_{Tracer} - R_{Mixture}}{(R_{Mixture} \times R_{Sample}) - 1}\right] \qquad (1)$$

The first two terms consist of known parameters: C_E^T is known the concentration of the element (E) in the tracer solution (T) [$\mu g\ g^{-1}$], m^T and m^S are the known weights of the tracer solution and the sample, respectively [g], M_E^S, M_E^T are the known relative atomic masses of the element in the sample and in the tracer, respectively [$g\ mol^{-1}$], X_k^T and X_i^S are the known isotopic abundances of the isotope k in the tracer and i in the

sample. The third term has no dimensions and consists of the known isotope ratios i/k in the tracer (R_{Tracer}), in the sample (R_{Sample}), and the measured isotope ratio i/k in the sample-tracer mixture ($R_{Mixture}$).

Besides high accuracy and precision, the advantage of ID is that once the sample/tracer homogeneity has been achieved there is no need for quantitative sample handling. Then, even the loss of some analyte during sample preparation does not diminish the quality of the result. Elements that have been determined by ID are given in Table 1.

2.2 Relative sensitivity factors (RSF)

Isotope dilution can only be applied if two or more interference free isotopes of an element are available. The concentration data of mono-isotopic elements (e.g., Nb, Ho, Th) or elements for which only one interference free isotope is available (e.g., Rb, Ta) can be improved by using ID determined elements as internal standards. The elements of interest and the internal standard are measured within one resolution mode (LR or HR, respectively) and within one acquisition run. The ion intensities of mono-isotopic elements are then normalized to those of the internal standard elements. The concentration $C^S_{E'}$ of such an element E' in the sample S can be calculated according to (modified after Jochum et al. [1988])

$$C^S_{E'}\ [\mu g\ g^{-1}] = \left[C^S_E \times \frac{X^S_{E,i}}{X^S_{E',l}} \times \frac{M^S_{E'}}{M^S_E} \right] \times \frac{R_{l,i}}{f^S_{E'}} \tag{2}$$

The first term contains only known parameters: C^S_E is the concentration of the internal standard element (E) in the sample (S) determined by ID [$\mu g\ g^{-1}$], $X^S_{E',l}$, $X^S_{E,i}$ are the natural isotopic abundances of isotope l and i of the elements E' and E, respectively [Rosman and Taylor, 1998], and $M^S_{E'}$ and M^S_E are the natural relative atomic masses [$g\ mol^{-1}$] of the element of interest and of the internal standard element, respectively Loss [2003]. The remaining variables of Eq. (2) are $R_{l,i}$ which is the measured ratio l/i of the ion intensities of isotope l of the element E' of interest and of isotope i of the internal standard element E, and the relative sensitivity factor (RSF, $f^S_{E'}$ in Eq. 2) that accounts for differences in the response between the element of interest and the internal standard element (ionization potential, transmission, mass dependent sensitivity of the detector system). It is defined as

$$f^S_{E'} = \frac{C^S_{E'}(meas)}{C^S_{E'}(true)} \tag{3}$$

where $C^S_{E'}(meas)$ is the apparent concentration of element E' obtained by reference to

the concentration of an internal standard element (E) and $C^S_{E'}(true)$ is the 'true' concentration in a standard solution containing all elements of interest.

The respective RSF values remain constant within their confidence intervals (1σ) over a time period of at least ten hours (see below), and thus have to be calibrated only once per day as long as the mass spectrometer operation conditions (torch position, gas flow rates, lens voltages, position of entrance slit) are kept constant. Elements that have been determined by RSF in this study are given in Table 1. Quantification of element abundances using RSF has been successfully applied to spark source mass spectrometry (SSMS) [Jochum et al., 1988, 2001], ICP-MS [Jenner et al., 1990; Meisel et al., 2003], and multiple collector (MC)-ICP-MS [Weyer et al., 2002].

Before the element ratios for the determination of element concentrations by RSF can be inserted into Eq. 3, the respective isotope i of the standard element E (Eq. 2) has to be corrected for the contribution of the tracer to the total intensity of the normalizing mass i. This is because non of the used tracers consists entirely of the enriched isotope, i.e. the ^{91}Zr tracer contains 3.24% ^{90}Zr and accordingly the Nb concentration (using the element ratio ^{93}Nb/^{90}Zr) would be underestimated if this contribution from the tracer on mass ^{90}Zr would not be corrected. If I is the measured ion intensity i of normalizing isotope i of the element that has been determined by ID, and L is the ion intensity of the isotope l of the element that has to be determined by RSF (see above), the required element ratio can be calculated as:

$$I \sim mol_i^S + mol_i^T \tag{4}$$

and accordingly,

$$\frac{L}{I_{corr}} = \frac{L}{I} \times \left[\frac{mol_i^S + mol_i^T}{mol_i^S} \right] \tag{5}$$

and

$$mol_i^S = m^S \times C_E^S \times X_{E,i}^S \times \frac{1}{M_E^S} \tag{6}$$

and

$$mol_i^S = m^T \times C_E^T \times X_{E,i}^T \times \frac{1}{M_E^T} \tag{7}$$

where $X^T_{E,i}$ is the known abundance of isotope i of element E in the tracer and all other variables are as defined above.

2.3 Mass fractionation

The accuracy of the determined concentration depends on the accuracy of the determined isotope or element ratio ($R_{Mixture}$ in Eq. 1 and $R_{l,m}$ in Eq. 2). It has been shown that the determination of isotope and element ratios by ICP-MS is biased by mass fractionation effects caused by the greater deflection of light compared to heavy ions due to mutual repulsion in the ion beam [Heumann et al., 1998]. Thus, mass fractionation (MF) is an important factor for the accurate determination of isotope ratios and their application to ID Longerich [1989]. Tentatively, the MF can be expressed as [Heumann et al., 1998]

$$MF\ [amu^{-1}] = \left[\frac{R_{true}}{R_{det}} - 1\right] \times \frac{1}{\Delta m_{i,k}} \tag{8}$$

where R_{true} is the true ratio of two isotopes i and k of one element obtained from tabulated isotopic compositions of elements [Rosman and Taylor, 1998], R_{det} is the determined isotope ratio and $\Delta m_{i,k}$ is the mass difference between both isotopes in amu. Mass fractionation may become > 0.01 per amu for masses smaller than 100 amu. A variety of mathematical functions (linear, power law, exponential law, e.g., Taylor et al. [1995] or Platzner et al. [1999] are routinely used for in-run mass fractionation correction by using normalizing isotope ratios with constant natural abundances. If the dissolved rock samples are analyzed directly by ID without previous separation of investigated elements or element groups, only two isobaric-free isotopes are available for most elements and thus direct in-run mass fractionation correction of individual isotope ratios is not possible due to the lack of an interference or tracer-free isotope ratio for normalization.

For a wide range of masses (e.g., ^{47}Ti to ^{238}U), the magnitude of mass fractionation varies systematically with mass (Becker and Dietze [2000]; see also Fig. 1). Therefore, it is possible to determine mass-dependent fractionation factors in-run by comparing determined ^{47}Ti/^{49}Ti, ^{99}Ru/^{101}Ru (in LR mode), ^{151}Eu/^{153}Eu (in HR mode) and ^{185}Re/^{187}Re ratios with known values [Rosman and Taylor, 1998].

This is done by determining the respective Ti, Ru, Eu, and Re isotope ratios simultaneously with those used for ID and RSF from the same solution. Re and Ru were added to the analyte during sample preparation. Interpolation yields empirical mass-dependent correction factors for indivual isotope ratios (Fig. 1) by fitting a power law function to the calculated mass fractionation factors for Ti, Ru, Eu, and Re, using the equation

$$MF\ [amu^{-1}] = a \times b^{m-c} + d \tag{9}$$

where m is the mass in amu [Loss, 2003], and a, b, c, and d are four coefficients that

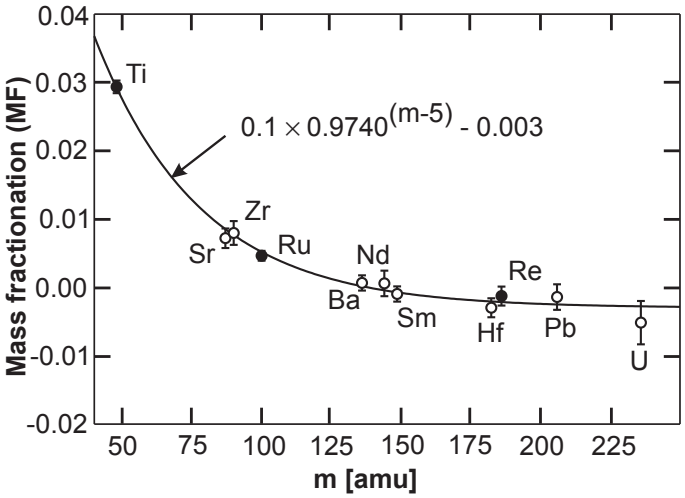

Figure 1: Mass fractionation (MF) as a function of mass [amu]. Also shown is a power law function fitted to the MF factors calculated from measured intensities of masses ^{47}Ti, ^{49}Ti, ^{99}Ru, ^{101}Ru, ^{185}Re, ^{187}Re. MF factors for elements Sr, Zr, Ba, Nd, Sm, Hf, Pb, and U determined from the measurement of not spiked BCR-1 agree with the empirical curve within confidence intervals (1σ). See text for explanations.

can be varied independently. Typical values are a: 0.05 to 0.30, b: 0.96 to 0.98, c: -10 to 10, and d: -0.005 to 0.005.

Determinations of isotope ratios for different elements in (not spiked) BCR-1 have shown that calculated mass fractionation factors for a number of elements across the entire mass range agree with this empirical curve within confidence intervals (1σ, Fig. 1). Determination of in-run mass fractionation with this method is independent of matrix composition, temporal variations in the response, and concentration, thus is superior to external mass fractionation corrections (e.g. by measuring a standard solution prior and after an unknown sample).

3 Experimental

3.1 Composition of multi-element tracer (MET) solutions

Twelve elements that span a wide mass range (86 to 235 amu) were spiked (Table 1) and determined by ID. To minimize the sample preparation procedure, single tracer solutions were combined into three multi-element tracer solutions (MET, Table 1). Optimum conditions for the sample-tracer mixture [Riepe and Kaiser, 1966] depend on the tracer concentration because the determined concentration in the unknown is a non-linear function of the isotope ratio of the sample/tracer mixture. This non-linearity leads to error

Table 1: Acquisition parameters, composition of multi-element tracer solutions (MET 1 to 3), and composition of stock standard solution in μg g^{-1}.

El.	Tracer	Ratio[a]	Mode[b]	Dil. factor[c]	Tracer conc.	Stand. conc.
Rb	-	^{85}Rb/^{88}Sr	LR	21000	-	16.6
Sr	^{86}Sr	^{86}Sr/^{88}Sr	LR	21000	106 (MET 1)	17.0
Y	-	^{89}Y/^{90}Zr	LR	21000	-	16.5
Zr	^{91}Zr	^{91}Zr/^{90}Zr	LR	21000	106 (MET 3)	16.4
Nb	-	^{93}Nb/^{90}Zr	LR	21000	-	16.4
Cs	-	^{133}Cs/^{137}Ba	LR	21000	-	16.7
Ba	^{135}Ba	^{135}Ba/^{137}Ba	LR	21000	59.7 (MET 1)	16.9
La	-	^{139}La/^{143}Nd	LR	21000	-	17.3
Ce	-	^{140}Ce/^{143}Nd	LR	21000	-	17.3
Pr	-	^{141}Pr/^{143}Nd	LR	21000	-	17.3
Nd	^{145}Nd	^{145}Nd/^{143}Nd	LR	21000	7.43 (MET 1)	17.3
Sm	^{149}Sm	^{149}Sm/^{147}Sm	LR	21000	2.16 (MET 1)	17.3
Eu	-	^{153}Eu/^{147}Sm	HR	1000	-	17.3
Gd	^{155}Gd	^{155}Gd/^{158}Gd	HR	1000	2.56 (MET 2)	17.3
Tb	-	^{159}Tb/^{158}Gd	HR	1000	-	17.3
Dy	^{161}Dy	^{161}Dy/^{163}Dy	HR	1000	4.12 (MET 2)	17.3
Ho	-	^{165}Ho/^{166}Er	HR	1000	-	17.3
Er	^{167}Er	^{167}Er/^{166}Er	HR	1000	2.54 (MET 2)	17.3
Tm	-	^{169}Tm/^{166}Er	HR	1000	-	17.3
Yb	^{171}Yb	^{171}Yb/^{172}Yb	HR	1000	1.92 (MET 2)	17.3
Lu	-	^{175}Lu/^{172}Yb	HR	1000	-	17.3
Hf	^{179}Hf	^{179}Hf/^{178}Hf	LR	21000	2.71 (MET 3)	16.4
Ta	-	^{181}Ta/^{178}Hf	LR	21000	-	16.4
Pb	^{207}Pb	^{207}Pb/^{208}Pb	LR	21000	2.03 (MET 2)	16.7
Th	-	^{232}Th/^{238}U	LR	21000	-	16.7
U	^{235}U	^{235}U/^{238}U	LR	21000	0.104 (MET 1)	16.7

[a] Determined ratio; [b] LR: $m\ \Delta m^{-1} = 300$, HR: $m\ \Delta m^{-1} = 10000$; [c] Dilution factor

magnification, which can become a serious problem when the determined ratio approaches either that of the tracer or the sample. Therefore, the concentrations of the tracer isotopes in the MES have been adjusted to natural variations of element concentrations in geological materials depending on the degree of enrichment of the respective trace elements in the analyzed rocks. As a first order approach, we grouped together elements of similar geochemical properties (e.g., ionic radius and charge) (see Table 1). Partial enrichment of one of these element groups in a rock can be met by adding the appropriate amount of the respective MET to the sample. As a second approach, we optimized the concentrations of individual tracers within each MET to cover the concentration interval that is commonly

encountered in geological materials. As a result, error magnification factors do not exceed a value of two, even when the concentration varies by three orders of magnitude (e.g. Ba concentrations that vary from 5 $\mu g\ g^{-1}$ in mid-ocean ridge basalts to 1000 $\mu g\ g^{-1}$ in some oceanic island basalts).

Concentrations in the MET solutions were calibrated by applying a 'reverse' ID against certified standard solutions (Alfa Aesar, specpure) using TIMS, MC-ICP-MS, and SF-ICP-MS. The results are shown in Table 1. The isotopic composition and respective uncertainties of the tracers (X_k^T in Eq. 1, and $X_{E,i}^T$ in Eq. 7) were taken from the certificates of the single tracers (Oak Ridge National Laboratory, Cambridge Isotope Laboratories, National Institute of Standards and Technology).

3.2 Composition of multi-element standard solution

The RSF have to be determined once per analytical run (e.g. once per day if operation parameters are kept constant) by measuring a multi-element standard solution. A highly concentrated multi-element stock solution (16-17 $\mu g\ g^{-1}$, Table 1) has been prepared from certified mono- or multi-element standard solutions by weighing (Alfa Aesar, Specpure; certified uncertainty on concentration $< 0.3\%$) taking into account the individual densities of mono-standard solutions (given by the manufacturer). Comparable concentrations of all elements in the stock solution (Table 1) were chosen to minimize the uncertainty related to cross contamination of mono-element solutions (e.g., the certified value for the Th blank in the 10000 $\mu g\ ml^{-1}$ Zr Alfa Aesar Specpure solution is 0.036 $\mu g\ g^{-1}$, but is negligible compared to 16 $\mu g\ g^{-1}$ Th in the shelf solution). Prior to each analytical run, the analyzed solution is prepared simply by diluting a few drops of the stock solution (concentration in the final solution approx. 1-5 $ng\ g^{-1}$). This simple preparation procedure can be applied because once the relative element abundances ($R_{l,i}$ in Eq. 2) are known in the multi-element standard solution they remain fixed irrespectively of the dilution factor.

3.3 Samples and sample preparation

Samples analyzed in this study are given in Table 2. All procedures were carried out under clean-room conditions. Purified water (18.2 $M\Omega\ cm^{-1}$ resistivity; Milli-Q system, Millipore, USA) was used throughout. All acids (HF, HCl, and HNO_3) were purified twice by sub-boiling distillation. After the addition of the three MET, about 100 mg of whole-rock powder were treated with a mixture of 1-2 ml HF (24 $mol\ l^{-1}$) and 0.2 ml HNO_3 (14 $mol\ l^{-1}$). Samples of basaltic composition or samples where no refractory minerals like zircon are expected, were placed on hotplates for 12 hours at 130°C in closed 15 ml

Savillex PFA vials. Samples containing refractory minerals (e.g. granites) were stirred for 7 days in closed 15 ml Savillex PFA vials in Parr bombs at 180°C. After 3 days the bombs were opened and 0.5 ml HF was refilled.

Table 2: Analyzed geochemical reference materials and issuing organizations.

Sample	Rock type	Split	Pos	Distributor
AGV-1	Andesite	35	13	USGS[a]
AGV-2	Andesite	1566		USGS
BCR-1	Basalt			USGS
BCR-2	Basalt	3924		USGS
BCR-2G	Basaltic glass			USGS
BIR-1	Basalt	858		USGS
BIR-1G	Basaltic glass			USGS
BHVO-1	Basalt	15	26	USGS
BHVO-2	Basalt	9351		USGS
BHVO-2G	Basaltic glass			USGS
G-2	Granite	58	23	USGS
JR-1	Rhyolite			GSJ[b]
KL2-G	Basaltic glass			MPI-DING[c]
ML3B-G	Basaltic glass			MPI-DING
NIST612	Synth. glass			NIST[d]
OU-6	Shale	5153		IAG[e]
PCC-1	Peridotite	10	32	USGS

[a] US Geological Survey, [b] Geological Survey of Japan, [c] Max-Plank-Institute for Chemistry, [d] National Institute of Standards and Technology, [e] International Association of Geoanalysts

After evaporation to incipient dryness at ca. 80°C, the samples were re-dissolved in a few drops of HNO_3 (14 $mol\ l^{-1}$) and again evaporated to incipient dryness. This step was repeated two times to remove insoluble fluorides. After the addition of 2 ml HCl (6 $mol\ l^{-1}$) the samples were heated at 80°C followed by another evaporation step at 50°C to form chlorides. Final uptake was carried out in 5 ml HNO_3 (7 $mol\ l^{-1}$). About 120 μl of this solution were diluted with HNO_3 (0.4 $mol\ l^{-1}$) to a total volume of 50 ml for LR resolution work and 2.5 ml of this solution were diluted with H_2O to a total volume of 50 ml for measurements in HR (final molarity 0.4 $mol\ l^{-1}$). To correct for mass fractionation during measurement, ca. 6 μl of a mixed Ru-Re solution (approximate concentration in the stock solution: 60 $\mu g\ g^{-1}$ Ru, 20 $\mu g\ g^{-1}$ Re) was added to each dilution.

3.4 Instrumentation and data acquisition

Measurements were carried out on a ThermoFinnigan ELEMENT2 mass spectrometer. This double focusing SF-ICP-MS system can be run in three fixed resolution modes (low resolution (LR), m $\Delta m^{-1} = 300$; medium resolution (MR), m $\Delta m^{-1} = 4000$; high resolution (HR), m $\Delta m^{-1} = 11000$). The acquisition of data was carried out in two steps. Elements for which no or negligible isobaric or polyatomic interferences are expected (Fig. 2) were carried out in LR mode. Because the flat-top peak shape in LR allows the reduction of the scan window to 10% of the whole peak width while maintaining a high level of precision (Fig. 2), this scan mode is favorable compared to the HR mode. Elements for which polyatomic interferences are expected, especially those of light REE oxides on heavy REE elements (e.g., Dulski [1994]), were acquired in HR mode. This is demonstrated in Fig. 3 where the mass spectrum of ytterbium in a natural sample in LR mode is compared with that in the HR mode. This example demonstrates that the HR mode of SF-ICP-MS devices is needed in order to achieve accurate results within reasonable measurement time.

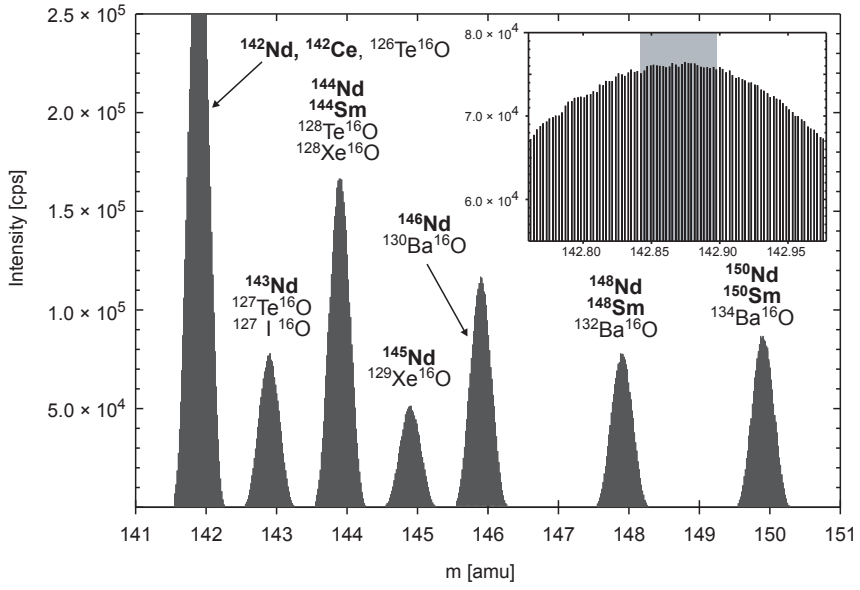

Figure 2: Mass spectrum of the rare-earth element Nd acquired in low mass resolution mode of a ThermoFinnigan ELEMENT2 mass spectrometer (m $\Delta m^{-1} = 300$). The isotopes ^{143}Nd and ^{145}Nd are free of isobaric interferences and are virtually interfered only by minor polyatomic interferences. Note that Te and I have generally negligible concentrations in geological samples (I/Nd < 0.04 in continental crust and < 0.004 in average basalt; Te/Nd < 0.0003 in continental crust and < 0.004 in average basalt). This is supported by the determined ^{143}Nd/^{145}Nd ratio of 1.46740 compared to the 'true value' of 1.46747. The inset shows an enlarged section of the flat-top ^{143}Nd peak and the conventionally scanned peak section (shaded range).

All samples were processed through one resolution mode before switching to the other

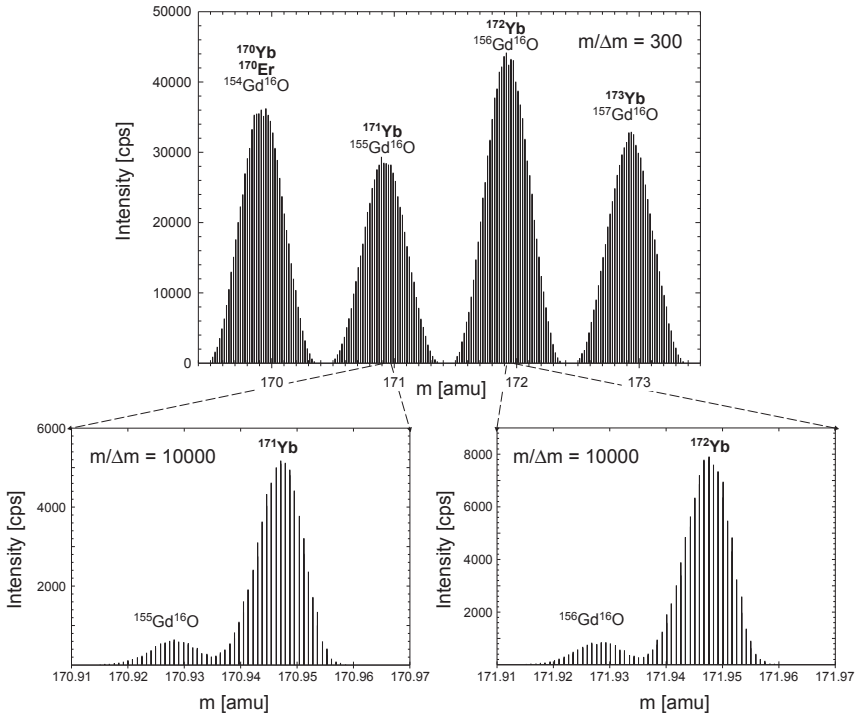

Figure 3: Spectrum of masses 170 to 173 of rare-earth element Yb acquired in low mass resolution mode of a ThermoFinnigan ELEMENT2 mass spectrometer (top; m Δm^{-1} = 300) and of masses 171 and 172 in high resolution mode (bottom; m Δm^{-1} = 10000) in a natural sample. The high mass resolution mode reveals the existence of GdO lines which could not have been resolved using the low mass resolution. Thus, the acquisition of intensities of masses that are potentially interfered by polyatomic lines in the high mass resolution is indispensable for the application of multi-element ID-ICPMS to maintain a low level of uncertainty on the final concentration.

mode. Otherwise, the RSF may change because of potential offset effects by moving the slit from one resolution to the other, as does the change of gas flows or torch position (see above). The ELEMENT2 was equipped with an ESI micro concentric Teflon nebulizer (flow rate ca. 100 $\mu l\ min^{-1}$) and an ESI Teflon spray chamber. The operation parameters are summarized in Table 3.

All intensities are acquired either in analog or counting mode depending on the expected count rates. This is because the range in acceleration voltage in the simultaneous mode (analog plus counting) for which the secondary electron multiplier (SEM) works under linear conditions is narrower than compared to either only analog or only counting mode (see Fig. 4) and requires frequent recalibration of SEM voltage.

Peaks were monitored in electrical scanning mode for 0.1 seconds. A total of 70 to 120 scans of the whole mass spectrum were performed for one analysis. Together with the settling times of the magnet this results in a total acquisition time of 10 minutes for one

Table 3: Operation parameters of ThermoFinnigan ELEMENT2.

RF power	1235 W
Cool gas flow rate	15 $l\ min^{-1}$
Auxiliary gas flow rate	0.9 $l\ min^{-1}$
Sample gas flow rate	1.0 $l\ min^{-1}$
Sample uptake rate	ca. 100 $\mu l\ min^{-1}$
Sample cone	Nickel 1.0 mm orifice
Skimmer cone	Nickel 0.5 mm orifice
Scan mode	Magnetic jump followed by electric scan
Dwell time per mass	0.1 seconds
Nebulizer	micro-concentric, Teflon
Spray chamber	Teflon

sample.

Two sample solutions with different concentration ranges have been prepared (see above, Table 1) since the response of an SF-ICP-MS device depends on the concentration of the specific element in the solution but also on the resolution used to acquire the data. This is because the transmission decreases by a factor of about 100 from the LR to the HR mode. Accordingly, a solution with a dilution factor of about 1000 was used to acquired the intensities for REE elements from Eu to Lu in HR mode. Intensities of masses without major polyatomic interferences (Rb to Sm and Hf to U) were measured in LR mode in a solution with a dilution factor of about 21000.

3.5 Data reduction

For off-line data reduction, all data (single values of integrated ion intensities of all masses) were exported to Microsoft Excel via the ThermoFinnigan software. Isotope ratios and element ratios of interest (Table 1) were calculated for every scan from blank corrected intensities (the blank values are obtained from an afore measured blank solution). Ten ratios were combined into one 'block' for which the mean value and standard deviation have been calculated. To account for outliers (caused by short term signal or amplifier instabilities), a Dixon outlier test was performed for each block [Miller and Miller, 1984]. Generally, less than one out of 120 ratios had to be excluded from the data set. Final isotope and element ratios have been calculated as the mean value of all scans (n = 70-

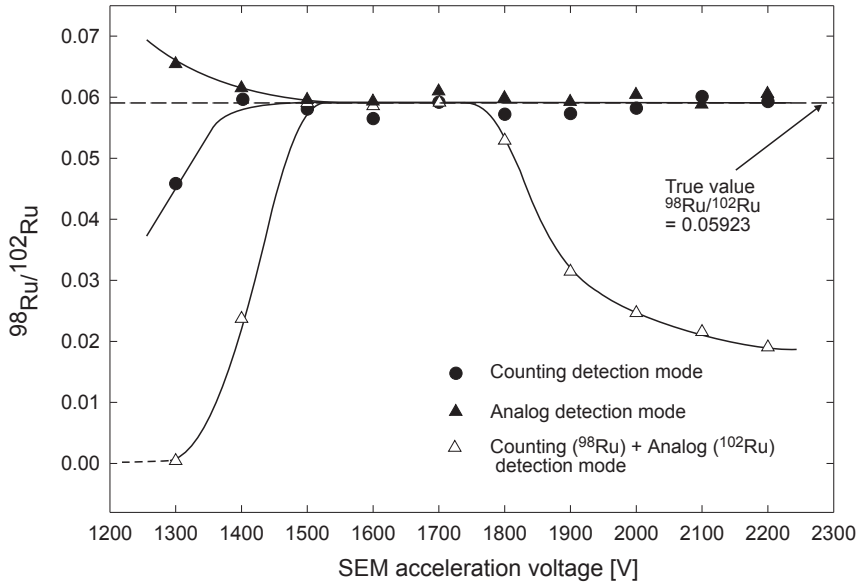

Figure 4: Measurements of $^{98}Ru/^{102}Ru$ ratios in a 2 $ng\ g^{-1}$ Re solution in counting mode (dots), in a 10 $ng\ g^{-1}$ Re solution in analog mode (triangles), and in simultaneous mode (counting/analog; open squares) for different secondary electron multiplier (SEM) acceleration voltages. True value of $^{98}Ru/^{102}Ru$ is 0.059. Measurements in either counting or analog mode display distinctive plateaus (over more than 700V for counting and about 300V in analog mode) whereas those acquired in simultaneous mode have only a narrow plateau (ca. 100V). Therefore it is advisable to acquire ion intensities used for isotope ratio determinations either in analog or counting mode.

120). After correction for mass fractionation using the correction factors obtained from Eq. 9, the mean values were used to calculate the trace element concentrations by ID using Eq. 1. After correction for the contribution of the tracer to the total intensity of the normalizing mass using Eq. 5 the trace element concentration by RSF were calculated using Eq. 2.

3.6 Limits of detection

Limits of detection (LOD) have been calculated according to the 3-σ criterion on a data set of 50 measurements in LR mode and 20 measurements in HR mode of total procedural blanks (including spiking). LOD as rock equivalents are shown in Fig. 5 and range between about 0.1 and 10 $ng\ g^{-1}$ sample equivalents for most elements. LOD decrease with increasing mass and are in good accordance with those described for other ICP-MS techniques (e.g., Eggins et al. [1997], Dulski [2001]). In addition, measurements of the low-concentrated RM PCC-1 (Appendix B) yielded a quantification limit of ca. 10 to 900 $ng\ g^{-1}$ for which results have RSD of better than 10%. This limit equals about 10 to 20

times the LOD for most elements.

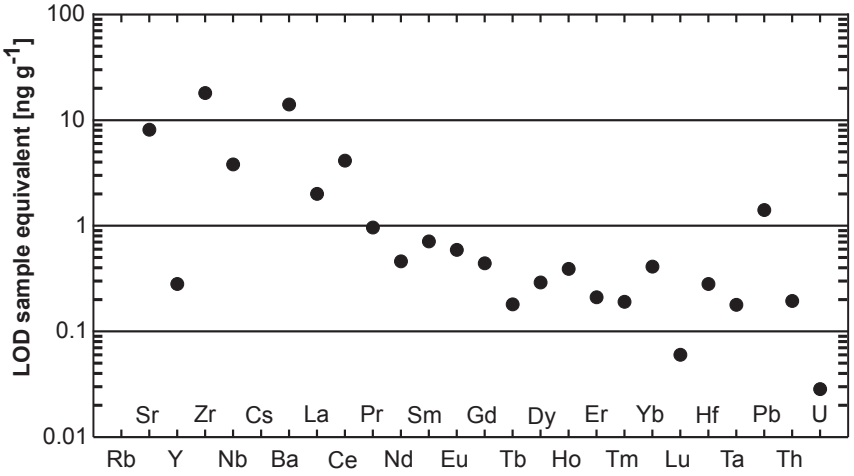

Figure 5: Limits of detection (LOD) in solid sample.

4 Combined standard uncertainty

The determination of the combined standard uncertainty of the measurements [Ellison et al., 2000] is important to evaluate the overall performance of multi-element ID-SF-ICP-MS data. In order to keep the chain of comparison traceable to a known standard we have used reference materials for the quantification of individual uncertainties. Thus, we demonstrate 'the property of the result of a measurement [...] whereby it can be related to stated references [...] through an unbroken chain of comparisons all having stated uncertainties' [Ellison et al., 2000]. The used reference materials include certified standard solutions from Alfa Aesar (SpecPure) and the well-known geological USGS RM BHVO-1. In the following, we use relative standard deviation (RSD) and relative standard error (RSE = RSD, divided by the square root of the numbers of analysis minus 1) to quantify these sources of error.

4.1 Sampling/Weighing

About 100 mg of rock powder is generally used for an analysis. This sample amount may not be representative of the solid geological reference material. The uncertainty, however, is assumed to be $< 0.2\%$ for fine-grained geological samples, as demonstrated by Raczek et al. [2001].

Table 4: Purity of single tracer salts and oxides [$\mu g\ g^{-1}$][a].

Element	**^{86}Sr**	**^{91}Zr**	**^{135}Ba**	**^{145}Nd**	**^{149}Sm**	**^{155}Gd**	**^{161}Dy**	**^{167}Er**	**^{171}Yb**	**^{179}Hf**	**^{207}Pb**	**^{235}U**
Rb	<10	<10	20	10	<10	<10	<10	40	20	160	20	7700
Sr	-	30	80	40	60	30	150	210	180	90	60	20600
Y	<10	<10	<10	<10	<10	<10	50	<10	<10	17	<10	80
Zr	<10	-	100	<10	<10	<10	390	<10	<10	1100	240	100
Nb	<10	10	30	<10	<10	<10	<10	<10	<10	20	90	30
Cs	<10	<10	<10	<10	<10	<10	<10	<10	<10	<10	<10	20
Ba	100	50	-	40	60	30	70	80	60	120	110	<10
La	<10	<10	<10	<10	<10	<10	20	<10	<10	<10	<10	70
Ce	<10	<10	10	20	<10	20	10	<10	<10	20	10	50
Pr	<10	<10	<10	<10	<10	<10	<10	<10	<10	<10	<10	<10
Nd	<10	<10	<10	-	20	10	10	20	<10	50	10	<10
Sm	<10	<10	<10	90	-	<10	<10	<10	<10	<10	<10	<10
Eu	<10	<10	^{137}Ba^{16}O	<10	<10	50	<10	4	3	<0.1	1	<0.1
Gd	<0.1	4	40	^{142}Nd^{16}O	40	-	^{158}Dy	30	80	<0.1	30	<0.1
Tb	<0.1	<0.1	<0.1	^{143}Nd^{16}O	<0.1	2	2	<0.1	<0.1	<0.1	<0.1	<0.1
Dy	<0.1	<0.1	1	^{148}Nd^{16}O	^{148}Sm^{16}O	7	-	^{164}Er	2	4	1	30
Ho	<0.1	<0.1	<0.1	<0.1	^{149}Sm^{16}O	4	10	10	5	<0.1	<0.1	<0.1
Er	<0.1	<0.1	1	^{150}Nd^{16}O	^{150}Sm^{16}O	<0.1	1	-	2	1	1	<0.1
Tm	<0.1	<0.1	<0.1	<0.1	<0.1	<0.1	<0.1	40	5	<0.1	<0.1	<0.1
Yb	<0.1	1	1	2	3	^{158}Gd^{16}O	4	2	-	^{174}Hf	1	<0.1
Lu	<0.1	<0.1	2	1	<0.1	1	<0.1	<0.1	4	9	<0.1	<0.1
Hf	1	250	6	<0.1	<0.1	<0.1	^{162}Dy^{16}O	< 0.1	<0.1	-	10	<0.1
Ta	2	160	4	<0.1	<0.1	<0.1	<0.1	<0.1	<0.1	30	6	60
Pb	6	2	400	70	30	270	50	40	40	90	-	<0.1
Th	<0.1	1	4	<0.1	<0.1	<0.1	10	2	2	2	3	2
U	<0.1	<0.1	<0.1	<0.1	<0.1	<0.1	<0.1	<0.1	<0.1	<0.1	<0.1	-

[a] Measurements have been carried out in low mass resolution. Therefore highly abundant mass lines caused by oxides or by isobaric interferences are cited.

Much higher values are expected for coarse-grained rocks, such as granites, or rocks where some elements are concentrated in refractory trace phases (e.g. Zr in the mineral zircon). In any case, where heterogeneous solid sample material is investigated, different amounts of sample material and different preparation procedures than those described herein have to be applied in order to ensure representative sampling. Uncertainties due to inaccurate weighing of samples and the tracer solutions are less than 0.2 %.

4.2 Homogeneity/chemical treatment of the sample

The transfer of a solid silicate sample into solution remains the most critical step in sample preparation because traceability chain is interrupted, every time the physical and chemical properties of the sample are changed [Kane and Potts, 2002]. In addition, achieving complete sample/tracer homogeneity is crucial for the success of ID. Applying the method described above, the chemical manipulation of the sample is kept at a minimum compared to other techniques that often imply element separation by cation exchange procedures. In addition it is widely accepted that a total recovery for most trace elements is achieved when applying a combined HF-HNO_3 procedure for the digestion of geological samples [Eggins et al., 1997]. This notion is supported by the fact that data for geochemical reference materials of this study (in particular for Zr, see below) agree well with those obtained by other techniques that do not involve acid digestion procedures, e.g. spark source mass spectrometry [Jochum et al., 1988] or X-ray fluorescence analysis [Jochum et al., 2000]. Although, we are not able to designate an analytical uncertainty related to sample digestion, almost all analytical techniques dealing with the digestion of geological samples are hampered by this fact and the discussion is beyond the scope of this study.

4.3 Purity of reagents

Acids that are used to dissolve the rock powder and to dilute the analyte can contaminate the sample. Total blank levels for acids that were used for dissolving the rock samples range at the *pg* level (e.g., 10 *pg* for Rb, 150 *pg* for Sr, 20 *pg* for Nd, and 5 *pg* for Sm). Since element abundances in the sample amount used for analysis are in the order of μg (1 μg Rb, 40 μg Sr, 2.5 μg Nd, and 0.6 μg Sm) these blank levels were insignificant for the analysis of basaltic reference materials. Blank levels of the 0.4 $mol\ l^{-1}$ HNO_3 that was used to dilute the analyte, range at the fg level. Although the abundances of elements in the final analyte are as low as 10 *pg* (Cs), blank levels are insignificant ($<$ 0.01%). Thus, all reagents used in this study do not significantly contribute to the overall uncertainty of this method. However, if rocks with low concentrations of trace elements are analyzed (e.g. peridotites, that can have trace element concentrations as low as 1 $ng\ g^{-1}$),

purity of reagents may become a source of error (about 0.2 to 1%). For each sample set, a blank solution was measured and a blank correction was applied to each sample. This is because it has been suspected earlier that most of memory/blank problems arise from sample introduction system and sample/skimmer cones [Jenner et al., 1990]. The estimated analytical uncertainty related to this blank correction is $< 0.05\%$.

4.4 Purity of tracer solutions

The sample can be contaminated with elements that are not determined by ID through the addition of MET solutions. We have therefore investigated the purity of each single tracer prior to mixing the MET solutions. The results in μg contaminant per g tracer element are listed in Table 4. The main contaminants are Ta, Rb and Nb. However, because the total amount of tracer that is added to the sample ranges in the μg scale, the concentration of contaminant elements ranges on the pg level. Comparing these concentrations to those naturally encountered in geological samples (e.g. BHVO-1) the uncertainty on the concentration that can be attributed to the introduction of contaminant elements by the tracer is $< 0.05\%$.

4.5 Reference solutions and reference material

In this study we have used certified mono-element standard solutions (Alfa Aesar, Specpure) to evaluate the extent of the analytical uncertainty of individual sources of error as well as to calibrate the RSF for each sample set (see above). The concentrations are known within 0.3%. Before preparing the multi-element standard solution, a careful screening of the purity of single certified mono mono-element standard solutions is necessary in order to avoid contamination of low concentrated elements in the multi-element solution by the other certified standard solutions. Using the certified blank values of standard solution (Alfa Aesar) we have calculated the extent of contamination taking into account the proportion in which the single standard solutions have been mixed. Uncertainties of trace element concentrations in the multi-element solution related to the impurity of mono-element solutions is less than 0.3%. Concentration data for the geochemical USGS RM BHVO-1 were adopted from Govindaraju [1994], Wilson [2005], Raczek et al. [2001], and Jochum and Hofmann [1995]. The uncertainty of these concentration data generally varies between 0.5% and 3%.

4.6 Calibration

Composition of multi-element tracer. The accuracy of the results depends on the quality of the calibration of the multi-element tracer solutions. Calibration errors mainly arise from uncertainties of concentration of certified standard solutions (0.3%), weighing of multi-element tracer solutions and standard solutions (0.3%), and the stability of tracer and standard solutions. In addition, the calibration was affected by uncertainties arising during isotope ratio measurements, as discussed below. The uncertainty of the tracer calibration procedure was estimated at about 0.5 to 1% depending on the individual element. The uncertainty of the certified isotopic composition of single tracers (Oak Ridge National Laboratory, Cambridge Isotope Laboratories, National Bureau of Standards) is less than 0.1% for Sr, Sm, Dy, Er, and Hf and less than 0.05% for all others.

Relative sensitivity factors (RSF). Similar to the tracer solutions, the error of RSF arise from the uncertainty of weighing, concentration of multi-element standard solutions, and the determination of element ratios, as discussed below. According to this, the RSF are known within 0.5 to 2%, depending on the individual element.

4.7 Drift

Drift effects, i.e. the increase or loss of ion sensitivity during the time of one acquisition interval is a serious source of error in external calibration ICP-MS [Cheatham et al., 1993]. For multi-element ICP-MS, drift is only a minor source of error for concentration data of elements that are determined by ID, because isotope ratios are measured at nearly the same time (uncertainty $< 0.5\%$).

For the determination of RSF, a multi-element solution is measured at the beginning of each sample set. To quantify the analytical uncertainty of RSF related to drift effects we have monitored the element ratios of $^{137}Ba/^{139}La$, $^{141}Pr/^{143}Nd$, and $^{232}Th/^{238}U$ twice over a time-period of ten hours. The results are shown in Fig. 6. All data agree with the internal error (RSE) of the individual analyses. The repeatability (RSD) of both long-term analyses (1 and 2 in Fig. 6) is less than 0.5% for $^{137}Ba/^{139}La$, less than 0.3 % for $^{141}Pr/^{143}Nd$ and less than 0.6% for $^{232}Th/^{238}U$.

Drift effects are a complex function of mass [Eggins et al., 1997] affecting higher masses more than lower ones. However, normalizing the count rates to an internal standard reduces the drift effect drastically, especially if the mass difference between measured isotope and internal standard is small (e.g., < 6 amu). Therefore, drift effects do not significantly affect the RSF and the related analytical uncertainty is $< 0.6\%$. In addition, we cannot detect any relation of drift to different ionization behavior of the elements since

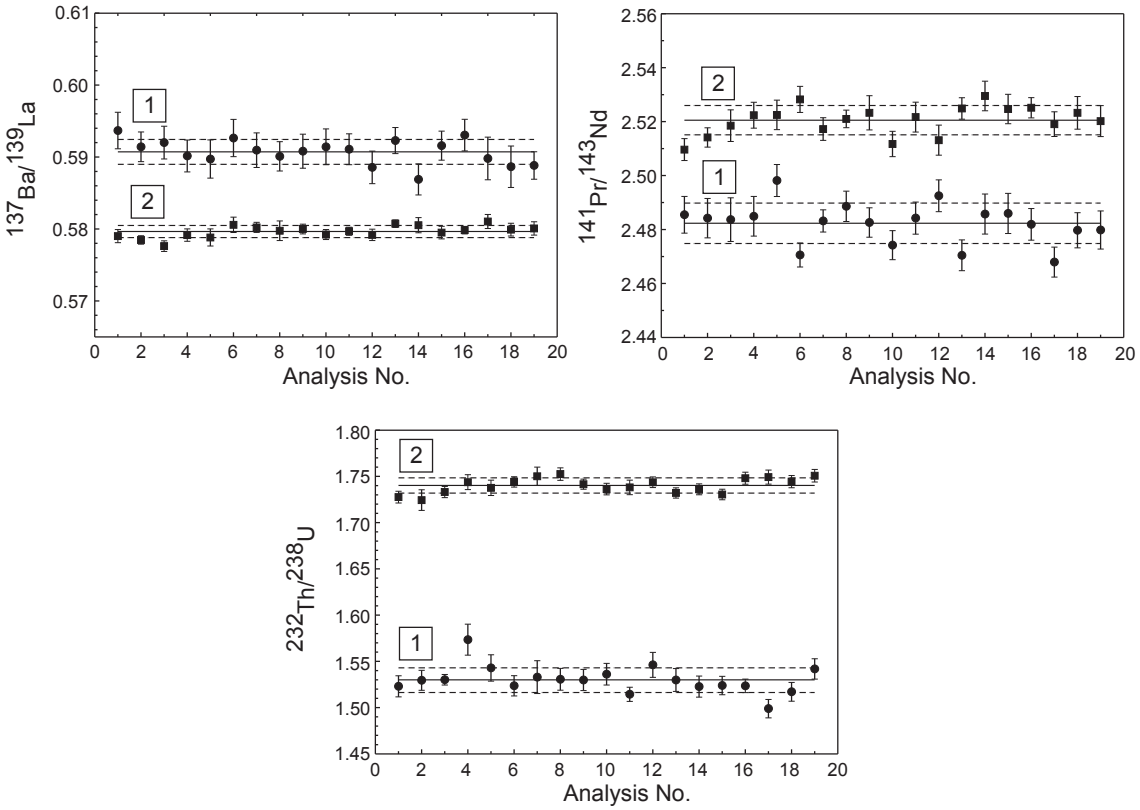

Figure 6: Results of two long term measurements (1 and 2 in figure, ca. 10 h each) of $^{137}Ba/^{139}La$, $^{141}Pr/^{143}Nd$, $^{232}Th/^{238}U$ ratios. Every determination comprises 120 mass scans. The measurements indicate that the element ratios are uniform within 0.3 to 0.6% (RSD). No drift effects are observable.

isotope ratios display similar errors ($< 0.4\%$ for $^{135}Ba/^{137}Ba$, $< 0.3\%$ for $^{143}Nd/^{145}Nd$, and $< 1\%$ for $^{235}U/^{238}U$; not shown in Fig. 6).

4.8 Robustness of isotope ratios

The accurate and precise determination of isotope ratios is the most important parameter in ID. The measurement isotope ratios has the advantage that it is robust according to a variety of instrument operation settings. Changing sensitivity of the detector system with time (see below) and spikes in intensity chromatograms that occur when large droplets of analyte get injected into the plasma, both affect the total ion counts during one analysis. Since these parameters influence the near-simultaneous measurement of different isotopes and elements in nearly the same way, the reproducibility can be improved, if isotope and element ratios are used to determine the concentrations. In Fig. 7, the isotope ratio measurements of standard solutions over a time period of 5 months are shown. Generally,

the total ion yields of individual isotopes agree within about 1% (RSE) during one analysis. However, analytical uncertainties of isotope ratio measurements are always better than 0.5% (RSE). Fig. 7 also shows the impact of different operation conditions on the results of isotope ratio measurements since operation conditions were varied day by day. Although the mean values of absolute count rates can differ by 50%, the isotope ratios remain constant and agree within their error limits. This demonstrates the robustness of isotope ratio measurements.

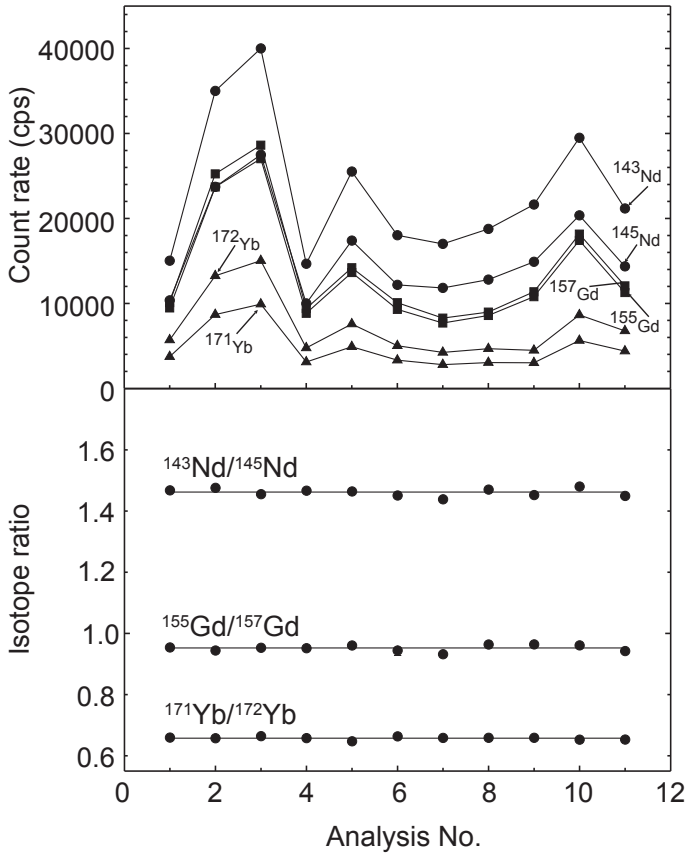

Figure 7: Absolute count rates and isotope ratios determined from analyses of multi-element solutions. The analyses were performed over a time period of 5 months. Each analysis consists of 120 mass scans. Although the absolute count rates can vary of about 50%, the isotope ratios agree within their $1\sigma_M$ intervals (equal to symbol size). This result emphasizes the robustness of isotope ratio measurements.

4.9 Spiking

Following the laws of error propagation [Riepe and Kaiser, 1966], any statistical error in the isotope ratio measurement is increased by an 'error magnification factor'. This factor depends on the measured isotope ratio of the sample/tracer mixture (in other words on

the amount of added tracer to the sample; Fig. 8). Accordingly, an optimum value for the measured ratio has to be obtained to keep the error magnification factor as low as possible. Error magnification factors in this study are between 1 and 2 for trace element concentrations most commonly encountered in geological samples (Fig. 8). However, if low-concentrated samples (e.g. peridotites) are analyzed, larger values of the error magnification factor may arise when using the same multi-element tracer solutions.

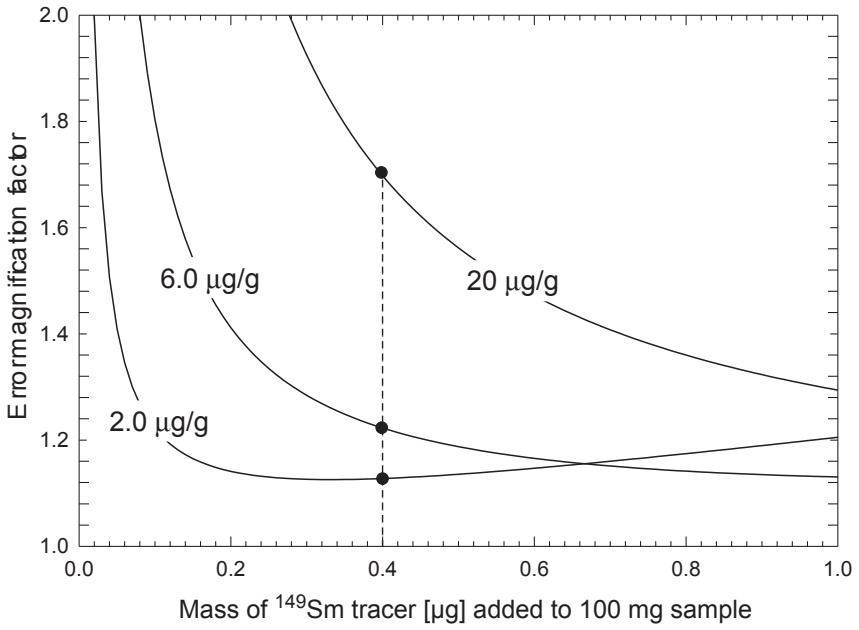

Figure 8: Calculated error magnification factors as a function of the amount of added tracer [μg] to 100 mg of sample powder (exemplified for the rare-earth element Sm). Even if the Sm concentration in the sample ranges between 2 and 20 $\mu g\ g^{-1}$, the error magnification factor on the precision of the determined isotope ratio (here $^{149}Sm/^{147}Sm$) is less than 2.

4.10 Instrument effects

Several aspects contribute to the overall machine bias that is specific for the used mass spectrometer.

Interferences and abundance sensitivity. The extent of polyatomic ions that interfere with the ions of the masses of interest are negligible for this study since most of them can be avoided using the HR mode. Another source of error is related to the superposition of the tail of a large mass peak with that of the mass of interest, if the latter is low compared to the interfering mass. The ability of a mass spectrometer to resolve such interferences is called 'abundance sensitivity'. Using a mass spectrometer with a double focusing reverse Nier-Johnson geometry (like in the case of the ELEMENT2), the tail corrections are min-

imal ($< 30 \times 10^{-6}$ for ^{86}Sr in LR mode for a solution with Rb/Sr = 1.8×10^6. Moreover, since abundances of neighbored mass peaks in natural samples do not vary by multiple orders of magnitude, we do not relate an analytical uncertainty to this issue.

Dead time of detector. For most isotopes that are acquired in counting mode, count rates range up to 2×10^6 cps and the dead time correction is less than 3%. The dead time was corrected online by the software and the analytical uncertainty related to this correction is $< 0.1\%$.

Instrumental background. The dark current of the multiplier itself is very low (< 0.2 cps). The background produced by charge exchange between ions and molecules varies between 5 - 30 cps. Since these intensities are negligible compared to those of the monitored masses, no background correction was performed. This results in an uncertainty of less than 0.04% on isotope and element ratios.

4.11 Matrix effects

The effect of concomitant elements (e.g., Al, Mg, Ca, Na, K) on the distribution of ions in the plasma does not significantly contribute to the analytical uncertainty of multi-element ID-SF-ICP-MS, because calibration is achieved internally by the added tracer. However, since the multi-element solution, that was used to calibrate the RSF, has a different matrix compared to that of the measured sample, possible matrix effects may have to be taken into account.

In order to investigate the uncertainty related to different matrices of analyte and multi-element solution we have determined the RSF from measurements of BHVO-1 and of the multi-element solution. The results are shown in Fig. 9. The uncertainty related to each RSF was determined taking into account the uncertainties of (1) concentrations in the geochemical reference material and the multi-element solution, respectively, (2) element ratio measurement, (3) correction of mass discrimination effect, and (4) weighing. The RSF agree within the analytical uncertainties of the individual measurements. Fig. 9b shows the RSF calculated from solutions of BHVO-1 and multi-element standard solutions that have been measured on three different days. On every day, RSF determined from BHVO-1 and multi-element solution agree within error limits. Moreover, the RSF determined from both solutions remain constant over a time period of at least three days if operation conditions are similar.

To test the linearity of the RSF according to different concentration levels, we have determined RSF from measurements of five different dilutions of the multi-element standard solution. Dilution factors cover a range of one order of magnitude (Fig. 10). The RSF of Y, Nb, La, Ce, and Pr determined for solutions with different concentrations all

agree within error limits. We therefore conclude that there is no dependency of RSF on the concentration of trace elements and, accordingly, we do not relate any uncertainty to this item.

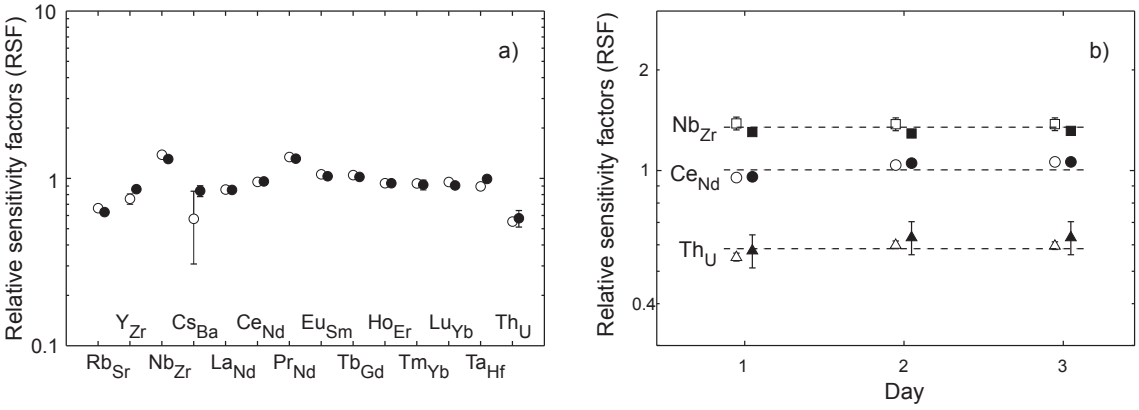

Figure 9: Relative sensitivity factors (RSF) obtained from analyses of a solution of the geological reference material BHVO-1 (open symbols) and a multi-element solution (filled symbols). Elements used as internal standards are given as subscripts. a) Calculated RSF from both solutions agree within the $1\sigma_M$ intervals for most elements (see text for discussion). b) RSF calculated for measurements of same solutions on three different days. RSF remain constant over a time period of three days if operation parameters are similar.

4.12 Mass discrimination

In order to evaluate the error that is related to the correction of MF we have measured a not spiked analyte of the BHVO-1 reference material and applied the correction as given in Eq. 9 to the data set. The deviation of the corrected measured value from the true value is a measure for the uncertainty that is related to the MF correction. The uncertainty is less then 1% for masses between 85 and 140 amu and less than 0.5% for masses higher than 140. We therefore assume a maximum value of 1% as an estimate for the uncertainty related to the correction of mass discrimination effect.

4.13 Values of constants

Isotope abundances and relative atomic masses are taken from Rosman and Taylor [1998] and Loss [2003]. Uncertainties of these constants lead to errors of 0.2 % for most elements with exception of Yb ($< 0.6\%$). Although the natural isotopic compositions of the respective elements in the samples are adequately known for the purpose of this study, the Pb isotopic composition is related to the U, Th, and Pb concentrations of the source of the rock. This is because the radioactive decay of ^{235}U to ^{207}Pb, ^{238}U to ^{206}Pb, and

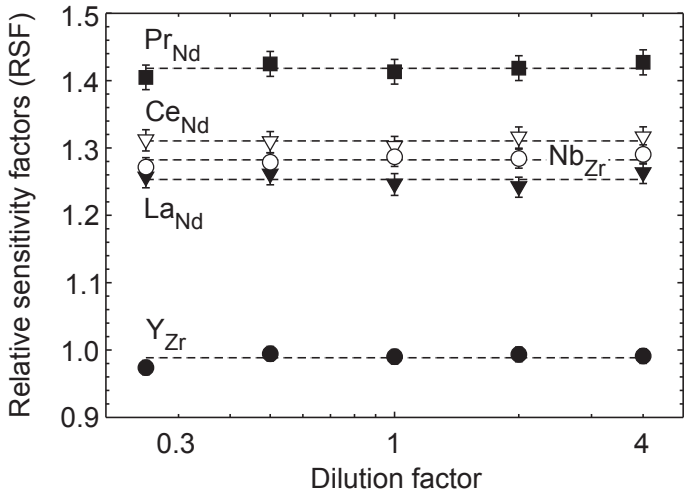

Figure 10: Relative sensitivity factors (RSF) obtained from different dilutions of a multi-element solution. Elements used as internal standards are given as subscripts. A solution with a dilution factor of 1 is routinely used for determination of RSF during analysis. RSF are uniform within error limits ($1\sigma_M$) for dilution factors that vary over one order of magnitude.

^{232}Th to ^{208}Pb over geological timescales (in the order of millions of years) causes variable Pb isotopic composition of different rocks. To asses the uncertainty of Pb concentrations related to the variable Pb isotopic compositions of unknown samples, we have compared the calculated Pb concentrations for BHVO-1 (see below) with its well known reference value for Pb assuming either average Pb isotope abundances [Rosman and Taylor, 1998] or high-precision Pb isotopic compositions determined for BHVO-1 by TIMS [Woodhead and Hergt, 2000]. The difference between both approaches is 0.4% (concentration of Pb: 2.13 $\mu g\ g^{-1}$ versus 2.14 $\mu g\ g^{-1}$, respectively).

4.14 Operator bias

The influence of operator bias during sample preparation, operation, and data reduction is difficult to quantify. However, the operator most efficiently influences the result during adjustment of operation conditions of the mass spectrometer (gas flows, torch position, lenses). Fig. 7 shows that differences in operational conditions of the mass spectrometer do not influence the accuracy and precision of the isotope ratio measurements. Moreover, the advantage of the multi-element ID-SF-ICP-MS technique is that operator bias during sample preparation is restricted to weighing (sample, multi-element tracer solutions). Beyond this, there is no need for quantitative sample handling since even the loss of sample solution would not have any influence on the trace element concentration results after the sample/tracer homogenization has been achieved. Therefore, we assume a maximum

uncertainty of 0.5% for operator bias.

4.15 Combined standard uncertainty

Summing up the individual components of uncertainty, we have calculated the combined standard uncertainty of multi-element ID-SF-ICP-MS following the rules of error propagation [Ellison et al., 2000] whereby we assume that individual components of uncertainty are independent. This results in an overall analytical uncertainty of 1 to 2% for trace element concentrations that are determined by ID and about 2 to 3% for trace element concentrations that are determined by RSF.

5 Results and discussion

Five independent analyses (different spiking/digestion) of BHVO-1 have been carried out over a time period of 4 months. Triplicate determinations have been performed for each digestion. The results are shown in Appendix A, together with the mean values of the triplicate determinations and their RSD. In Appendix B, the results of three to four independent analyses of 16 other reference materials are given together with the mean value and RSD. Only one digestion has been prepared for the USGS reference glasses BCR-2G, BHVO-2G and BIR-1G, and NIST SRM 612 respectively and has been measured three to four times.

5.1 Accuracy and reproducibility

Data obtained by isotope dilution. The repeatability of trace element concentrations as determined by the RSD of triplicate determinations of one digestion of BHVO-1 (Appendix A) is generally better than 1%. Highly concentrated elements (e.g., Sr > 350 $\mu g\ g^{-1}$) have lower RSD values for triplicate analysis compared to low concentrated elements (e.g. U < 0.5 $\mu g\ g^{-1}$), a fact that is related to better counting statistics for highly concentrated elements. Also, the higher RSD values for element concentrations obtained in HR mode (1-2%) are probably related to the reduced transmission in the HR mode. As an example, for a given concentration level of about 2 $\mu g\ g^{-1}$, the RSD for Yb, which has been determined in HR mode is about 1% whereas the RSD for Pb, which has been determined in LR, is < 1%. The reproducibility of all five digestions of BHVO-1 (n=5, Appendix A) differs only slightly from the that of every triplicate determinations and demonstrates that the overall reproducibility of trace element concentrations is mainly limited by the reproducibility of the mass spectrometer measurements.

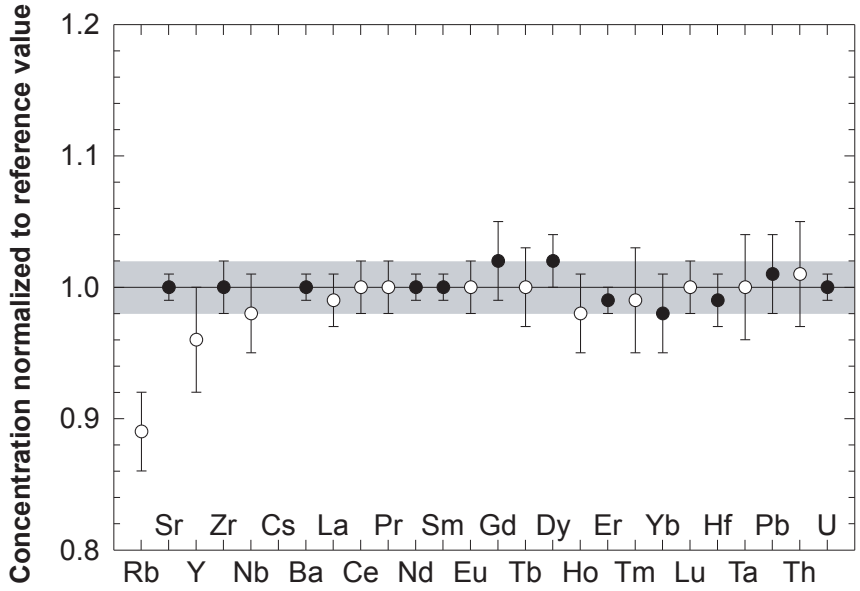

Figure 11: Comparison of trace element data of BHVO-1 (n=5) to ID-TIMS [Raczek et al., 2001], ID-MIC-SSMS [Jochum et al., 2001] data, and data of Govindaraju [1994]. Filled symbols = data obtained by isotope dilution, open symbols = data obtained by relative sensitivity factors. Note that confidence intervals (68%) also include uncertainties of reference values that range between 1 to 4%.

The mean concentration values agree within about 1-2% with respective ID multi-ion counting-(MIC)-SSMS and ID-TIMS data (Fig. 11) from our laboratory [Raczek et al., 2001; Jochum et al., 2001]. It has to be noted, that in all cases different tracers and procedures have been used. Moreover, when compared with other sets of ID data for BHVO-1 (e.g., poly-isotopic REE and Pr data by Baker et al. [2002]) the results agree within the given confidence intervals (1σ). In the following discussion we use, whenever possible, highly precise ID data as reference values for comparison.

Data obtained by relative sensitivity factors (RSF). Repeatability (RSD) of triplicate determinations of elements that have been determined in the LR mode is better than 1%. Similar to concentrations determined by ID, the reproducibility (RSD) depends on the concentration level and on the resolution mode. The reproducibility of data acquired in HR is diminished due to poorer counting statistics. The overall reproducibility of all measurements of BHVO-1 (n = 5) ranges between 1 and 2% (Appendix A). Exceptions are Rb and Cs for which RSD of 3% and 18% are obtained. We cannot attribute these findings to instrumental bias since the repeatability of triplicate determinations of one solution is excellent (e.g., 0.1% for Cs in BHVO-1 (5), Appendix A). We infer environmental reasons such as blank or memory effect to explain this observation. An increasing memory for Cs during the course of the day was observed repeatedly and is probably related to poor

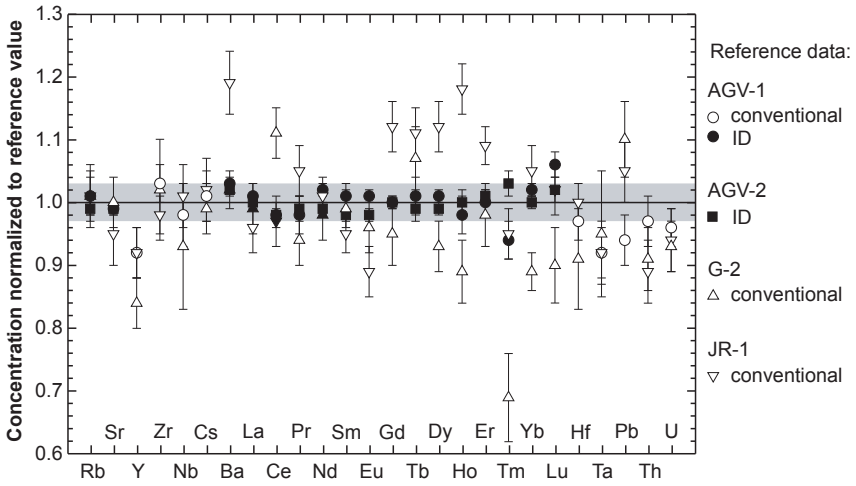

Figure 12: Comparison of concentration data of silica-rich geological reference materials AGV-1, AGV-2, G-2, JR-1 with reference values (Appendix B). Filled symbols = reference values obtained by isotope dilution (ID) and internal standardization using ID values. Note that confidence intervals (68%) also include uncertainties of reference values that range between 1 to 7%. Inferred uncertainties for reference values from Govindaraju [1994] are: recommended values 3%, proposed values 5%, and information values 7% (RSD).

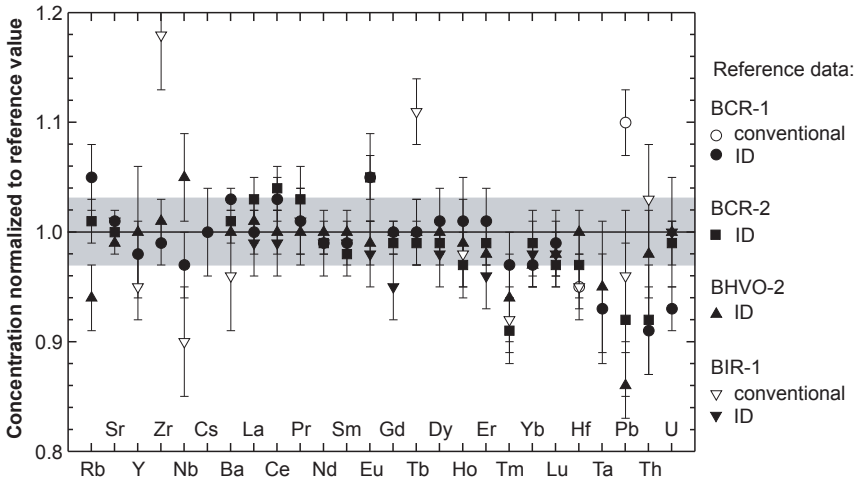

Figure 13: Comparison of concentration data of basaltic geological reference materials BCR-1, BCR-2, BHVO-2, BIR-1 with reference values. Filled symbols = reference values obtained by isotope dilution (ID) and internal standardization using ID values. Note that confidence intervals (68%) also include uncertainties of reference values that range between 1 to 7%. See Fig. 12 for inferred uncertainties of reference values from Govindaraju [1994].

washout characteristics for Cs in our tubing system, despite the use of Teflon tubes. These effects may become severe for concentrations $< 5\ \mu g\ g^{-1}$ for Rb and $< 0.1\ \mu g\ g^{-1}$ for Cs. However, these findings do not obliterate the principle use of RSF for the determination of element concentrations since these problems can be largely avoided by using different washout and sample preparation procedures. In Fig. 11, our data are compared to literature values obtained by ID-MIC-SSMS and ID-TIMS [Raczek et al., 2001; Jochum et al., 2001]. Both data sets agree within about 2-4%. Our Rb value deviates about 10% from the respective reference value supporting our interpretation that environmental reasons (over-correction of blank background) caused the offset of this value.

5.2 Data for geological reference materials - special features

The reproducibility (RSD) of three to four independent determinations (different spiking/digestions, Appendix B) of different reference materials is, in most cases, better than 1% for elements determined in the LR mode and better than 2% for elements determined in the HR mode. These findings are in good agreement with the long-term reproducibility obtained from the analysis of BHVO-1 (see above). In Figures 12, 13, and 14, relative deviations (mean value/reference value) of concentration data for silica-rich rock samples, basalts, and glasses are shown. Most data agree within 3-4% with reference values that have been determined by ID and by external calibration using ID values as internal standards (filled symbols; Raczek et al. [2001]; Jochum et al. [2001]; Baker et al. [2002]).

Exceptions are the Pb concentrations of BCR-2 and BHVO-2 (Fig. 13) that are up to 14% lower than the values of Jochum et al. [2001]. Assuming our values to be correct, the lower Pb concentrations in new USGS reference materials (BCR-2, BHVO-2, AGV-2) compared to higher Pb concentrations in original samples (BCR-1, BHVO-1, AGV-1) can be explained by Pb contamination during the sample preparation of the original samples, a finding which is consistent with different Pb isotopic compositions between both generations [Woodhead and Hergt, 2000]. In addition, the U and Th concentrations in BCR-1 and the Th concentration in BCR-2 are up to 10% lower than the respective values from Jochum et al. [2001]. Yet, the Th/U ratios of 3.22 and 3.21 in BCR-1 and BCR-2 of this study are in better accordance than the respective values of 3.30 and 3.48 in Jochum et al. [2001].

Reference materials containing refractory minerals or having low concentrations of trace elements have significantly larger uncertainties of about 4 to 9% for some elements (e.g., Zr, Hf, Pb, U in G-2 or Sm, Ta in PCC-1). They also show larger relative deviations from published values (up to 60%). This can be related to (1) variable digestion yields especially of refractory mineral phases (e.g., zircon in G-2), (2) a too small test sample

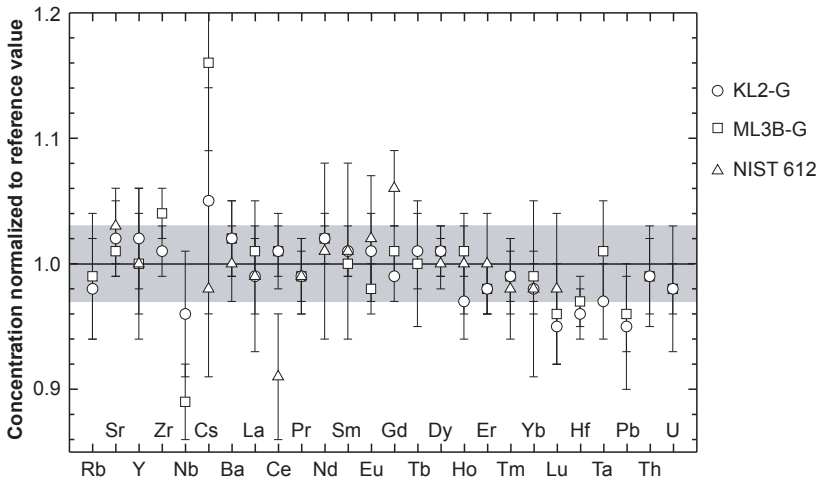

Figure 14: Comparison of concentration data of geological reference glasses KL2-G, ML3B-G, NIST SRM 612 with reference values (Appendix B). Note that confidence intervals (68%) also include uncertainties of reference values that range between 1 to 8%.

size especially if the reference material was produced from a coarse grained rock and the powder itself is not fine grained enough, (3) the low concentration levels of trace elements in the analyzed sample (e.g., 30 - 100 $ng\ g^{-1}$ for REE in PCC-1), or a combination of 2) and 3).

In Fig. 15, trace element data for the new USGS reference glasses BCR-2G, BHVO-2G, and BIR-1G are compared with those of their original rock powders. Most data agree within the given uncertainty levels of both determinations (ca. 3% relative deviation). The elevated U and Pb concentrations in BIR-1G (almost 300% and 7% higher compared to original powder) are significant features and are probably related to U and Pb contamination during the preparation of the BIR-1G reference glass by the USGS. There is a good agreement for Pb concentrations in BHVO-2G and BHVO-2 (ca. 2% depletion of Pb in BHVO-2G). However, a significant depletion of Pb in BCR-2G relative to BCR-2 is observed (ca. 10% relative deviation). We relate this to the loss of Pb during the preparation of BCR-2G. Similar depletion of Pb during the preparation of melt beads for laser ablation ICP-MS has been observed in our laboratory. This is probably related to increasing volatility of Pb with increasing melting temperature and time of melting.

In NIST SRM 612 the concentration levels for trace elements range between 20 and 80 $\mu g\ g^{-1}$ [Pearce et al., 1997] leading to large spectroscopic interferences that are commonly not encountered in natural samples. These interferences are $^{69}Ga^{16}O$ on ^{85}Rb,$^{74}Ge^{16}O$ on ^{90}Zr (affecting both the Zr and Nb concentration; see Table 1), $^{162}Dy^{16}O$ on ^{178}Hf, and $^{165}Ho^{16}O$ on ^{181}Ta. In addition, inadequate spiking leads to increased error magnification

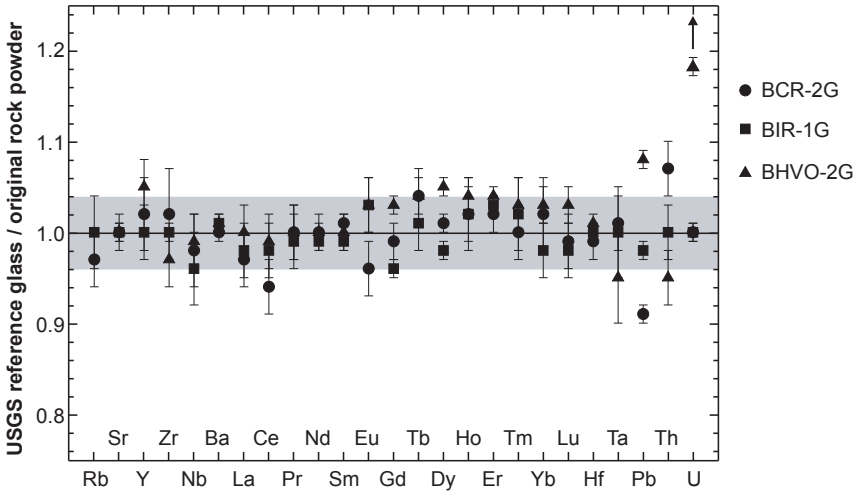

Figure 15: Comparison of trace element concentrations for new USGS reference glasses BCR-2G, BIR-1G, BHVO-2G with the results obtained for the original USGS reference materials (Appendix B).

for Pb and U due to the high concentrations of these elements in NIST SRM 612 that strongly contrast those in natural samples. We therefore have omitted concentration data for Rb, Zr, Nb, Hf, Ta, Pb and U for NIST SRM 612 in Appendix B.

6 Overall performance of multi-element ID-SF-ICP-MS

In the following, we discuss the advantages and disadvantages of ID-SF-ICP-MS in the light of the most prominent obstacles in ICP-MS and TIMS analysis. As a result, we propose that multi-element ID-SF-ICP-MS fulfills the requirements of advanced geochemical investigations for data with low uncertainty and short analysis time.

6.1 Matrix effects

Matrix effects can considerably diminish accuracy of ICP-MS analyses if external calibration is applied. It has been shown that only matrix-matched standardization (e.g., the use of reference materials as calibration standards) can account for variation in instrument sensitivity due to matrix effects [Cheatham et al., 1993]. However, if only one reference material is used for standardization (e.g. BHVO-1) the accuracy can be diminished due to the uncertainty of concentrations in the used reference material [Eggins et al., 1997].

Matrix effects can be eliminated by the use of ID because the sensitivity of the instrument is determined within the sample matrix itself by the added tracer [Heumann,

1986]. In addition, matrix effects on concentration data that are determined by RSF can be significantly reduced by the use of several internal standards if there is a close mass matching between the element of interest and the internal standard [Longerich et al., 1990; Field and Sherrell, 1998]. Accordingly, matrix effects are eliminated or largely avoided by the use of multi-element ID-SF-ICP-MS.

6.2 Instrumental drift

Temporal variations in instrument sensitivity (e.g., clogging of cones, thermal effects, defocusing of ion beam) are the most important factors restricting the reproducibility in conventional ICP-MS. The problem of instrumental drift in conventional ICP-MS can only be solved by the use of several internal standards spaced in small intervals across the mass spectrum and by frequent recalibration [Longerich et al., 1990; Eggins et al., 1997; Dulski, 2001].

The instrumental drift of a sector field ICP mass spectrometer has only a negligible effect on the reproducibility of ID determined concentrations since isotope ratios are used for the determination of concentrations. These findings are consistent with the results of other ID techniques (e.g., Xie and Kerrich [1995]; D'Orazio and Tonarini [1997]; Griselin et al. [1999]; Raczek et al. [2001]; Weyer et al. [2002]; Baker et al. [2002]). In addition, diminishing effects of instrumental drift are achieved by the simultaneous determination of trace element concentrations by RSF. Therefore, multi-element ID-SF-ICP-MS, compared to conventional ICP-MS, is less sensitive to errors induced by signal drift.

6.3 Spectroscopic interferences

If multi-element methods are applied to TIMS or ICP-MS, polyatomic and isobaric interferences on masses of interest can cause severe problems concerning the accuracy of determined isotope intensities (e.g., Prohaska et al. [1999]; Robinson et al. [1999]; Raczek et al. [2001]). In TIMS and for some MC-ICP-MS techniques, isobaric and polyatomic interferences (e.g. interferences of light REE oxides on heavy REE) can only be avoided by time consuming chemical separation procedures [Raczek et al., 2001; Weyer et al., 2002; Baker et al., 2002]. Reduction of oxide formation in ICP-MS by using desolvation nebulization systems [Field and Sherrell, 1998] is hampered by increased wash out times of up to several minutes (e.g., for Cs, Ta, and Th). Also, corrections for oxide interferences that include the determination of oxide formation rates prior to the analysis of unknowns are faced with the problem of temporal or matrix induced variation of oxide formation [Longerich, 1989; Lichte et al., 1987; Longerich et al., 1990; Jenner et al., 1990]. The

latter can only partly been overcome by frequent recalibration of oxide correction factors [Dulski, 1994] during each analytical run.

Multi-element ID-SF-ICP-MS is less sensitive to spectroscopic interferences related to matrix and operation conditions especially for those of light REE on heavy REE, if the HR mode is used to determine the intensities of isotopes that are potentially interfered by polyatomic ions [Prohaska et al., 1999; Robinson et al., 1999]. The elimination of oxide corrections from the determination of concentration improves the accuracy of the result by minimizing the error propagation associated with this correction.

6.4 Multi-element capability

In principle, all elements can be determined near simultaneously by multi-element ID-SF-ICP-MS for which two stable and interference free isotopes are available. As it is demonstrated in this study, the tracer concentrations in the MET have been designed for a broad spectrum of concentrations and require only a rough knowledge of the concentration in the sample. All other element concentrations can be determined by RSF (e.g., mono-isotopic elements) by using ID determined elements as internal standards, yielding reproducible and accurate results.

6.5 Time

ICP-MS compared to TIMS allows rapid analysis capabilities and sampling at atmospheric pressures. A drawback of multi-element ID-SF-ICP-MS compared to conventional ICP-MS is the time consuming and effort-rich preparation and calibration of tracer solutions. However, once the MET have been prepared and calibrated, the mass spectrometer runtime can be improved significantly compared to conventional ICP-MS.

During the course of this study, a total analysis time of ca. 20 minutes per sample was achieved including the measurement of blank, standard solution, washout, as well as the acquisition of masses for mass fractionation correction and masses of elements that were determined by RSF. This results in a mass spectrometer efficiency of almost 90% (mass spectrometer time that can be used to measure unknown samples). In comparison, a mass spectrometer efficiency of about 70 to 50% is achieved in conventional ICP-MS due to frequent measurement of standard solutions for recalibration (e.g. Eggins et al. [1997]; Dulski [2001]). Thus, labor and time intensive preparation of tracer solutions in multi-element ID-SF-ICP-MS is relativized by higher mass spectrometer efficiency.

6.6 Reproducibility and accuracy

The reproducibility of an ID method is limited by the precision of the determined isotope ratio, which, on the other hand, is always better than that for the absolute intensity. By using multiple detection systems, ID-TIMS and ID-MC-ICP-MS are able to eliminate any instability of ion intensities and thus yield highly reproducible results with less than 0.5% RSD and accuracies that agree within 1-2% relative to respective reference values [Weyer et al., 2002; Raczek et al., 2001; Baker et al., 2002].

It has been shown that due to the flat-top peak shape of SF-ICP-MS (as in the case of this study) precise isotope ratios of about 0.5% RSD can be achieved [Vanhaecke et al., 1996; Kerl et al., 1997; Becker and Dietze, 2000]. In addition, the use of several internal standards also improves the precision of determined elemental ratios. The achieved reproducibility of 1-3% (RSD) and accuracy of 2-3% (relative deviation) of this study for a broad range of elements determined by ID and RSF are in good agreement with similar values by Xie and Kerrich [1995] and Joannon et al. [1997] for the determination of Zr and Hf, and Th and U by ID. Compared to a reproducibility of 3-7% (RSD) and an accuracy of 3-7% (relative deviation) for conventional ICP-MS [Jenner et al., 1990; Dulski, 2001], a two to three fold improvement is achieved. In the case of matrix matched standardization (e.g., Eggins et al. [1997]) the accuracy is strongly restricted by the uncertainty of element concentrations in the reference materials, which can be significantly higher than 5% for some elements.

6.7 Combined standard uncertainty

The combined standard uncertainty of a method is a direct measure for the quality of its results [Ellison et al., 2000]. To our knowledge, the combined standard uncertainty has been evaluated only for a few of the analytical techniques used in geosciences (e.g., Stoll and Jochum [1999]). However, we can make some basic estimates concerning the combined standard uncertainty of conventional ICP-MS techniques for comparison with multi-element ID-SF-ICP-MS: Conventional ICP-MS using several internal standards (e.g. Eggins et al. [1997]) requires at least six measurements of ion intensities (isotope of interest and two internal standard isotopes, each in sample and calibration solution) each assumed to have an uncertainty of $\leq 1\%$. The uncertainty of concentrations in the reference material calibration solutions can be as high as 5%, especially with respect to the instability of HFSE that are prone to form insoluble precipitates in the absence of HF and HCl [Weyer et al., 2002].

Table 5: Comparison of three different isotope dilution techniques used at the MPI for Chemistry for trace elemental analysis of geological materials.

Technique	**TIMS**	**MC-ICP-MS**	**SF-ICP-MS**
Mass separation	magnetic field	electric/magnetic field	magnetic/electric field
Acquisition mode	static	static	scanning
Detection	multiple collector (Faraday)	multiple collector (Faraday)	single collector (SEM)
Quantification	ID	ID/external	ID/external
Determable elements	elements with low first ionization potential (P-TIMS)	all elements	all elements
Multi-element capability (simultaneous determination)	low (ca. 2 elements)	low (ca. 3-4 elements)	high (whole mass spectrum)
Matrix effects	negligible	negligible (ID)/low (RSF)	negligible (ID)/low (RSF)
Drift effects	negligible	negligible (ID)/low (RSF)	negligible (ID)/low (RSF)
Spectroscopic interferences	conditionally negligible	conditionally negligible	low (HR mode)
Time consumption	high	high	low
Limit of detection ($ng\ g^{-1}$ in rock)	very low (0.01)	very low (0.01-0.1)	low (0.1-10)
Mass fractionation	correctable	correctable	correctable
Reproducibility	very high (RSD $< 1\%$)	very high (RSD $< 1\%$)	high (RSD 1-3%)
Accuracy	very high (1-2%)	very high (1-2%)	high (2-4%)
Analytical uncertainty	very low (0.5-1%)	low (ca. 1% ID, 2-10% RSF)	low (1-2% ID, 2-3% RSF)

Applying an oxide correction to the data set and assuming a conservative uncertainty of 2% for oxide correction, the individual errors sum up to a provisional combined standard uncertainty of about 6%. This suggests that multi-element ID-SF-ICP-MS yields a two to three fold improvement of combined standard uncertainty compared to conventional multi-element techniques.

6.8 Comparison with other isotope dilution techniques

Table 5 summarizes the experiences with other ID techniques (ID-TIMS, ID-MC-ICP-MS) used in our laboratories at the MPI for Chemistry in Maniz. The overall performance of multi-element ID-SF-ICP-MS is comparable to TIMS and MC-ICP-MS although the accuracy and reproducibility are slightly better for TIMS and MC-ICP-MS. This small handicap of multi-element ID-SF-ICPMS is easily compensated by the unbeatable easy and fast sample preparation effort and by its multi-element capability.

7 Conclusions

Multi-element ID-SF-ICP-MS in combination with external standardization is an accurate and precise method for the determination of trace element concentrations in a wide range of geological materials. It provides an up to three fold better reproducibility than conventional ICP-MS techniques and a significant improvement in analysis time compared to ID-TIMS or ID-MC-ICMPS while maintaining multi-element capability and a high level of accuracy and precision. It is capable to overcome the major drawbacks of conventional ICP-MS (matrix effects, instrumental drift, poly-atomic interferences), it enhances machine time efficiency and it is fairly easy to use once the tracer/sample equilibration has been achieved.

Following the rules of method validation [Ellison et al., 2000] we have identified and evaluated the major components of uncertainty that are related to multi-element ID-ICP-MS. We have estimated the combined standard uncertainty of trace element concentrations that are determined by ID at 1 to 2%, and for all other elements at 2 to 3%.

The analysis of geological reference materials yielded an overall good accordance with published high quality reference values (relative deviation less than 4%). Most data of new USGS reference glasses agree with those of respective original reference materials within the combined standard uncertainty although we found a significant enrichment of U in BIR-1G (almost 300 %) compared to the original reference material.

Part II

Mantle end-members: the trace element conundrum

8 Introduction

On the basis of their isotopic composition White [1985] and Zindler and Hart [1986] classified ocean island basalts (OIB) into three isotopically different families or groups: HIMU (= high $^{238}U/^{204}Pb$) and two varieties of enriched mantle (EM-1 and EM-2; see Fig 16). Weaver [1991b] has argued that each of these isotopically different families has certain common trace element characteristics that distinguish them from one another and so substantiated this classification. Thus by the early 1990's an apparently coherent picture emerged, favoring recycling of oceanic crust (HIMU) and different types of sediment as the most plausible explanations for the isotope and trace element systematics in oceanic basalts ("pelagic" sediment for EM-1 and "terrigenous" sediment for EM-2). In the meantime, however, the global trace element database of OIB has more than quadrupled and the quality of the trace element data has improved significantly. Here, we reassess the global trace element systematics in oceanic basalts on the background of the isotope relationships observed in OIB using new high-quality trace element data for OIB from several key islands: St. Helena, Tristan da Cunha (referred to as Tristan in the following) and Gough, in addition to recent data from the literature. Our database includes data on more than 300 basalts from 15 ocean islands with major and trace element concentrations determined on the same samples (plus isotope data when available).

It will be shown here that HIMU basalts have very similar trace element compositions and likely derive from one common source reservoir. Despite the fact that there are some characteritics common to EM basalts in general, each suite of EM basalts has its unique trace element composition, which distinguishes it from any other suite of EM basalts. The trace element systematics of EM-type OIB therefore do not support grouping into two different types, EM-1 and EM-2, as suggested by the isotopic relationships, nor can any other grouping be identified. Is it justified, therefore, to maintain the distinction between only two types of EM basalts based on their isotopic characteristics only, or do the trace element systematics indicate that EM sources are best evaluated by considering each island chain/group individually? Moreover, how can sources with similar time-integrated parent/daughter ratios but apparently different trace element signatures be produced, and is it conceivable that such sources share a similar genetic origin? In other words, the general question that arises from this analysis of the trace element systematics in OIB is the following: How can the isotope and trace element systematics in oceanic basalts be reconciled?

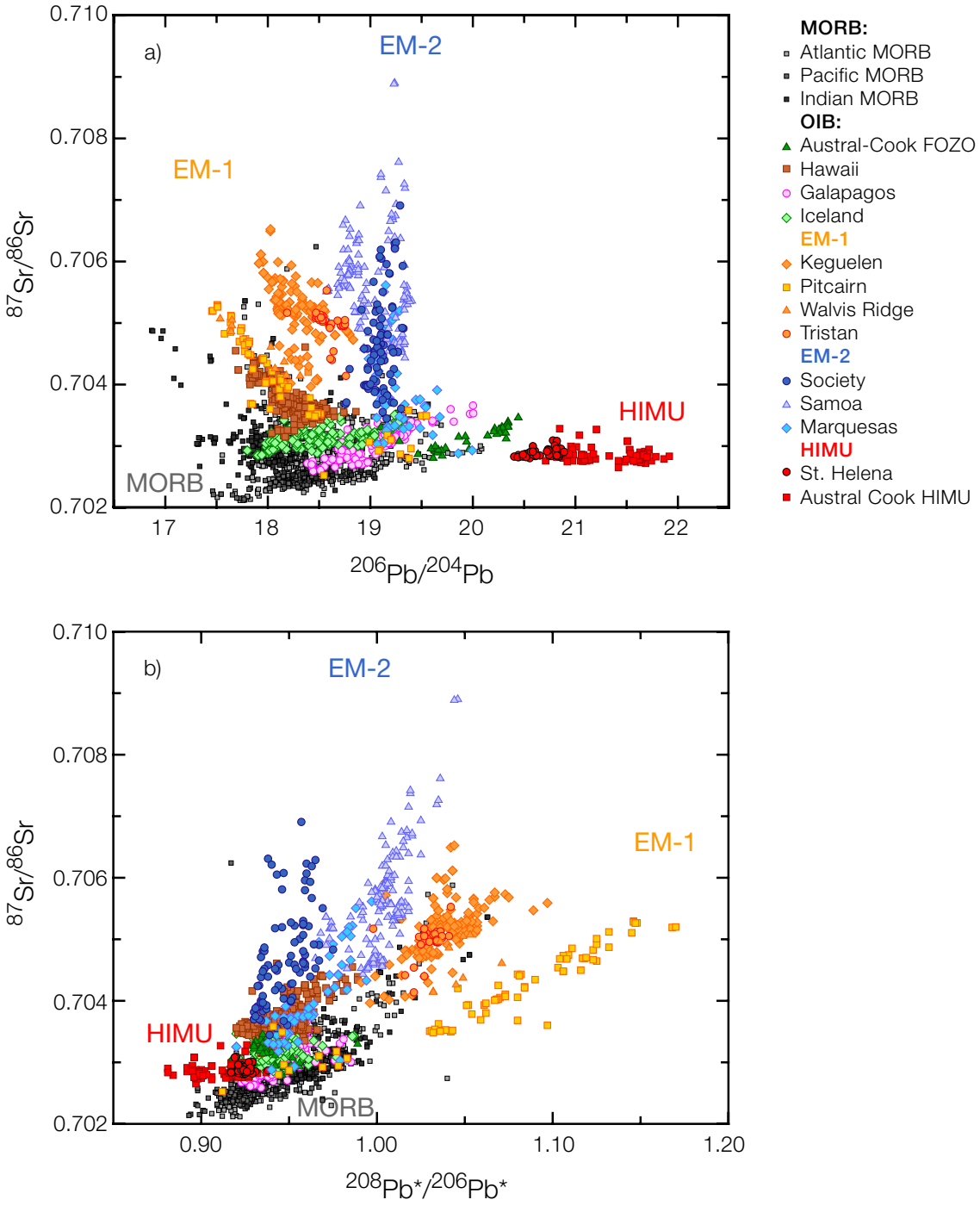

Figure 16: Mantle end-members as inferred from Sr and Pb isotope systematics. a) $^{87}Sr/^{86}Sr$ versus $^{206}Pb/^{204}Pb$ and b) $^{87}Sr/^{86}Sr$ versus $^{208}Pb^*/^{206}Pb^*$ [Galer and O'Nions, 1985]. HIMU basalts have high $^{206}Pb/^{204}Pb$ and low $^{208}Pb^*/^{206}Pb^*$, and $^{87}Sr/^{86}Sr$, whereas EM-1 basalts have low $^{206}Pb/^{204}Pb$, high $^{208}Pb^*/^{206}Pb^*$ and intermediate $^{87}Sr/^{86}Sr$ and EM-2 basalts have intermediate $^{206}Pb/^{204}Pb$, $^{208}Pb^*/^{206}Pb^*$, and high $^{87}Sr/^{86}Sr$. Data from GEOROC database (http://georoc.mpch-mainz.gwdg.de/georoc/).

9 Analytical techniques

New high-precision trace element data on OIB from the islands of St. Helena, Gough and Tristan in the Atlantic Ocean are presented in Appendix C and Appendix D. Major elements have been determined by XRF at the University of Mainz. Sr, Zr, Ba, Nd, Sm, Hf, Pb, and U concentrations have been measured by ID-SF-ICP-MS (see Part I) at the MPI for Chemistry, Mainz. The remaining trace element concentrations were determined by laser ablation (LA)-ICP-MS using a ThermoFinnigan ELEMENT2 mass spectrometer coupled to a New Wave UP-213 laser ablation system. LA-ICP-MS measurements were done on glass beads made from about 50 mg of sample powder using an electronically controlled Ir-strip heater [Jochum et al., 2004]. The NIST SRM 612 has been used for calibration. The MPI-DING reference glasses KL2-G and ML3B-G [Jochum et al., 2000] and the USGS reference material BHVO-1 have been used for quality assurance (Appendix E).

Conventionally, Ca is used as an internal standard element for LA-ICP-MS measurements. By using the eight trace elements previously determined by ID-ICP-MS (Sr, Zr, Ba, Nd, Sm, Hf, Pb, and U), an up to three-fold improvement in both, accuracy and reproducibility can be achieved compared to using Ca only. The reproducibility (as determined by 12 independent measurements of BHVO-1) is better than 2% (RSD) for all elements except for Rb and Th (both 3%, RSD) and Cs (4%, RSD). The accuracy, determined relative to literature data for BHVO-1 [Raczek et al., 2001; Jochum et al., 2001; Govindaraju, 1994], is better than 2% with the exception of Cs, Tb, and Ho (about 5%). The overall uncertainty of the determined concentrations, which, among others, includes uncertainty of measurement, sample heterogeneity, uncertainty of spike concentrations, and uncertainty of calibration factors, is less than 2% (RSD) for elements determined by ID (Sr, Zr, Ba, Nd, Sm, Hf, Pb, and U) and less than 5% (RSD) for all remaining lithophile elements (see also Part I, section 4).

10 The database

In addition to the newly determined data on samples from St. Helena, Tristan and Gough, the overall dataset includes data from ocean islands representing all major isotopic families (HIMU, EM-1 and EM-2). The additional data were taken from the GEOROC database (http://georoc.mpch-mainz.gwdg.de/georoc/). For the purpose of this study, the selected localities are restricted to those islands of each island group/chain that define the most extreme isotopic compositions (Fig. 16). HIMU basalts are from St. Helena in the Atlantic Ocean, and from the islands of Mangaia, Tubuai, and Rururtu (young and old series lavas) of the Cook-Austral chain. EM-1 basalts are from Pitcairn Island, in addition to our new

data for samples from Gough and Tristan. EM-2 basalts are from the Marquesas (Tahuata and Ua Pou), and the Samoan (Malumalu and Savaii, including its post-erosional (PE) suite) and Society Islands (Tahaa, Moorea, and Hauhine). In addition, samples from the Azores (Sao Miguel) are included.

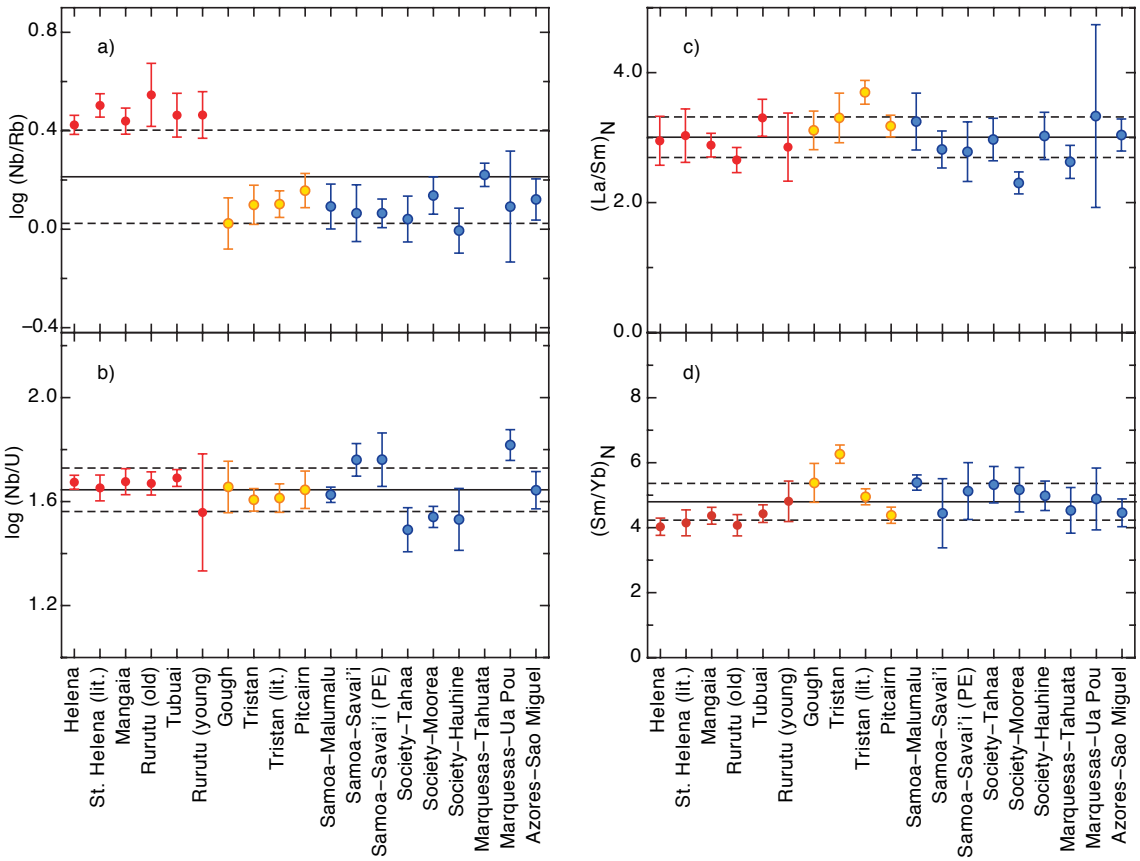

Figure 17: Averages and standard deviations (1σ) of a) log(Nb/Rb) and b) log(Nb/U) ratios and of average CI normalized c) La/Sm and d) Sm/Yb ratios for individual islands. Note that due to the log-normal distribution of very incompatible elements (VICE) [Ahrens, 1954] all averages and standard deviations of ratios of VICE are calculated from log values in order to obtain a normal distribution of the data sets. Although the absolute Nb/Rb ratios are different from island to island the variation within each suite is <10% indicating freshness of samples. Nb/U values of all islands are close to the 'canonical' value of 47 (corresponding to log 47 = 1.67) for oceanic basalts [Hofmann et al., 1986]. All island suites have comparable and high La/Sm (2.99 ± 0.3) and Sm/Yb ratios (4.79 ± 0.56) indicating that all OIB have been produced by comparable degrees of partial melting in the garnet-stability field. Normalizing values from Anders and Grevesse [1989].

All samples are alkaline rocks belonging to the alkali-olivine-basalts series [Irvine and Baragar, 1971]. For each individual island, samples were screened to exclude highly differentiated samples. In general, the cut-off is chosen at a sharp decrease in CaO, FeO, and TiO_2 and increase in SiO_2 and Na_2O concentrations with decreasing MgO. As a re-

sult, only samples containing more than 4-5 wt.% MgO are included in the final dataset. Selected samples include only samples with major and trace elements determined on the same sample (with the exception of some of the Society samples). The entire dataset was further screened to exclude altered samples by investigating ratios of fluid-mobile (e.g. Rb, K, U) and fluid-immobile elements (e.g. Th, Nb). The absolute Nb/Rb ratios, for example, vary from island to island, whereas the total range in Nb/Rb within one individual suite is small (<10%; Fig. 17). The average Nb/U ratios in samples from individual islands agree within error with the overall average value of 44.8. Note that this value is close to the 'canonical' value of 47 for oceanic basalts [Hofmann et al., 1986]. This coherent behavior of fluid-mobile and fluid-immobile elements suggests that alteration effects in the samples from the entire dataset are relatively insignificant.

In addition to alteration effects, different extents of partial melting and/or fractional crystallization may obscure the source characteristics. Whereas the rare-earth element (REE) abundances are a good proxy for the extent of crystal fractionation, La/Sm ratios are a sensitive indicator for the degree of melting. The chemistry of most of the samples investigated here is mainly influenced by fractionation of olivine and clinopyroxene. Unless more than 30% of clinopyroxene have fractionated, La/Sm ratios are not significantly affected by crystal fractionation (e.g., less than 10% deviation of La/Sm from the assumed initial ratio). At low degrees of melting (F = 0.01), however, La can be enriched up to eight-fold over Sm compared to the source values, but is only little fractionated from Sm at higher degrees of melting (F > 0.3). The uniformly high La/Sm ratios from different islands indicates that all suites have undergone low, but similar degrees of melting (Fig. 17) and/or that all OIB derive from sources with similar La/Sm. It is therefore expected that differences in trace element ratios due to differences in degree of partial melting are of minor importance (especially for elements that are more incompatible than La).

Very incompatible elements (VICE; bulk distribution coefficients, D $\ll$ 1) are almost quantitatively removed from the source after only a few percent of melting (< 3-5%). The ratios between such highly incompatible elements are thus equivalent to those in their sources. The relative compatibility difference between two elements can be tested using log-log plots of trace element concentrations [Hofmann, 2004]. If the concentrations of two elements A and B are related by a function $f(x, y)$, which accounts for partial melting (x) and fractional crystallization (y) effects, then

$$A = f(x, y) \times B \tag{10}$$

$$\log A = \log f(x, y) + \log B \tag{11}$$

For the special case where the abundances of A and B do not (or only to a small extent) depend on the degree of melting and/or fractional crystallization, $\log f(x, y)$ is a constant

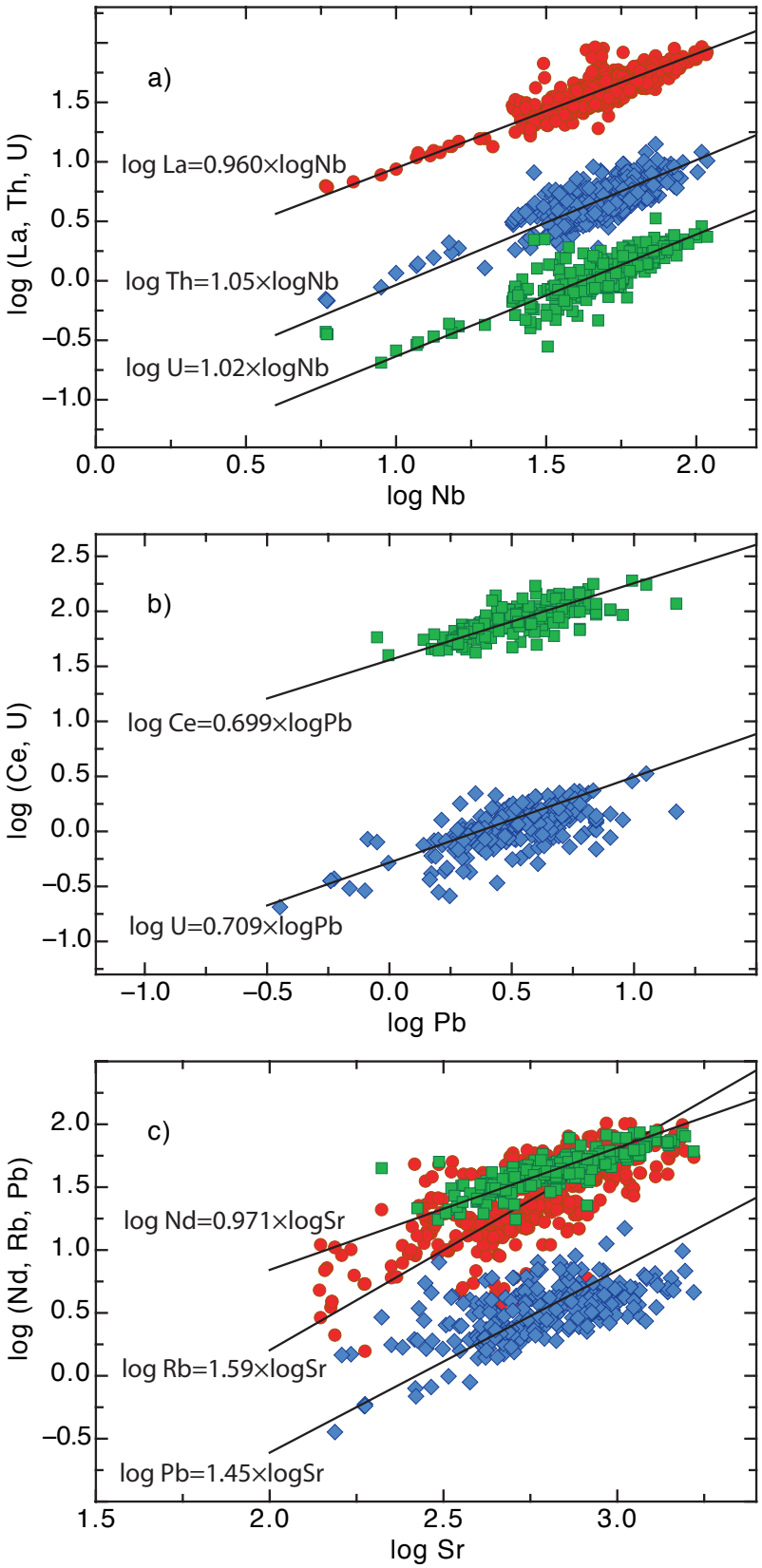

Figure 18: Log-log plots of concentrations of a) Nb versus La, Th, and U, b) Pb versus Ce, and U, and c) Sr versus Nd, Rb, Pb. Correlations of very incompatible elements (a) and Sr-Nd (c) have a slope of close to unity suggesting that these elements are not fractionated during partial melting. To some degree this is also valid for other, more compatible elements (b, c). See text for discussion.

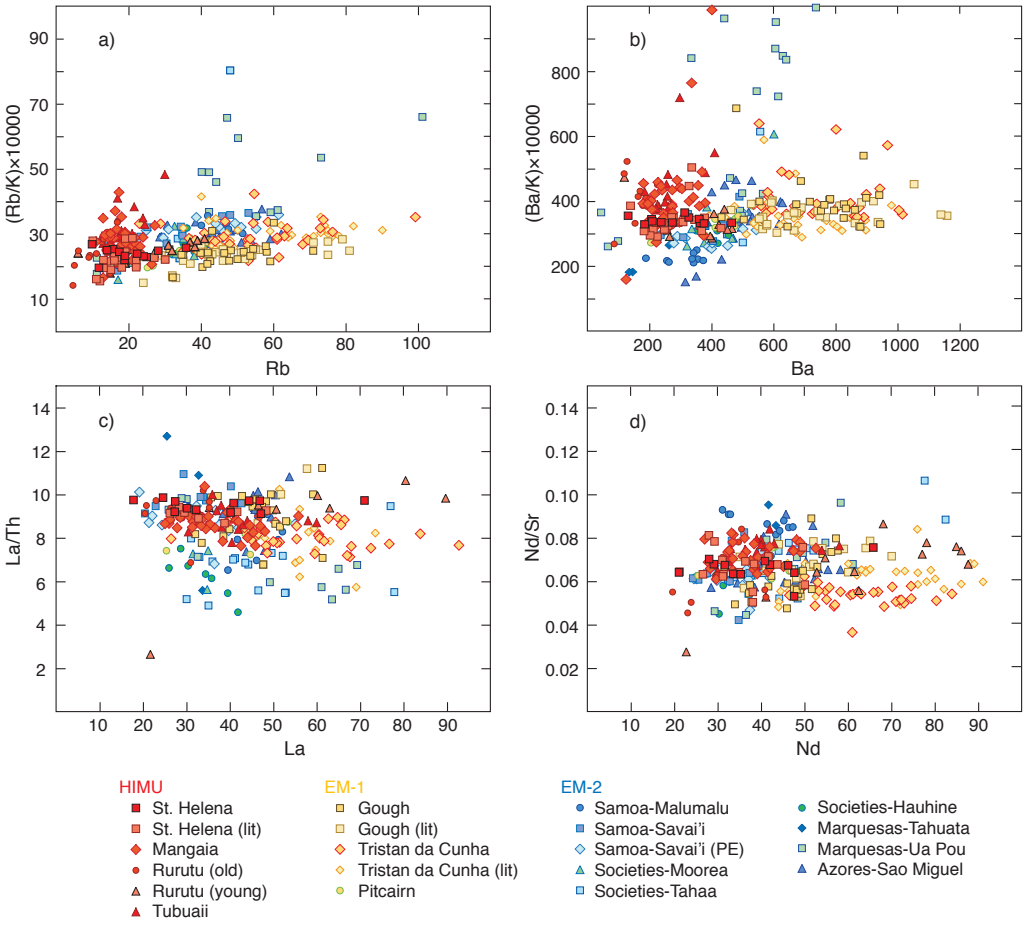

Figure 19: Data of ocean island basalts in a) Rb/K versus Rb, b) Ba/K versus Ba, c) La/Th versus La, and d) Nd/Sr versus Nd space. Ratios of Rb, Ba, K, and La/Th, Nd/Sr are rather uniform and do not vary with absolute concentrations indicating that these ratios are source characteristics that are common to all OIB-suites.

and Eq. 11 is a linear function with a slope of unity [Hofmann, 2004]. Fig. 18 shows log-log plots for some VICE. Nb-La, Nb-Th, Nb-U (Fig. 18a), and Sr-Nd relations (Fig. 18b) have a slope close to unity, whereas Pb-U, Pb-Ce, Sr-Rb and Sr-Pb (Fig. 18b and c) can deviate up to 50% from unity. Similar exercises involving other VICE (Rb, Ba, Th, U, Nb, Ta, K, La) also yield a slope close to unity. This confirms that for the VICE fractionation during partial melting and/or fractional crystallization is indeed relatively insignificant. These elements are therefore expected to provide reliable information about the composition of their mantle sources. To a lesser degree this also holds for some element pairs with larger compatibility differences (e.g., U-Pb, Rb-Sr, Ce-Pb; see Fig. 18b and c).

11 Trace element characteristics of OIB and their sources

11.1 Common characteristics to all OIB

All OIB investigated in this study have subparallel rare-earth element (REE) patterns and are enriched in light REE (LREE) relative to average CI chondrite and 'primitive upper mantle' (PUM; Appendix F). All samples are depleted in heavy REE (HREE) relative to middle REE and LREE (Fig. 17) suggesting that melting is dominated by melting in the garnet stability field. The ratios between the alkali and earth alkali elements Ba, Rb, K and the La/Th and Sr/Nd ratios are similar in all OIB (Fig. 19). Note that although the absolute concentration of the denominator elements vary by up to a factor of 5 within each suite, all suites plot in a narrow range of Rb/K, Ba/K, and La/Th and Sr/Nd ratios (with the exception of some samples from Ua Pou (Marquesas); Fig. 19).

Similar Ba-Rb-K ratios (and similar Ba, Rb, and K abundances in HIMU basalts) might be due to buffering of Rb, Ba, and K by residual hydrous phases during partial melting (e.g., Hart [1988]; Sun and McDonough [1989]). In the presence of accessory residual phases such as phlogopite or amphibole, cogenetic suites should have uniform Rb/Nb, Ba/Nb K/Nb ratios as well as uniform Nb abundances because of the high partition coefficients for these elements in phlogopite and amphibole (Kd (Rb, Ba, Nb) > 1 in phlogopite, Kd (Rb, Ba, Nb) $= 0.4$ to 0.8 in amphibole). HIMU-type OIB have remarkably similar Rb/Nb and Ba/Nb ratios (Fig. 20a), but have a large variation in Nb abundances. In all other OIB, Rb/Nb, Ba/Nb, and K/Nb ratios and Nb abundances are highly variable. Note that HIMU-type OIB also define a narrow range in La/Th-Rb/Th space (Fig. 20b). Since La/Th and Rb/Th are element pairs that are fractionated by melting in the presence of residual phlogopite and/or amphibole, the alkali and alkali earth element (plus Nb and Th) systematics show that hydrous phases such as phlogopite and amphibole do not have a major influence on the composition of the erupted melts, i.e. these phases cannot be residual phases during partial melting (see also Hofmann et al. [1984]), even for the low degrees of melting commonly attributed to OIB. As a corollary, titanite minerals (which may buffer Nb, Ta, and Ti abundances in the melt) are not residual phases during melting [Sun and McDonough, 1989] which is confirmed by the small range of and nearly chondiritc Ti/Eu ratios in all OIB (not shown; total average is 7080 ± 540; chondritic value is 7790 [Anders and Grevesse, 1989]).

Relatively uniform Nd/Sr ratios in all OIB (Fig. 19d) are a feature that is expected from both the linear mixing trends in Sr-Nd isotope space (see, for example, Hart [1988]) and the similar compatibility of Sr and Nd during OIB melting (Fig. 19c). Similar Sr/Nd ratios of OIB sources, however, can only be preserved in case plagioclase fractionation

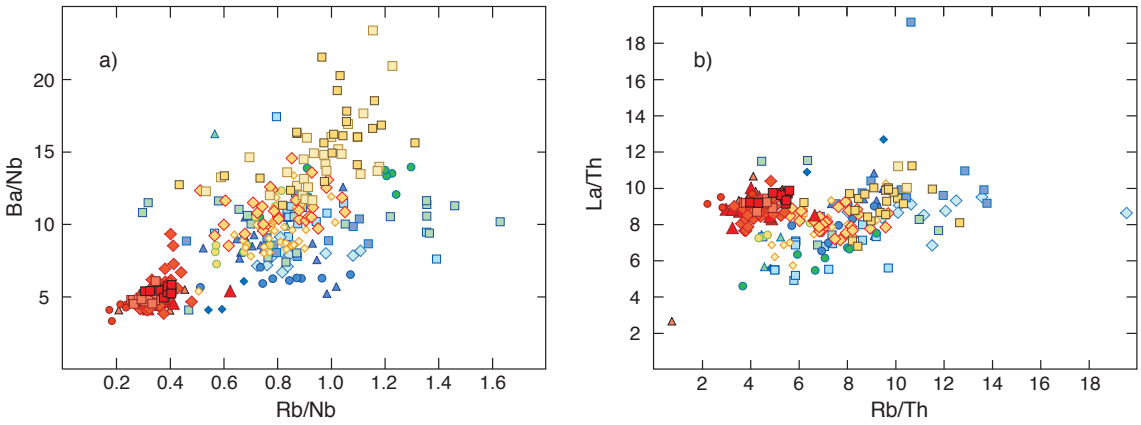

Figure 20: Data of ocean island basalts in a) Ba/Nb versus Rb/Nb, and b) La/Th versus Rb/Th space. Data of HIMU-type OIB are rather uniform with respect to Ba-Rb-Nb systematics but also with respect to Rb-La-Th ratios suggesting that their sources rather have uniform compositions with respect to VICE systematics than contain residual hydrous phases. Ba/Nb and Rb/Nb ratios are lower in HIM-type suites than in EM-type suites indicating that the source of HIMU-type OIB is enriched in Nb (Ta) relative to other very incompatible elements (VICE). Symbols as in Fig. 19. See text for discussion.

during magma evolution is negligible. The small range in Sr/Nd in all OIB (Fig. 19d) therefore not only confirms that the investigated samples are not significantly affected by plagioclase fractionation, they also confirm that the OIB investigated here are formed by similar degrees of melting of sources with similar Sr/Nd ratios.

On the background of the similar degrees of melting, the relatively uniform La/Th ratios in all investigated OIB (Fig. 20b) indicate that although VICE/LREE ratios in general can be highly variable, La and Th represent a common anchor for LREE-VICE depletion/enrichment patterns in all OIB sources.

11.2 HIMU-type OIB

Our new data compilation shows that HIMU basalts from different localities have remarkably similar trace element compositions (Appendix F). All HIMU basalts are enriched in Nb and Ta (Fig. 20a) relative to Ba and Rb and are overall depleted in Pb (Fig. 21a), Rb and Ba (Fig. 21b) relative to EM-type OIB. HIMU basalts also have the lowest Rb/Sr ratios of all OIB (Fig. 21c). Although Fig. 18c suggests that the Rb/Sr ratios are likely to be disturbed by partial melting and/or fractional crystallization processes, the Rb/Sr ratios in HIMU-type OIB are remarkably similar over a wide range of Sr concentrations (Fig. 21c). In combination with their relatively constant $^{87}Sr/^{86}Sr$ ratios (Fig. 16), this implies that all HIMU-type OIB sources have similar Rb/Sr ratios.

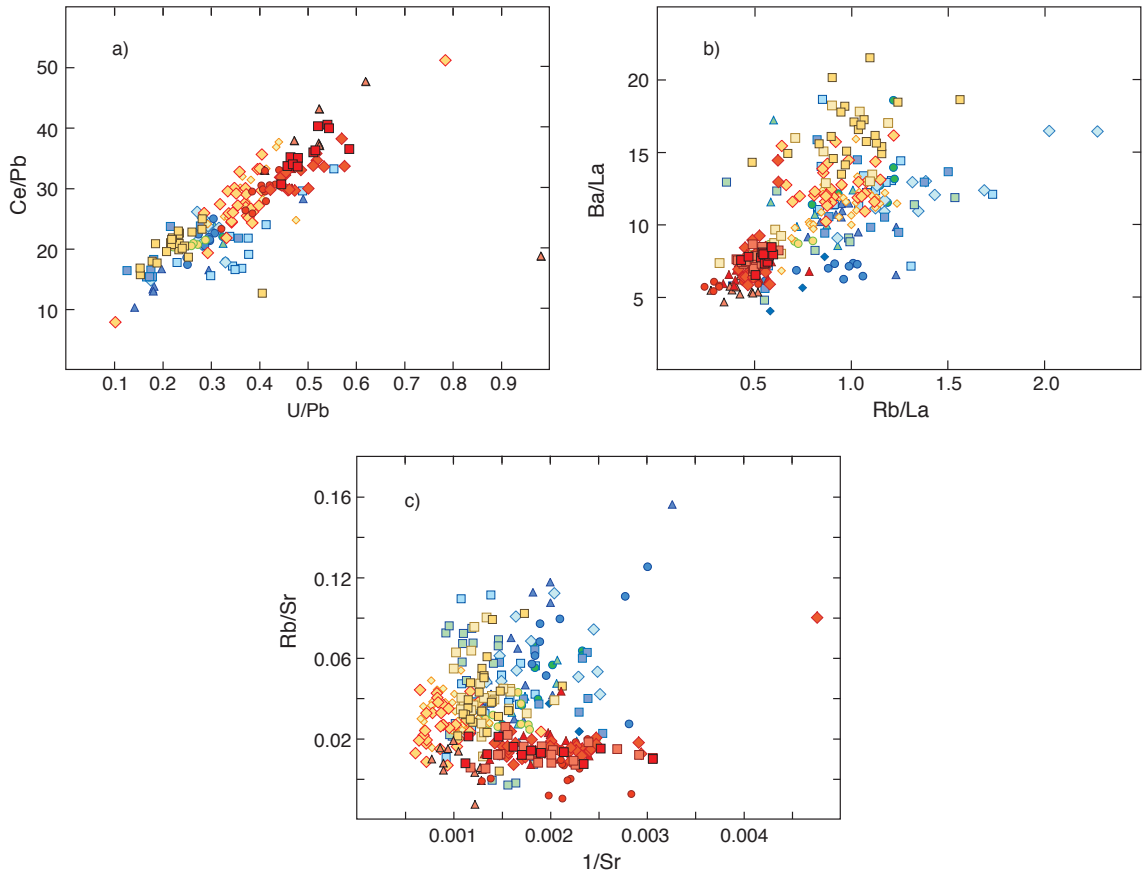

Figure 21: Data of ocean island basalts in a) Ce/Pb versus U/Pb, b) Ba/La versus Rb/La, and c) Rb/Sr versus 1/Sr space. High Ce/Pb and U/Pb and low Ba/La and Rb/La ratios indicate that HIMU-type OIB are more depleted in Pb, Ba, and Rb than EM-type OIB. HIMU-type OIB have consistently lower Rb/Sr ratios than in EM-type OIB. Symbols as in Fig. 19.

The decrease in normalized concentrations from Nb to Cs is a unique feature of HIMU basalts that distinguishes them from all EM basalts (Appendix F). We have previously inferred that all OIB result from low degrees of melting in the presence of residual garnet. Estimated trace element abundances in the source of an average St. Helena basalt (Fig. 22a), calculated assuming fractional batch melting (see also Hofmann and White [1982]), are shown in Fig. 22b. Different degrees of melting or different assumptions concerning the modal composition of the source (garnet-peridotite or eclogite) or the used partition coefficients affect both the absolute concentrations of the HIMU source and the relative fractionation between some trace elements [Stracke et al., 1999].

The use of four different sets of recently published partition coefficients (Fig. 22c; Kelemen et al. [2003], Stracke et al. [2003], Workman et al. [2004], Salters and Stracke [2004]), however, does not obliterate the general outcome of these source models and we

have therefore used the average of all four sets for our calculations. Despite the remaining uncertainties, some general inferences about the composition of the HIMU sources are possible: The HIMU source must be depleted in Cs, Rb, Ba, Th and U and enriched in most other elements with respect to Bulk Earth. In addition, the LREE must be depleted relative to the HREE. As a consequence, the HIMU source is characterized by VICE/REE and Rb/Sr ratios lower than, and by Sm/Nd ratios higher than Bulk Earth. These conclusions are consistent with the low Ba/La, Rb/La, and Rb/Sr ratios (Fig. 21) and the Sr-Nd isotope systematics in HIMU basalts ($^{87}Sr/^{86}Sr$ lower than and $^{143}Nd/^{144}Nd$ higher than Bulk Earth), and hold even for different modal compositions of the source (eclogite and garnet-peridotite) and for degrees of melting up to 20% (Fig. 22b).

11.3 EM-type OIB

EM basalts are characterized by large variations in trace element ratios, both within and between samples from individual localities. Some trace element characteristics are common to all EM-type OIB and clearly distinguish them from HIMU-type basalts. As shown earlier, the La/Th and La/Sm ratios are relatively constant in all OIB. Trace element ratios with La as the denominator element should thus be a good tool to show the relative enrichments and depletions of trace elements in different OIB suites. Similar systematics are obtained using Th as a denominator element, which verifies the success of this approach (compare Figs. 23d and 24f). Exceptions are the samples from the Societies (Tahaa, Moorea, Hauhine) that have higher Th/La than all other OIB (Fig. 23a), which is probably related to elevated Th concentrations in the samples from the Societies (note that their La/Sm ratios lie well within the range of $(La/Sm)_N$ in all other OIB; Fig. 17).

The consistently low U/Th ratios in EM compared to HIMU-type OIB are perhaps the most conspicuous general feature of the EM-type signature in OIB (Fig. 24f). The Sao Miguel suite, however, is exceptional, since it is the only EM-type suite with HIMU-like U/Th ratios. The higher Rb/La, Rb/Th, Ba/La, Ba/Th and K/La ratios further suggest enrichment of Rb, Ba, and K in EM compared to HIMU basalts (Fig. 23). The consistently and uniformly high Rb/La and Rb/Th ratios in all EM-type basalts confirm that this is indeed the case for Rb. There are, however, some exceptions to the rule for Ba and K, since some EM-type suites (Samoa-Malumalu, Marqueses-Tahuata and Ua Pou) have, on average, Ba/La and K/La ratios as low as HIMU basalts. In general, EM-type OIB are also depleted in Nb (Ta) relative to HIMU-type OIB, as indicated by their lower Nb/La (Fig. 23e) and Nb/Th ratios (not shown). An exception are the Samoa-Savaii and Savaii post-erosional (PE) samples with low REE and Th concentrations, which cause their elevated Nb/La and Nb/Th ratios (see Appendix F and also Figs. 11 and 12 in Workman et al. [2004]).

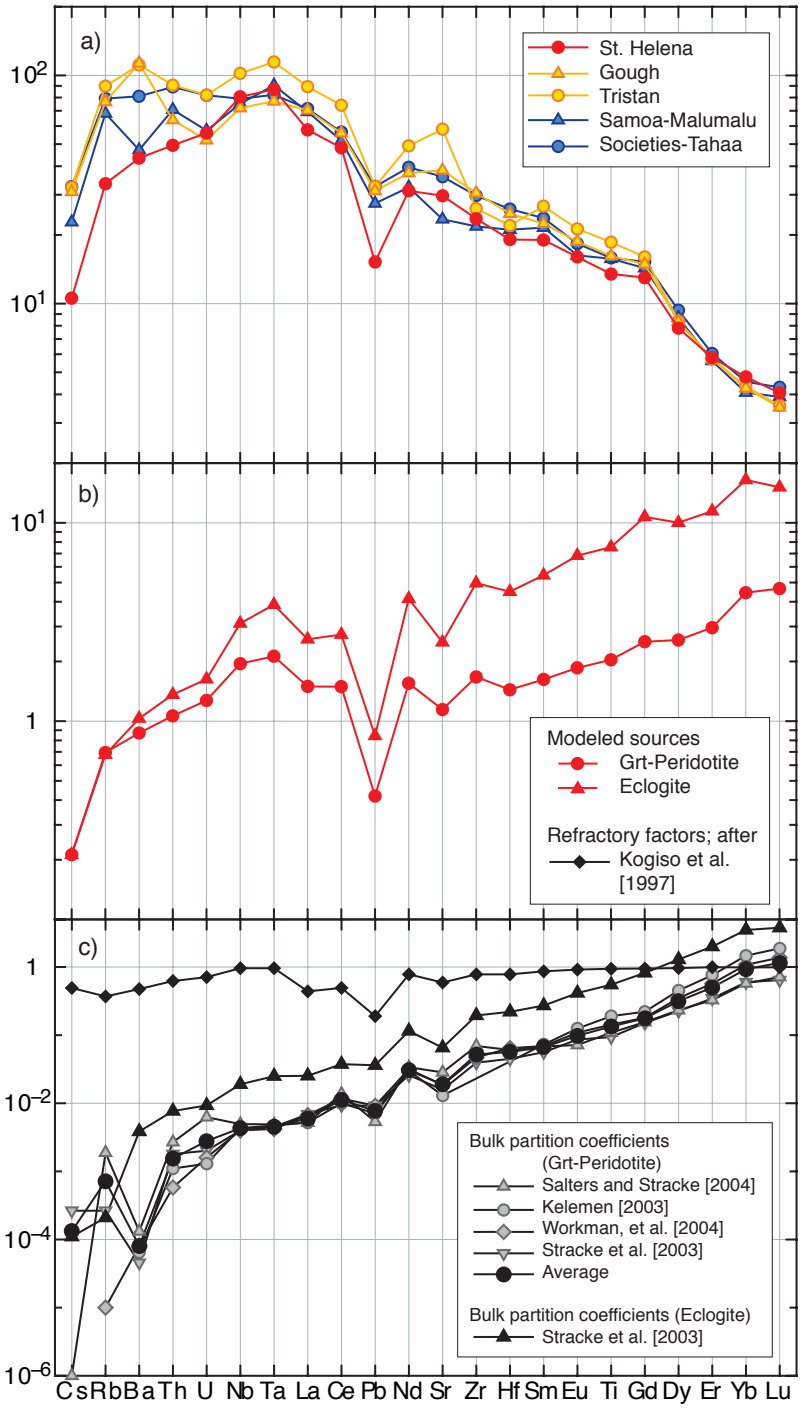

Figure 22: Modeled source of HIMU-type OIB (St. Helena). a) Average trace element composition of St. Helena, Gough, Tristan, Samoa-Malumalu, and Societies-Tahaa basalts. b) Inferred source composition of average St. Helena basalt calculated by assuming 2% batch melting of a eclogite and garnet-peridotite source using the average of partition coefficients shown in c). c) Compilation and average of literature bulk partition coefficients for garnet-pyroxenite using data from Kelemen et al. [2003], Stracke et al. [2003], Workman et al. [2004], and Salters and Stracke [2004]. Also shown are the alteration factors in a fluid-rock system [Kogiso et al., 1997]. Note that the fluid-rock mobility factors have been converted to 'refractory factors' (= 1-mobility factor) and reflect the fraction that is retained in the source. Although the absolute values differ, increasing compatibility towards heavy REE and depletions in Pb and Sr relative to Nd are common to all data sets. Independent of the melting model, the HIMU source is depleted in very incompatible elements (VICE) and light REE relative to heavy REE. Note that inversion modeling by partial melting produces smooth patterns of VICE and negative anomalies for Pb and Sr and positive anomalies for Nb and Ta in the source. Thus, the trace element pattern of the calculated source is inconsistent with a pure magmatic evolution. Comparison with rock-fluid alteration factors (after Kogiso et al. [1997]) suggests that the HIMU source must have experienced fluid-rock interaction during its evolution.

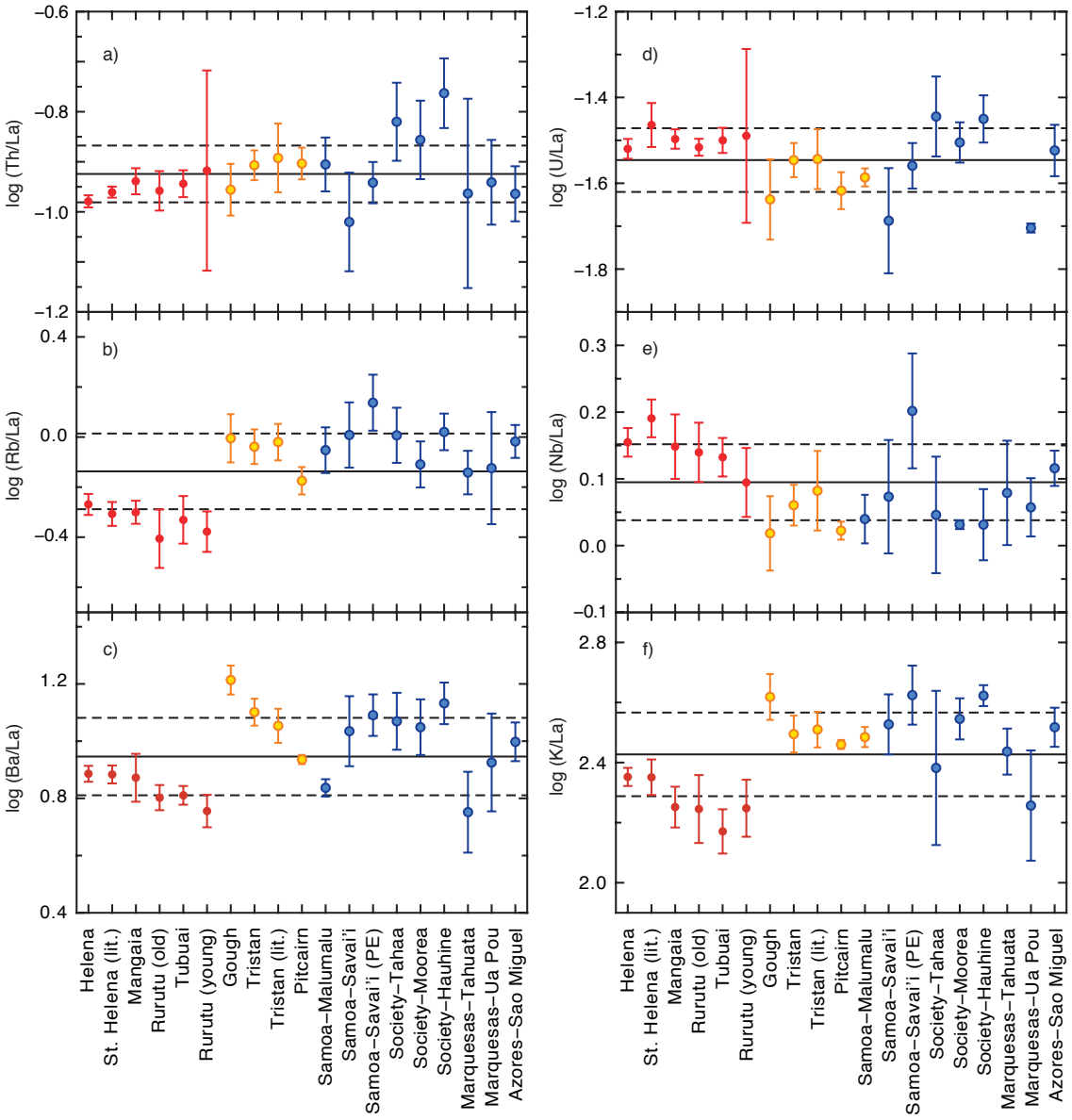

Figure 23: Averages and standard deviations (1σ) of log (VICE) / log (La) ratios for individual island suites. Note that HIMU-type islands (St. Helena, Mangaia, Rurutu (old/young), and Tubuaii) are distinct in their ratios relative to EM-type OIB (with the exception of Th/La) indicating different source compositions. Each EM-type suite (all others) owns a unique signature that is different to those of any other suite and thus do not allow unambiguous discrimination between EM-1 (yellow symbols) and EM-2-type OIB (blue symbols).

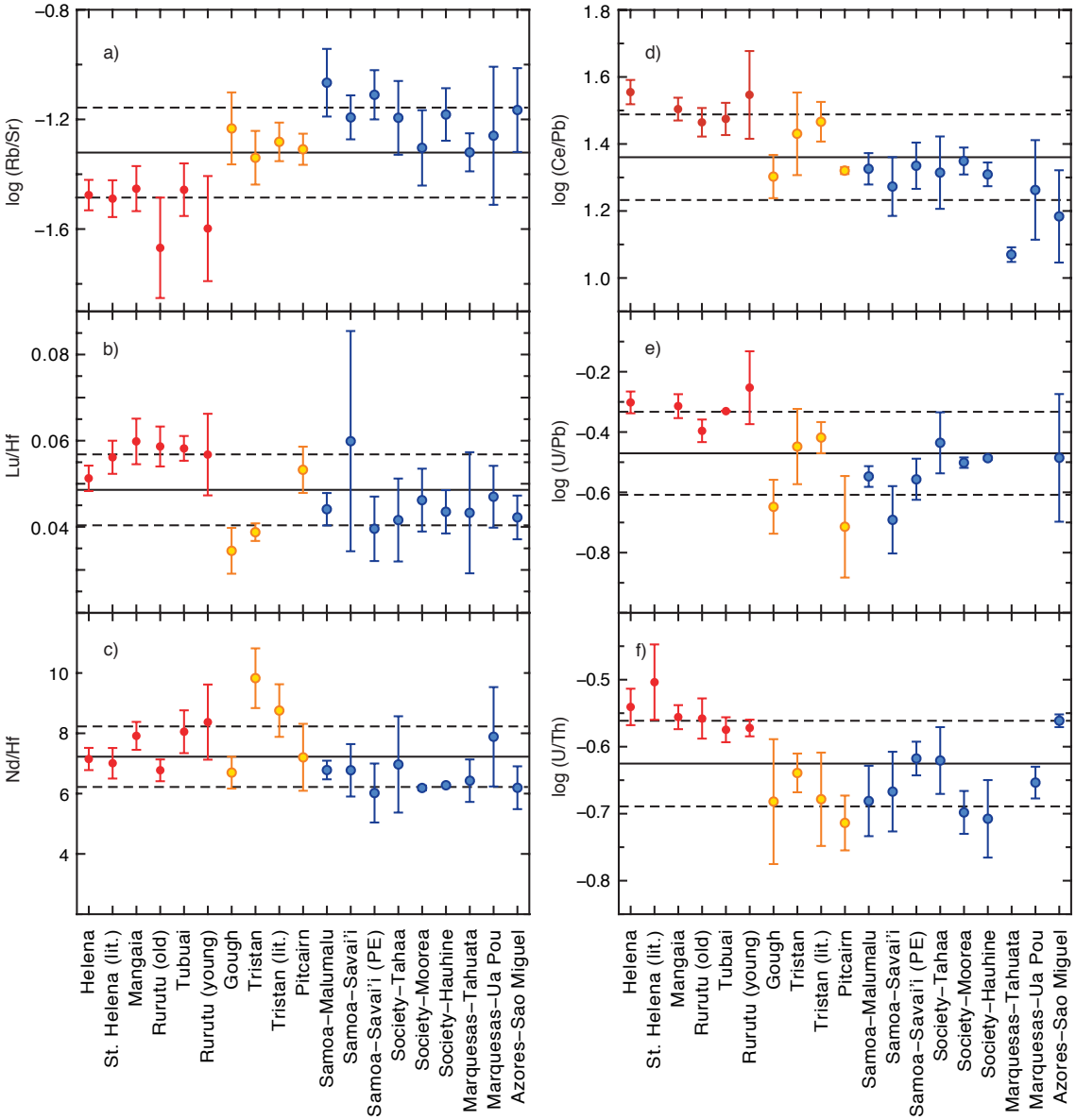

Figure 24: Averages and standard deviations (1σ) of log of parent/daughter ratios of Sr, Pb, and Hf isotope decay systems as well as log (Ce/Pb), log (U/Th), and Nd/Hf ratios for individual island suites. EM-type suites have higher Rb/Sr, and lower Lu/Hf, U/Pb, Ce/Pb ratios compared to HIMU-type suites. Note that EM-type OIB have consistently lower U/Th ratios compared to HIMU-type OIB (see text for discussion).

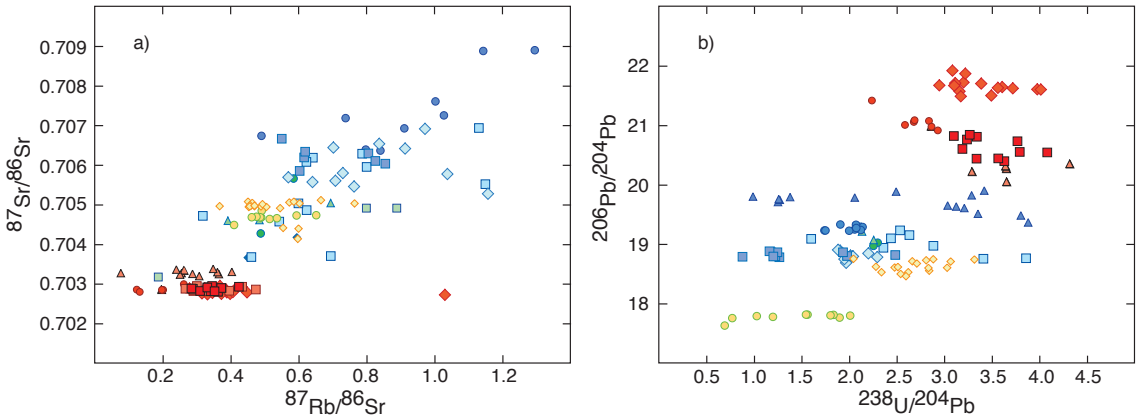

Figure 25: $^{87}Sr/^{86}Sr$ and $^{206}Pb/^{204}Pb$ isotopes versus respective parent/daughter ratios in ocean island basalts. a) $^{87}Sr/^{86}Sr$ versus $^{87}Rb/^{86}Sr$; b) $^{206}Pb/^{204}Pb$ versus $^{238}U/^{204}Pb$. Despite the large variations in parent/daughter ratios caused by fractionation effects, EM-type OIB have higher $^{87}Rb/^{86}Sr$ and lower $^{238}U/^{204}Pb$, consistent with higher $^{87}Sr/^{86}Sr$ and lower $^{206}Pb/^{204}Pb$. The positive correlations further suggest that variations in $^{87}Sr/^{86}Sr$ and $^{206}Pb/^{204}Pb$ between different OIB are the result of systematic variations of $^{87}Rb/^{86}Sr$ and $^{238}U/^{204}Pb$ of different sources and are not caused by different source ages. Symbols as in Fig. 19.

As shown previously, some ratios of highly and moderately incompatible trace elements are little disturbed by partial melting or crystallization (Fig. 18b and c) and so allow further characterization of EM-type OIB (and their sources). Ce/Pb and U/Pb ratios, for example, are generally lower in EM compared to HIMU-basalts (Fig. 24d and e); a feature that is probably related to, on average, higher Pb abundances in EM relative to HIMU basalts (Fig. 21). Exceptions are the samples from Tristan that have slightly elevated Ce/Pb and U/Pb ratios compared to all other EM-type suites. This might be caused by larger relative fractionation of U-Pb (Ce-Pb) in the Tristan samples due to slightly lower degrees of partial melting compared to all other OIB (note that the Tristan samples have the highest La/Sm and Sm/Yb ratios of all OIB in Fig. 17), or, alternatively, by a slightly different source composition. EM-type suites have consistently lower Lu/Hf but comparable Nd/Hf ratios with regard to HIMU-type OIB. Most likely, fractionation during partial melting and/or crystallization is also responsible for some of the scatter of the parent-daughter ratios Rb/Sr, Lu/Hf, U/Pb and also the Ce/Pb ratios (Fig. 24). However, a rough positive trend in $^{238}U/^{204}Pb$ versus $^{206}Pb/^{204}Pb$ and $^{87}Rb/^{86}Sr$ versus $^{87}Sr/^{86}Sr$ space (Fig. 25) is in good agreement with the isotope systematics, which indicates that the HIMU sources developed with higher $^{238}U/^{204}Pb$ and lower $^{87}Rb/^{86}Sr$ than the EM sources.

In summary, EM basalts in general are characterized by lower U/Th ratios, enrichment in Rb, Ba, K and Pb and depletion in Nb and Ta relative to HIMU basalts. The variations

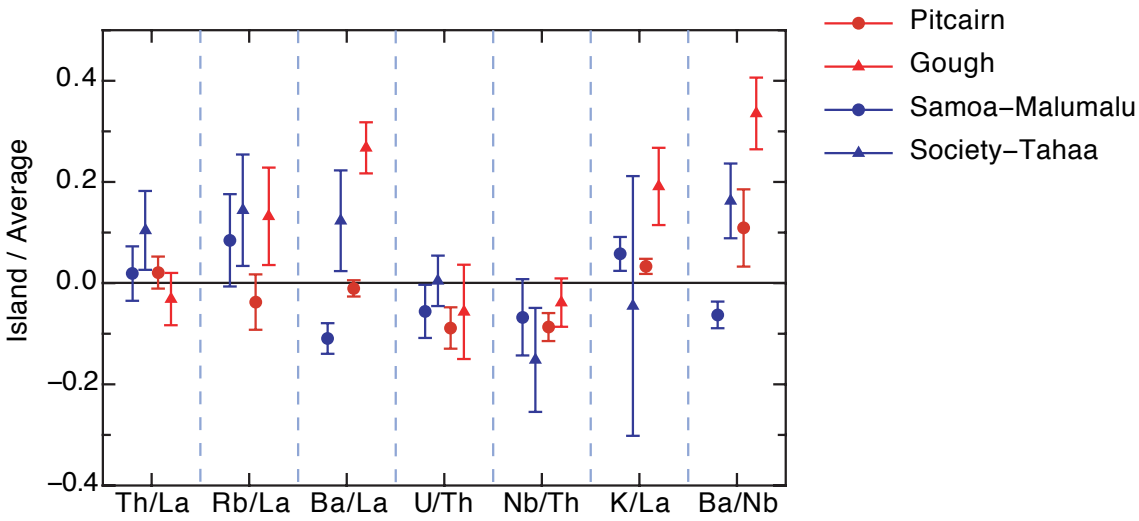

Figure 26: Comparison of trace element ratios of EM1-type (Pitcairn, Gough) and EM2-type (Samoa-Malumalu, Society-Tahaa) suites normalized to mean value of all suites (HIMU-, EM1-, and EM2-type, see Figs. 23 and 24). Also shown are the variations of respective ratios within each suite (1σ). The islands have been chosen because of the most extreme isotopic composition of their samples. None of the trace element ratio is unambiguously indicative for either EM-1 or EM-2. The same observation is made using different element ratios of VICE.

in Th/La, Rb/La, Ba/La, U/Th, Nb/Th, K/La, and Ba/Nb in four of the isotopically most extreme EM-1 and EM-2 localities (Fig. 26; Pitcairn and Gough for EM-1, and Samoa-Malumalu and Society-Tahaa for EM-2) show no systematic enrichment or depletion of individual highly incompatible elements (Rb, Ba, Th, U, Nb, Ta, K, La) or ratios thereof, which is typical for either EM-1 or EM-2 sources. Ba/Nb ratios, in particular, have often been used to discriminate between EM-1 and EM-2 basalts. Previously, Weaver [1991a] and Weaver [1991b] have argued that high Ba abundances (high Ba/Nb, Ba/Th, Ba/La ratios) and high Th/Nb and Th/La ratios are typical for EM-1 basalts, and absent in EM-2 basalts. With the more comprehensive dataset used here, however, systematic differences between the Th/La, Th/Nb, and especially the Ba/Nb ratios in EM-1 and EM-2 basalts, cannot be confirmed. The highest and lowest Ba/Nb ratios are found in both, EM-1 and EM-2 basalts. Samples from Gough and Society-Tahaa have the highest, and samples from Pitcairn and Samoa-Malumalu have the lowest Ba/Nb ratios, respectively (Fig. 26). Similar observations are made if this type of analysis is extended to other trace element ratios. Rather, each suite of EM-type OIB appears to have its own unique VICE signature that is different from those of any other suite of EM basalts. Thus, on the basis of the comprehensive dataset used here, EM-like OIB cannot be grouped into EM-1 and EM-2, nor can any other grouping be identified.

Similar to the HIMU source, the likely concentrations in EM sources can be inferred from the melt concentrations using partial melting models with reasonable assumptions for bulk partition coefficients and the degree of partial melting. Calculated sources derived from the average concentrations in four EM-type suites (Gough, Pitcairn, Samoa-Malumalu, and Society-Tahaa) are given in Fig. 27. Despite the large variability of trace element abundances in the EM-type melts and their corresponding sources (see also discussion above), there are some general features common to all calculated EM-type sources. Similar to the HIMU sources, EM sources are enriched relative to Bulk Earth, but depleted in LREE and VICE relative to HREE. Pb and Sr are also depleted relative to neighboring elements (e.g., Ce, Nd). These findings are almost independent of the assumed mineralogical composition of the source (garnet-peridotite or eclogite) and hold for degrees of melting up to 10%. In contrast to HIMU sources, however, U is consistently depleted in EM-type sources relative to Th although the relative fractionation of elements between Nb and Ba (Rb) for different EM sources does not follow a coherent pattern (see discussion above).

12 Implications for the origin of OIB source compositions

12.1 The nature of the HIMU source

The apparent depletion of the most incompatible elements (Cs-U) and the enrichment of most other trace elements in HIMU sources with respect to Bulk Earth suggest that the HIMU sources are most likely produced by melting VICE and LREE depleted precursors. Although mid-ocean ridge basalts (MORB) display a large compositional variety ranging from depleted to enriched REE patterns [Hofmann, 2004], melting of the depleted mantle is the only known process that yields large volumes of incompatible element enriched (with respect to Bulk Earth), but VICE and light REE depleted rocks (i.e. MORB). The smooth trace element patterns in MORB fit the smooth normalized trace element patterns from Rb to U and between REE of the calculated HIMU source (Fig. 22).

Some observations, however, are inconsistent with a pure magmatic evolution (single or multi-stage) of HIMU sources. Pb and Sr are depleted whereas Nb and Ta are enriched to a degree that is hard to reconcile with partial melting alone. Bulk partition coefficient ratios (see Fig. 22b) indicate that Nb and Ta are hardly fractionated from neighboring elements (e.g., U, La) and bulk partition coefficients for Pb and Sr are slightly lower than those of Nd. Thus no enrichment of Nb and Ta relative to U and La and slight enrichment of Pb and Sr relative to Nd would be expected in derivative melts. Retention of elements during fluid-rock exchange (Fig. 22b; [Kogiso et al., 1997]), on the other hand,

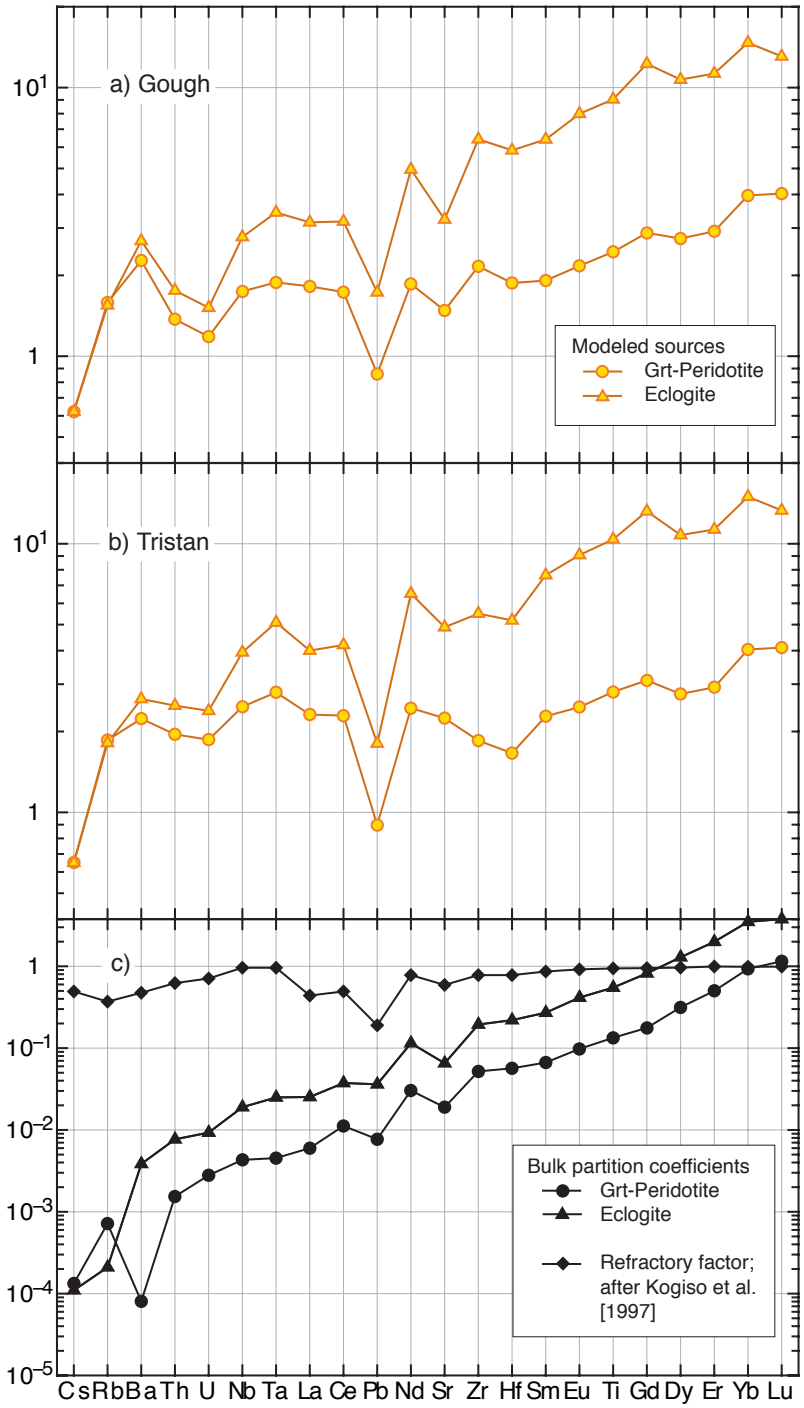

Figure 27: Modeled sources of EM-type OIB. a) Gough, b) Tristan, and d)Samoa-Malumalu, e) Societies-Tahaa (next page). See Fig. 22 for average composition of EM-type OIB and details on the melting model. Independent of the melting model (c, f), the EM source is depleted in very incompatible elements (VICE) and light REE relative to heavy REE. Note that inversion modeling by partial melting produces an irregular pattern of VICE and negative spikes for Pb and Sr in the source. The trace element pattern of the calculated source is similar to the HIMU source with regard to the less incompatible elements (La to Lu) and is inconsistent with a pure magmatic evolution because of negative anomalies for Pb and Sr. Comparison with rock-fluid alteration factors [Kogiso et al., 1997] suggests that the EM source must have experienced fluid-rock interaction during its evolution. The more enriched VICE pattern of the EM-type sources compared to the HIMU-type sources requires a more enriched component. Continued. See text for full discussion.

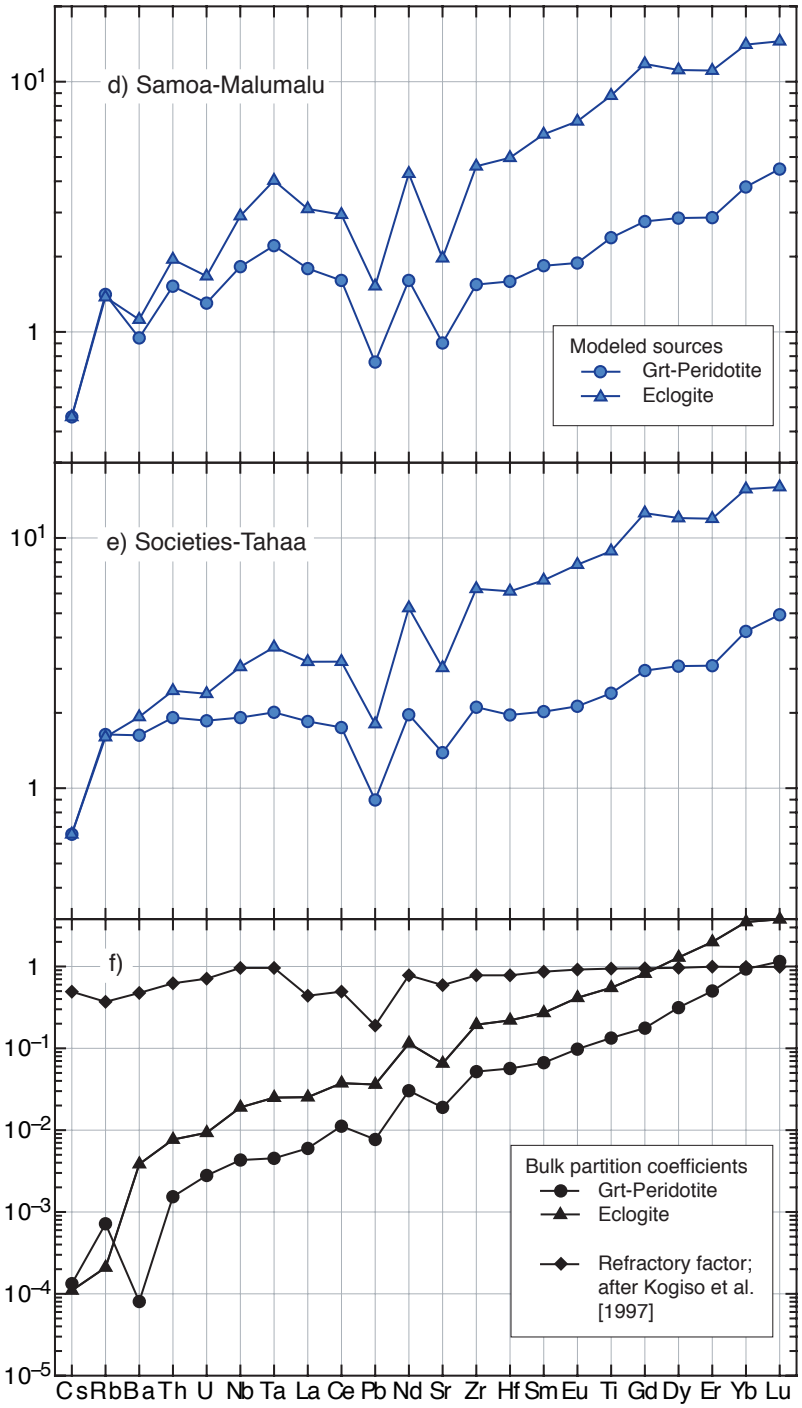

Figure 27: Continued.

decreases smoothly from U-La towards Cs and Rb, and is significantly lower for Pb and Sr compared to Nd and significantly higher for Nb and Ta compared to U and La. This indicates that the Pb, Sr, and Nb-Ta inventory of the HIMU source might be influenced by fluid-rock interaction during dehydration of the oceanic crust possibly during the transfer of the oceanic lithosphere to the mantle by subduction. From the composition of arc lavas and experimental studies of fluid-rock interaction in sub-arc environments, it has been inferred that dehydration of subducted MORB leads to net loss of Cs, Rb, Ba, K, light REE, Pb and Sr but net gain of Nb, Ta due to fluid removal and/or the retention of these elements in a Ti-phase or amphibole (e.g., Pearce and Peate [1995]; Pearce et al. [1995]; Kogiso et al. [1997]; Ionov and Hofmann [1995]; Brenan et al. [1994]; Tiepolo et al. [2000]; Stalder et al. [1998]; McCulloch and Gamble [1991]). Note that although Cs, Rb, Ba, and La, Ce are significantly removed from the oceanic crust during dehydration (Fig. 22b) the depletion during fluid-rock interaction increases systematically from U to Cs. Thus, although the absolute abundances of the fluid mobile elements are changed, fluid-rock interaction preserves the smoothly decreasing VICE pattern (U-Cs) in MORB, albeit with slightly different slope. Note that the expected high U/Pb and Th/Pb ratios in the HIMU source are in good agreement with their radiogenic Pb isotope signatures, which indicate a long-term evolution with high U/Pb (= high μ) ratios.

These inferred characteristics of the HIMU source (e.g. general enrichment of incompatible enrichment in the HIMU source over PUM, depletion of VICE relative to light REE, enrichment of Nb-Ta relative to U and La, and depletion of Pb relative to Nd) provide a strong case that HIMU sources were formed by melting VICE and LREE depleted sources which were subsequently modified by fluid-rock alteration processes in the sub-arc environment. In other words, the trace element systematics strongly support the notion that HIMU sources represent ancient subduction-modified oceanic crust (e.g., Chauvel et al. [1992]; Chauvel et al. [1997]; Halliday et al. [1988]; Hart [1988]; Hauri and Hart [1993]; Hauri et al. [1996]; Hofmann [1997]; Hofmann [2004]; Lassiter and Hauri [1998]; Nakamura and Tatsumoto [1988]; Palacz and Saunders [1986]; Reisberg et al. [1993]; Roy-Barman and Allegre [1995]; Salters and White [1998]; Vidal et al. [1984]; Weaver [1991a]; Zindler and Hart [1986]). The composition of subduction-modified oceanic crust is eventually the result of a complex interplay of a number of hard-to-constrain parameters, such as the bulk composition of the oceanic crust before subduction, its age, and the mode of modification during subduction and storage in the mantle [Stracke et al., 2003, 2005]. The uniform trace element composition of all HIMU basalts (and their corresponding sources) in combination with their comparatively small range in isotopic composition therefore suggests that despite the potentially large compositional variability of subduction-modified oceanic crust [Stracke et al., 2003], the HIMU sources must have evolved with remarkably uniform composition for similar time periods. Consequently, it appears most likely that the HIMU

sources were formed under similar conditions at roughly the same time, i.e. the HIMU source is likely to represent a real mantle reservoir.

12.2 The nature of the EM sources and the trace element conundrum

In general, the similarities between EM and HIMU sources (LREE depleted pattern of the EM source and the depletion of Pb and Sr relative to Ce and Nd) suggest that a precusor similar to those of the HIMU source (i.e. subduction-modified oceanic crust) is also involved in the genesis of EM sources. However, Th/U and Rb/Sr are consistently higher, Ce/Pb and Lu/Hf ratios are lower, and the VICE are more enriched whereas Nb and Ta are less enriched in EM compared to HIMU sources.

Bulk partition coefficient values do not allow for significant fractionation of U and Th to cause the differences in U/Th between the EM and HIMU sources by melting processes alone (Fig. 27). Regular variation of both bulk partition coefficient values and mobility factors for the elements between U and Rb further suggests that both magmatic differentiation and/or fluid-rock interaction are unlikely to be responsible for the irregular variation of the highly incompatible trace elements (and their ratios). Furthermore, the complex enrichment and depletion patterns in VICE (especially for Ba and U) are source-dependent, and are contrasted by the consistent, though variable depletion in U/Pb and Lu/Hf, and enrichment in Rb/Sr ratios in all EM sources.

Different, or additional, processes must therefore be responsible for the trace element composition of EM compared to HIMU sources. As a consequence, a more complex evolution, possibly involving an additional (enriched) component is suggested. On the other hand, the broadly similar isotope ratios in EM-1 and EM-2 relative to HIMU-type OIB (lower $^{143}Nd/^{144}Nd$, $^{206}Pb/^{204}Pb$, higher $^{87}Sr/^{86}Sr$, $^{208}Pb^*/^{206}Pb^*$ ratios) indicate that at least two general patterns exist with respect to the long-term evolution of parent/daughter ratios (e.g. Rb/Sr, Sm/Nd, Lu/Hf, U/Pb, Th/Pb) in EM sources in general. Despite these similarities in parent/daughter ratios, other trace element ratios clearly reveal compositional differences between individual EM-1 and EM-2 sources (e.g. Ba/La ratios; Fig. 23c), in addition to compositional variability between EM sources from one isotopic family alone (EM-1 or EM-2, respectively). Compare, for example, the variation in Ba/La, Rb/La (Fig. 23b and c), and U/Th ratios (Fig. 24f) in samples from the EM-1 islands Gough, Tristan and Pitcairn. As a family, therefore, EM basalts have common trace element characteristics that distinguish them from HIMU, but each suite of EM basalts appears to have a unique trace element composition, which is ultimately related to a unique source compositions. The highly incompatible trace element systematics therefore suggest that there are many, not only two, EM sources (see also Sun and McDonough [1989]), whereas

the isotopic relationships could be explained by a minimum of two enriched mantle components (EM-1 and EM-2). Identification of processes leading to reservoirs that evolve, with time, along distinct isotope paths but retain different incompatible element contents could resolve the apparent trace element conundrum.

The two principal reservoirs, which together host almost the entire trace element inventory of the Earth, are the Earth's mantle and crust. Melting of the Earth's mantle has ultimately created the oceanic and continental lithosphere. Although heterogeneous on a global scale [Hofmann, 2004; Salters and Stracke, 2004], the depleted mantle and its derivative melts are, in contrast to the continental crust, more homogeneous and characterized by low Rb/Sr, and high Sm/Nd and Lu/Hf that have evolved to low time-integrated $^{87}Sr/^{86}Sr$ and high $^{143}Nd/^{144}Nd$ and $^{176}Hf/^{177}Hf$ ratios. The continental crust is highly heterogeneous on both large and small scales, owing to complex intra-crustal differentiation processes (melting of the continental crust, fluid-rock exchange, weathering, erosion and sedimentation etc.). Nevertheless, two chemically distinct reservoirs within the continental crust have developed: the upper and the lower continental crust (e.g., Taylor and McLennan [1985]; Rudnick and Fountain [1995]; Rudnick and Gao [2004]). In addition, both the oceanic and continental lithospheric mantle may develop unique chemical characteristics.

Chemical heterogeneity in the Earth's mantle, as witnessed by the chemical and isotopic composition of OIB, must either be directly related to mixing or to interaction between two or several of these reservoirs. In addition to being a plausible solution for the chemical composition of OIB sources, the mechanism(s) suggested for the generation of the OIB sources have to be physically and geologically plausible. In the discussion above, we have advocated recycling of ancient subduction-modified oceanic crust as the principal mechanism for generating the HIMU reservoir. Since there is ample evidence for subduction of oceanic crust and its alteration during subduction zone processing, a reasonable mechanism for introducing subduction-modified oceanic crust into the mantle exists. Consequently, this scenario is geochemically, geologically, and physically plausible. In the following, we will discuss and/or suggest potential scenarios for the origin of EM sources.

12.3 Sediment recycling

Almost 20 years ago, the presence of recycled sediments and oceanic crust in EM sources has been invoked on the basis of the isotopic composition of EM basalts (e.g., Cohen and O'Nions [1982]; White and Hofmann [1982]; Beske et al. [1981]; Wright and White [1987]; Zindler and Hart [1986]). Subsequently, Weaver [1991a] proposed, based on the trace ele-

ment systematics in OIB, that recycling oceanic crust plus ancient (1-2 Ga) "pelagic" sediments generates EM-1 sources, whereas recycling oceanic crust plus ancient "terrigenous" sediments generates EM-2 sources. In the following, this scenario has often been invoked and has become somewhat of a paradigm for explaining the geochemical and isotopic systematics in OIB (e.g., Barling and Goldstein [1990]; Blichert-Toft et al. [1999]; Chauvel et al. [1992]; Eisele et al. [2002]; Hart [1988]; Hauri and Hart [1993]; Hauri et al. [1996]; Hemond et al. [1994]; Hofmann [1997]; Hofmann [2004]; Le Roex et al. [1990]; Rehkämper and Hofmann [1997]; Roy-Barman and Allegre [1995]; Weis et al. [1993]; White and Duncan [1996]; Woodhead and Devey [1993]; Woodhead and McCulloch [1989]). Owing to the limited knowledge of the geochemical composition of modern "pelagic" and "terrigenous" surface sediments in the early 1990's [BenOthman et al., 1989], however, it has been difficult to adequately assess the role of recycled sediments. Recently, the compilation of Plank and Langmuir [1998] has dramatically increased our knowledge about the geochemical composition of sediments. Most importantly for investigating sediment recycling, Plank and Langmuir [1998] have shown that modern sediments have a large range of chemical compositions, which is independent of their depositional environment ("pelagic" versus "terrigenous"), but depends mainly on the lithological constituents of the sediments (clastic, biogenic, hydrothermal).

The alkaline elements (Cs, Rb, K), Sr, REE and HFSE are largely hosted in detrital components in marine sediments and thus have average abundances comparable to those of the upper continental crust. Second-order variations in the alkaline and Sr abundances can be caused by variable proportions of biogenic phases such as opal, nannofossils, and foraminiferal oozes. Fe-Mn oxyhyrdoxides or fish-debris scavenge REE from seawater, which can lead to enrichment of REE over high field strength elements (HFSE; e.g. high Lu/Hf ratios) in slowly depositing sediments. Precipitation of U from seawater is enhanced by the decomposition of organic matter in environments with high biological activity (anoxic environments) whereas U forms soluble complexes in oxidizing environments. As a consequence, modern biogenic processes appear to control the total variation in parent/daughter ratios (e.g., Rb/Sr, Lu/Hf, and probably U/Pb) in present-day sediments. Biogenic carbonates (nannofossils, e.g. foraminifera), vertebrate remains (e.g. fish teeth) and other biogenic matter must have been virtually absent from oceanic sediments prior to Cambrian times. In addition, the occurrence of banded iron formations is taken as evidence for the existence of an oxidized ocean early in the Earth's history [Stanley, 1989]. The U concentration in Precambrian sediments should therefore have been controlled mainly by the detrital input.

Depending on the proportion of their constituents (detrital, biogenic, hydrothermal components), even similar types of present-day sediments therefore have highly variable

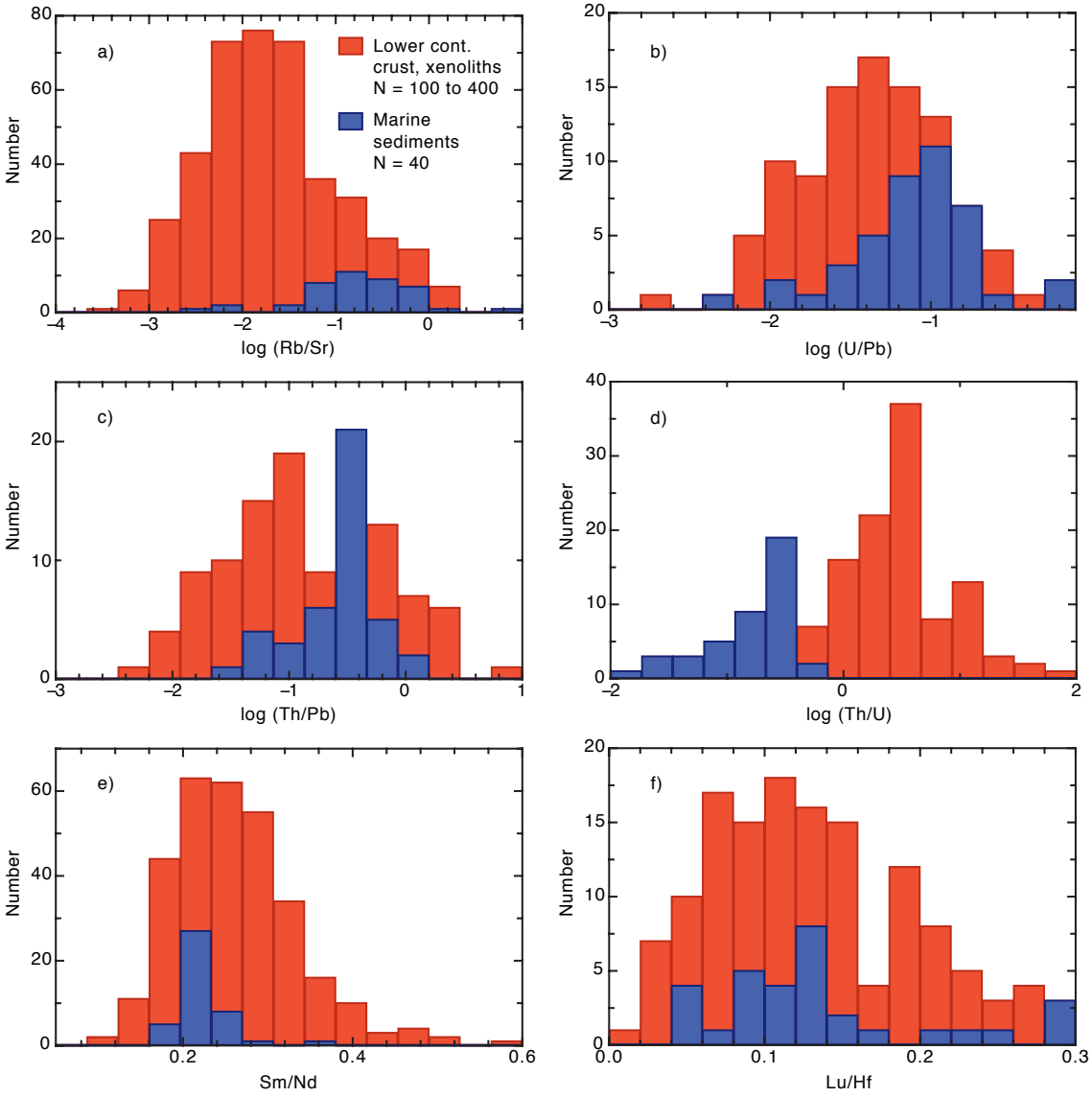

Figure 28: Histograms showing the log-normal distribution of parent/daughter ratios of isotope decay systems in presently subducted sediments (data from Plank and Langmuir [1998]). Also shown are distributions of the parent/daughter ratios in lower continental crust xenoliths (data from compilation in Rudnick and Gao [2004]). Both sets display uni-modal patters though with slightly different but significant maxima for Rb/Sr, U/Pb, Th/Pb, Th/U ratios, but not for Sm/Nd, and Lu/Hf ratios.

chemical compositions [Plank and Langmuir, 1998]. In addition to this inherent chemical variability of each type of sediment, assessing the chemical composition of subducted sediments is complicated by the fact that the sediment cover on the oceanic plate is usually composed of different types of sediment strata. In other words, when evaluating the significance of sediments in mantle sources, it has to be taken into account that certain types of surface sediments alone are unlikely to be representative of subducted sediments [Plank and Langmuir, 1998]. Although the bulk compositions of present-day subducted sediment packages differ, their chemical composition, at least with respect to parent/daughter ratios, is unimodal (Fig. 28; see also Stracke et al. [2003]), and their average composition is similar to those of the upper continental crust [Plank and Langmuir, 1998]. Note that the average global subducted sediment (GLOSS; Fig. 18 in Plank and Langmuir [1998]) has an REE pattern that strongly increases from La to Eu and then flattens out towards Lu (even when corrected for autigenic carbonate and opal production). Since such convex upward REE patterns and enrichment of REE are typical features of biogenic apatite (e.g., Toyoda and Tokonami [1990]; Trueman and Tuross [2002]), we speculate that the REE concentrations in modern marine sediments could be governed by biogenic input. The lack of such biogenic sediments and the probably oxidized state of the oceans in archean or early proterozoic times may have had the effect that pre-Cambrian sediments were even closer in composition to the upper continental crust than present-day sediments.

Since subducted sediments contain large amounts of water, dehydration and partial melting during subduction causes large parts of the original sediment signature to be lost, which is obvious from the chemical composition, in particular the ^{10}Be and Th/Rb signatures, of island arc volcanics (e.g., White and Dupré [1986]; Stern and Kilian [1996]; Elliot et al. [1997]; Hoogewerf et al. [1997]; Tatsumi [2000]; Morris et al. [1990]) and experimental data (e.g. Nichols et al. [1994]; Stalder et al. [1998]; Johnson and Plank [1999]). There is ample evidence, therefore that sediments make its way into the mantle. Exactly how much of the original sediment cover survives sub-arc processing, however, and makes its way into the deeper mantle remains unresolved. Thus the significance of subducted sediments (in composition and mass) for controlling the final chemical composition of the subducted lithsophere is not clear.

Although recycling of oceanic crust plus overlying sediments, is a possible mechanism to explain some of the enriched (EM) signatures in OIB sources (e.g., Chauvel et al. [1992]; White and Duncan [1996]; Eisele et al. [2002]; Woodhead and Devey [1993]; Hemond et al. [1994]; Weis et al. [1993]), it can certainly not account for the two broadly similar types of EM sources (EM-1 and EM-2) defined by the isotope systematics, and so leaves the trace element conundrum open.

12.4 Recycling lower continental crust

The two key parameters that determine the isotopic composition of any type of material are its parent/daughter ratio and age. Thus two sources with similar parent/daughter ratios can have different isotopic composition, provided they have different ages and/or initial isotopic composition. In contrast, similar isotopic signatures may simply indicate that sources with different isotope evolution paths fortuitously cross at the present time.

Such a scenario, however, appears unlikely to be responsible for the common isotopic trends of EM-1 and EM-2 sources, because all EM-1-type OIB have negative, whereas EM-2-type OIB have near vertical or positive slopes in $^{87}Sr/^{86}Sr$-$^{206}Pb/^{204}Pb$ space (Fig. 16a). High $^{87}Sr/^{86}Sr$ ratios (Rb/Sr) are therefore always coupled to low $^{206}Pb/^{204}Pb$ ratios (U/Pb) in EM-1 sources (note also the positive trends in $^{87}Sr/^{86}Sr$-$^{87}Rb/^{86}Sr$ space and in $^{206}Pb/^{204}Pb$-$^{238}U/^{204}Pb$ space, Fig. 25). This coherent behavior is indicative of a common, but different genetic origin of EM-1 and EM-2 sources, respectively. As a consequence, the parent/daughter ratios in EM-1 and EM-2 sources, respectively, have to be similar, despite the differences in VICE ratios. This behavior could most easily be explained in case parent-daughter element fractionation is determined by one common process, but this same process allows for different fractionation and/or preservation of different initial highly incompatible trace element ratios.

Intracrustal differentiation has led to the formation of two geochemically heterogeneous, but distinct, reservoirs: the lower and the upper continental crust (e.g., Taylor and McLennan [1985]; Rudnick and Fountain [1995]; Rudnick and Gao [2004]). These differentiation processes, caused by a variety of magmatic and non-magmatic processes, have led to variable but systematic differences in the trace element abundances of the upper and lower continental crust [Rudnick and Gao, 2004]. However, ratios among the highly incompatible elements (e.g. Th/Nb, Rb/K) or elements with similar geochemical behavior (e.g., Sr/Nd, Lu/Hf) should be less affected than ratios between elements with higher compatibility or different geochemical behavior. No matter what the exact processes involved in intracrustal differentiation are, in case these processes follow a systematic pattern, systematic differences between trace element ratios would be expected, and be most pronounced the larger the compatibility and/or mobility differences between two elements are. Despite the large uncertainties of lower crust composition when compared to those of the upper crust, our knowledge of the composition of the lower continental crust has increased significantly in recent years. Fig. 28 shows the variation in parent-daughter ratios and Th/U ratios for xenoliths from the lower continental crust (see data compilation in Rudnick and Gao [2004]) and subducted sediments (data from Plank and Langmuir [1998]) serving as a proxy for the average composition of the upper continental crust. Indeed, there are small

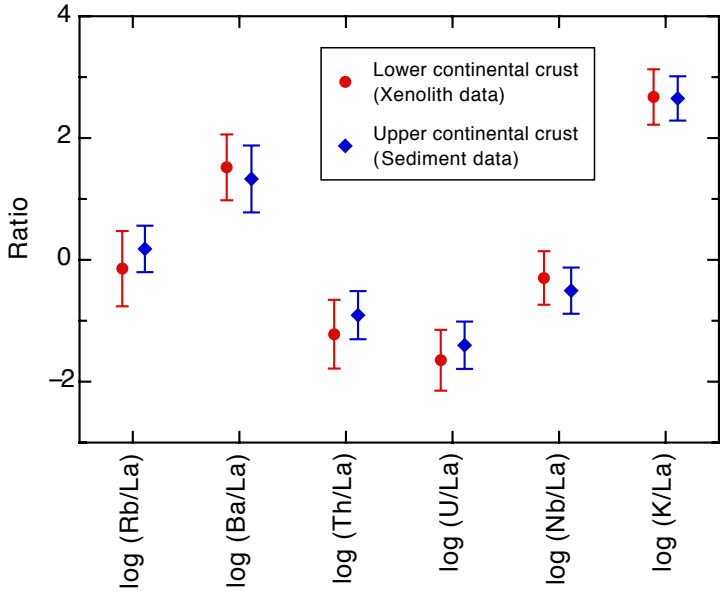

Figure 29: Comparison of ratios of VICE in the upper and lower continental crust. Averages and variations (1σ) have been calculated using data of marine sediment (N = 40, data from Plank and Langmuir [1998]) as an estimate for the upper continental crust as well as data of xenoliths from the lower continental crust (N = 100 to 400, data compilation in Rudnick and Gao [2004]). There is broad overlap in all trace element ratios for the upper as well as for the lower continental crust.

but considerable differences in the distribution patterns and maxima for parent/daughter ratios (Rb/Sr, U/Pb, Th/Pb) and Th/U in the upper and lower continental crust resulting in an overall bimodal distribution pattern in the continental crust. Although small, these differences can, over time, evolve along considerably different isotope evolution paths due to the early formation and high average age of the continental crust (first formation at ca. 4 Ga (e.g., Bowring et al. [1989], with a present-day average of ca. 2 Ga [Goldstein et al., 1984]).

In this respect, the time, as an additional component, acts as a 'magnifying glass' for the small compositional gross differences between the upper and lower continental crust. Accordingly, the lower crust develops consistently low $^{87}Sr/^{86}Sr$, $^{206}Pb/^{204}Pb$, and $^{208}Pb/^{204}Pb$ and high $^{208}Pb^*/^{206}Pb^*$ well distinct from those of the upper continental crust. These findings are in good agreement with the low $^{87}Sr/^{86}Sr$, $^{206}Pb/^{204}Pb$, and $^{208}Pb/^{204}Pb$ and high $^{208}Pb^*/^{206}Pb^*$ isotope systematics of the most extreme EM-1 basalts in contrast to EM-2 basalts (Fig. 16). Very incompatible trace element ratios in both the upper and lower continental crust, respectively, are highly variable and overlap considerably (Fig. 29). Small systematic differences in relative abundances of VICE between the upper and lower continental crust, however, are diminished given the large

differences in absolute and relative abundances of highly incompatible elements between the continental crust and MORB in general. Thus highly incompatible element ratios in the upper and lower crust retain their comparable variance in mixtures of upper/lower continental crust and MORB. Rather, each enriched mixture would result in a unique trace element composition.

These characteristics of the upper and lower continental crust may thus provide a possible solution to the trace element conundrum in EM sources. Mixing small amounts of predominantly lower continental crust and upper continental crust (or ancient subducted sediment) to altered oceanic crust, respectively, should lead to the observed isotope evolution of EM-1 and EM-2 sources (see also discussion in Zindler and Hart [1986]), while preserving similar, but variable highly incompatible trace element characteristics.

12.5 Mixing relationships

The trace element composition of EM-1 and EM-2 basalts (average of Pitcairn, Tristan and Gough; Samoa-Malumalu, and Society-Tahaa; Fig. 30) can successfully be modeled by mixing subducted MORB with lower or upper continental crust, respectively. Especially the relative enrichment in VICE, the less pronounced positive Nb-Ta and negative Pb anomalies compared to HIMU source are successfully reproduced by the model calculations. Calculations are done based on the model described in detail in Stracke et al. [2003]. Mixing about 1 to 10% lower continental crust [Rudnick and Gao, 2004] and 1 to 10% of upper continental crust [Taylor and McLennan, 1985] with altered oceanic crust, respectively, creates suitable EM-1 and EM-2 sources. The modeled EM-1 and EM-2 melts assume partial melting of eclogitic sources (F = 0.02 to 0.05). The calculated heavy REE concentrations in the melts are lower than those in EM-type OIB, which is attributed to the large abundance of garnet in the source and the uncertainty of bulk partition coefficients.

Preliminary modeling of the isotopic composition of EM-1 and EM-2-type OIB, using the same compositions and mixing proportions as for the trace elements, also successfully reproduce the isotopic compositions of EM-1 and EM-2 basalts [Stracke et al., 2004] This is in good agreement with the conclusions of Escrig et al. [2004] and Hanan et al. [2004], who suggested that the EM-1-like isotope signatures in Indian MORB are consistent with the presence of delaminated lower continental crust in the sub-Indian Ocean mantle.

In Ba/Rb versus Th/Rb space (Fig. 31a), all OIB form a triangular pattern with the EM-type OIB (large spread in Ba/Rb at low Th/Rb) fanning out from the HIMU-type OIB at the apex (high values for Th/Rb and intermediate values for Ba/Rb). Interestingly, the arrays of most EM-type suites do not trend towards the HIMU field, but are more or less, with some exceptions, oblique to it (Fig. 31a). Similar patterns are observed for other trace

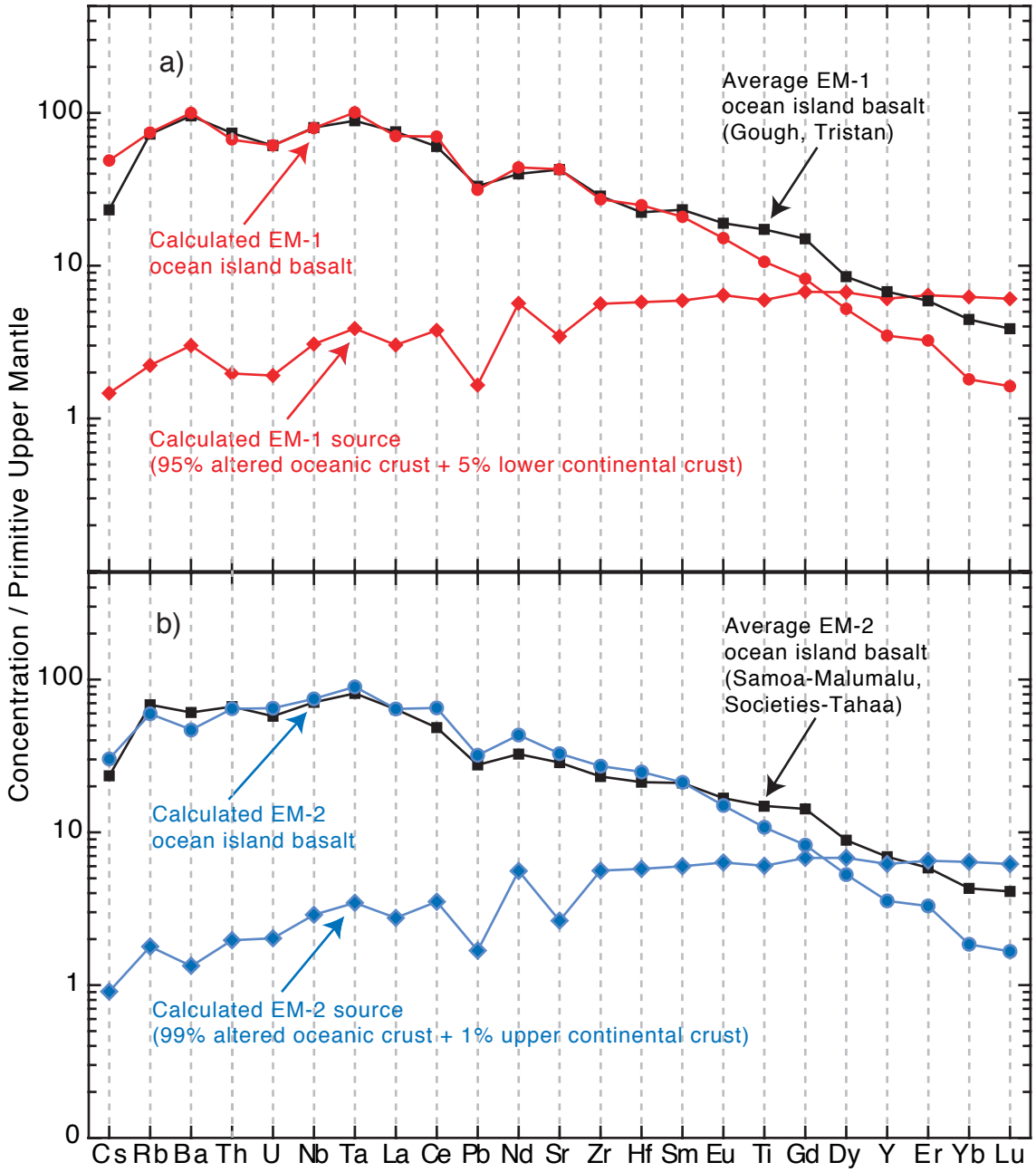

Figure 30: Comparison of average EM-type OIB with modeled trace element patterns. a) Modeled EM-1 source assuming mixing of altered oceanic crust with 5% average lower continental crust [Rudnick and Gao, 2004] followed by 3% batch melting of eclogite to produce the modeled EM-1 basalt. Measured EM-1 basalt is average of Gough and Tristan samples. b) Modeled EM-2 source assuming mixing of altered oceanic crust with 1% average upper continental crust [Taylor and McLennan, 1985] followed by 3% batch melting of eclogite to produce the modeled EM-2 basalt. Measured EM-2 type basalt is average of Samoa-Malumalu and Societies-Tahaa samples. See Appendix G for a full description of the model.

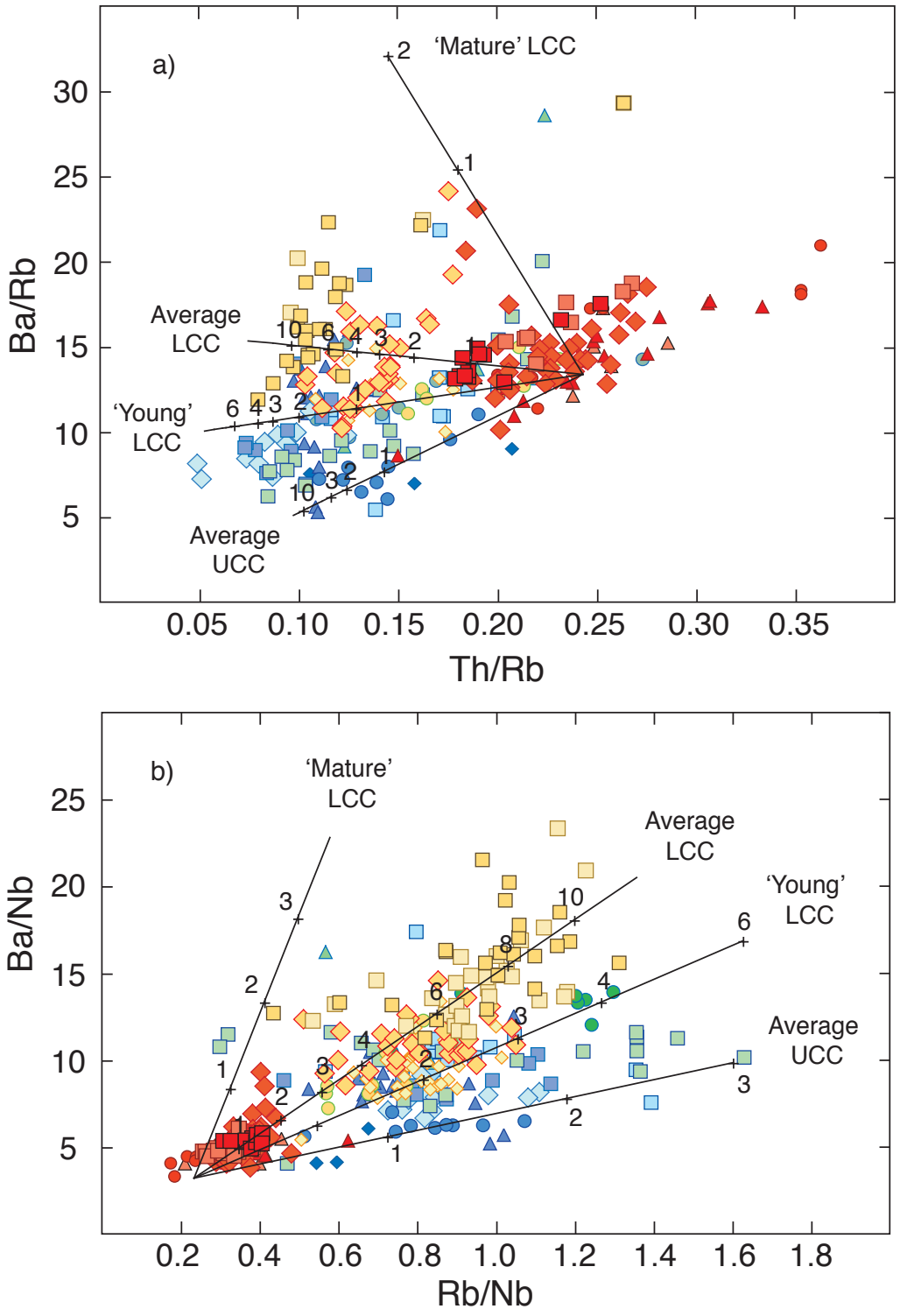

Figure 31: Modeling the variation of a) Ba/Rb versus Th/Rb and b) Ba/Nb versus Rb/Nb for different OIB suites. Modeled mixing trajectories using different average compositions of the lower continental crust suggest that the large variation in within single suites can be explained by admixing 1 to 6% of lower continental crust (LCC) with different bulk composition (average, young, and mature lower continental crust), and up to 1 to 3% average upper continental crust (UCC). See Appendix G for a full description of the model. Numbers at tick marks refer to percent of continental crust. Note that, with a few exceptions, trends of individual suites run oblique to the trajectories HIMU-EM suggesting that each suite contains a rather fixed mixture of HIMU and an ultimately heterogeneous enriched end-member (upper continental crust, lower continental crust). See text for discussion. Symbols as in Fig. 19.

element ratios (e.g. Ba/Nb versus Rb/Nb; Fig. 31b) or isotopes (e.g., $^{208}Pb/^{204}Pb$ versus $^{206}Pb/^{204}Pb$ isotopes, not shown). These patterns are consistent with mixing recycled oceanic crust with compositionally heterogeneous (due to various proportions of different kinds of continental crust all having different but characteristic composition) but relatively reproducible proportions of predominantly upper or lower continental and oceanic crust, i.e. each individual EM source contains a rather constant amount of compositionally heterogeneous continentally derived material. Thus mixing of recycled oceanic crust with the compositionally heterogeneous, enriched component is likely to occur during the generation of the EM source (e.g., during subduction), and does not occur by mixing different EM-type mantle reservoirs with recycled oceanic crust somewhere in the convecting mantle (e.g., Zindler and Hart [1986], Hart [1988]). As a consequence, each EM source reflects its own unique composition, determined by mixing recycled oceanic and continental crust. In contrast to the HIMU signature (see discussion in Part II, section 12.1), therefore, the EM signature does not appear to be related to real mantle reservoirs, i.e. parts of the mantle that share a similar genetic origin and age, and that have a relatively homogeneous geochemical and isotopic composition.

12.6 Mechanisms for recycling lower continental crust

The preceding discussion shows that the trace element and isotope systematics of EM-1 and EM-2 basalts can successfully be explained by recycling oceanic and various proportions of lower and upper continental crust, respectively, but leaves one important question unanswered: How can the lower continental crust be recycled into the mantle?

Delamination of the lower continental crust has previously been proposed (e.g., Rudnick [1995]; McKenzie and O'Nions [1983]; Tatsumi and Kogiso [1997]; Kay and Kay [1993]; Tatsumoto and Nakamura [1991]; Escrig et al. [2004], Hanan et al. [2004]). Although this is certainly a viable process, delamination of the lower continental crust without the attached subcontinental lithospheric mantle may require special conditions [Escrig et al., 2004]. Although the composition of the subcontinental lithospheric mantle is hard to constrain, it appears to have a characteristically unradiogenic $^{187}Os/^{188}Os$ signature [Pearson et al., 2004]. The lack of such unradiogenic $^{187}Os/^{188}Os$ signatures in OIB suggests that the subcontinental lithospheric mantle is not a major constituent of present OIB sources (e.g. Eisele et al. [2002], Escrig et al. [2004]). The apparent presence of subduction-modified oceanic crust in the EM sources (see preceding discussion) also implies that mechanisms other than delamination, but most likely closely related to subduction of oceanic crust, are responsible for recycling lower continental crust. Recent studies of global convergent plate margins reveal the importance of erosive versus accretionary margins for the global mass flux at subduction zones (see Clift and Vannucchi [2004] for a recent review and Uyeda

[1982], von Huene et al. [2004], and Vannucchi et al. [2004]). Mass flux calculations suggest that up to 100 km^2 continental material per million years per km trench can be eroded by the down-going plate [Clift and Vannucchi, 2004]. Prolonged bending of the oceanic crust during subduction causes rocks at the base of the upper plate to be fractured and dragged into the subduction channel where it is, together with the subduction-modified oceanic crust, ultimately subducted [von Huene et al., 2004]. Erosive margins are characterized by net-loss of continental crust to the mantle, high orthogonal convergence rates and a thin sediment veneer. The latter is probably related to the short transient time of the oceanic plate through the fore arc region. Accretionary margins are characterized by net-growth of continental crust, slow convergence rates and long transient times of the oceanic plate through the fore arc, which cause accumulation of thick piles of continentally derived sediments in accretionary prisms. Thus, loss of continental crust by subduction is balanced by crustal accretion through sediment underplating and arc volcanism. Nevertheless, crustal material is recycled at both, erosive and accretionary margins.

Recycling of continental crust through subduction erosion not only provides a valid mechanism for recycling of continental material, it is also consistent with the inferred additional presence of subduction-modified oceanic crust in EM sources (see discussion above), and is thus a geochemcially, geologically and physically consistent scenario. More speculatively, recycling of continental crust via subduction erosion might also be a possible explanation for the bimodal pattern of EM signatures (EM-1 and EM-2). EM-1 sources could be created predominantly at erosive margins through preferential erosion and recycling of lower crustal material, whereas a EM-2 sources could be formed predominantly at accretionary margins through preferential recycling of sediments or eroded upper continental crust. Whether sediment subduction or erosion of upper crust is more important is hard to address. In either way, this new model for the source generation of EM-type OIB incorporates the classic model of recycling oceanic crust plus continentally derived material but places more detailed constraints on the chemical diversity of the continental crust itself.

12.7 Alternative models: metasomatic processes

Similar to the scenario proposed in this study, Tatsumi [2000] suggested that the EM-1 sources are formed by pyroxenitic restites that delaminate during the anatexis of the initially basaltic lower continental continental crust at destructive margins. The modeled trace element composition of the pyroxenitic source of Tatsumi [2000] is, however, highly enriched in VICE relative to light REE, has a pronounced negative Nb anomaly and a large positive Pb anomaly (see Fig. 2 in Tatsumi [2000]). These features are inconsistent with the flat but irregularly shaped very incompatible trace element pattern (Cs-U), the

positive Nb anomaly and the negative Pb anomaly of all OIB investigated in this study.

Recenly, Niu and O'Hara [2003] have argued that oceanic crust is inappropriate to generate the isotopic and trace element composition of OIB. Similar to Stracke et al. [2003], Niu and O'Hara [2003] have argued that dehydration during subduction potentially leads to variable parent/daughter ratios in the subduction-modified crust, which, if a general feature of subduction-modified oceanic crust, would lead to irreproducible Sr-Nd-Hf isotope systematics. These would then be difficult to reconcile with the relative chemical and isotopic homogeneity of HIMU basalts. The geochemical and isotopic homogeneity of HIMU sources, however, requires that they are produced by similar processes at roughly the same time, irrespective of their presumed origin (see Part II, section 12.1 and Stracke et al. [2003]). According to Niu and O'Hara [2003], Sr-Nd-Hf isotope ratios in recycled MORB are also too depleted to be suitable EM sources. We agree with Niu and O'Hara [2003] that pure oceanic crust is not appropriate for explaining the isotopic composition of EM sources. The trace element pattern of both HIMU and EM sources, however, provides good evidence that incompatible element enriched material (with respect to Bulk Earth, see preceding discussion) similar to partial melts from a depleted mantle, which was subsequently modified during subduction, is indeed involved in both HIMU and EM sources. As an alternative mechanism responsible for the isotopic diversity in OIB sources, Niu and O'Hara [2003] proposed the formation of phlogopite- and amphibole-bearing pyroxenites by metasomatic processes. Small-degree melt impregnation of oceanic lithosphere may be a common feature, but the presence of hydrated residual phases (phlogopite/amphibole) is inconsistent with the observed trace element characteristics of both HIMU and EM sources (see discussion in Part II, section 11.1) and also fails to explain the bimodal composition of enriched mantle components (EM-1 and EM-2).

Similarly, Workman et al. [2004] argued that the composition of the source of Samoan basalts (EM-2) is consistent with metasomatized oceanic lithosphere. Although the isotopic composition of the Samoan lavas may be successfully explained by this approach, the smoothly increasing incompatible trace element concentrations from La to Cs in the modeled EM-2 source, however, is inconsistent with the irregular and almost horizontally sloped incompatible trace element pattern of the Samoan basalts (low Cs-Ba-U-K/La and high Rb/La ratios). If anything, melting of the proposed EM-2 source [Workman et al., 2004] would lead to an even steeper sloped incompatible element pattern.

Fluid-rock or small-degree melt-rock interaction in the oceanic lithosphere is perhaps a widespread phenomenon and may contribute to the compositional variability of some OIB sources. However, our understanding of the chemical composition of potential metasomatic agents and metasomatized materials, the scale of such processes and the ways by which metasomatized material may end up as source material for OIB remains limited

and is characterized by uncertainties probably similar to or even exceeding those related to recycling of oceanic crust. Whether recycling of oceanic crust plus small amounts of continental material, or interaction of essentially basaltic melts with the depleted oceanic lithosphere is responsible for potential enriched signatures in OIB sources, is difficult to assess. While there is ample evidence of subduction of oceanic crust and continental material at least to upper mantle levels, as testified by arc volcanism, evidence for widespread fluid/melt-rock interaction in the sub-oceanic mantle is ambiguous. We therefore favor recycling of oceanic crust as the principal mechanism for introducing chemical heterogeneity into the Earth's mantle

13 Conclusions

HIMU basalts have more depleted very incompatible element abundances (Cs-U), more pronounced Nb and Ta enrichment and Pb depletions, and are characterized by higher U/Th, lower Rb/Sr ratios relative to EM basalts. As a group, HIMU basalts and their corresponding mantle sources are geochemically and isotopically remarkably homogeneous. This implies that the HIMU sources are produced by similar processes and have roughly the same age. The HIMU signature is therefore most likely related to a real mantle reservoir.

EM basalts are overall more enriched in very incompatible elements compared to HIMU basalts. Each suite of EM-type OIB appears to have its own unique very incompatible trace element signature (Cs-U) that is different from those of any other suite of EM basalts. The highly incompatible trace element systematics therefore suggest that there are many, not only two, EM sources in contradiction the isotopic definition of EM-1 and EM-2 basalts.

Similarities between calculated EM and HIMU sources (similar La/Th, La/Sm ratios, light REE depleted patterns, depletion of Pb and Sr and enrichment of Nb and Ta relative to neighboring elements) suggest that both HIMU and EM, and thus OIB sources are formed by melting trace element enriched (with respect to Bulk Earth) but very incompatible elements and light REE depleted sources, which were subsequently modified by fluid-rock alteration processes, i.e. in a sub-arc environment (subduction-modified oceanic crust).

Owing to the bimodal composition and high average age of the continental crust, addition of preferentially lower and/or upper continental crust to oceanic crust via subduction erosion and/or sediment recycling could, over time, explain the diverging isotopic trends in EM-1 and EM-2 type OIB while maintaining a large variance in trace element com-

position in the resulting mixture. Modeling the trace element compositions of EM-1 and EM-2 type OIB assuming different estimates for the chemical composition of the lower continental crust supports this hypothesis.

14 Acknowledgments

My special thanks go to (in the order of appearance) my advisor Ernst Hegner for introducing me to geochemistry and to mass spectrometry and for being around (although far away in Munich) whenever there were problems to solve; to Klaus Peter Jochum for his unconditional support and for teaching me all the skills and tricks in mass spectrometry and trace element analysis; and to Andreas Stracke for introducing me to mantle geochemistry and also for the many discussions that helped me to sort out my thoughts. All three of them gave me complete freedom to explore my ideas but have always been there for discussions whenever the question marks became "too big". I really appreciate their integrity and reliability!

I would like to thank Al Hofmann for giving me the opportunity to work at the MPI for Chemistry and for his straightforward support.

Brigitte Stoll, Michael Seufert, Kirstin Herwig, Macho Amini, and Klaus Peter Jochum not only supported me during my work but also created a great atmosphere that made my stay in Mainz much more convenient, especially during the first couple of months.

I want to thank Frau I. Raczek for her assistance and helpfulness in the lab and during the preparation of the spikes.

Karin Geiger, Frau R. Gross, Frau G. Feyerherd, Frau I. Bambach, Alex Rocholl, Heinz Feldmann, Frau R. Löhr, and Frau H. Prager are thanked for their assistance and for their unconventional help whenever I needed it most.

Andreas Gaab is thanked for "refreshing" my LaTeX skills. Without him this thesis would not look like as it actually does.

I also would like to acknowledge the professional help and support of all the people at the MPI for Chemistry.

At last, great thanks to Andreas and Ella for being good friends and for building me up again, whenever things went wrong!

References

Ague, J., 2004. Fluid flow in the deep crust. In: Rudnick, R. (Ed.), Treatise on Geochemistry, vol. 3, The Crust. Elsevier-Pergamon, Oxford, 195–228.

Ahrens, L., 1954. The lognormal distribution of the elemenets (A fundamental law of geochemistry and its subsidiary). Geochimica et Cosmochimica Acta 5, 49–73.

Anders, E., Grevesse, N., 1989. Abundances of the elements: Meteoritic and solar. Geochimica et Cosmochimica Acta 53, 197–214.

Anitha, S., Shanmugavelu, P., Gazula, V. R., Shankar, S. K., Menon, R. B., Rao, R. V., Rao, J. K. S., Zecca, L., 2002. Molecular understanding of aluminium bioinorganic chemistry in relevance of the pathology of Alzheimer's disease. Group 13 Chemistry: from fundamentals to applications ACS symposium series 822, 228–245.

Baker, J., Waight, T., Ulfbeck, D., 2002. Rapid and highly reproducible analysis of rare earth elements by multiple collector inductively coupled plasma mass spectrometry. Geochimica et Cosmochimica Acta 66, 3635–3646.

Barbante, C., Schwikowski, M., Doring, T., Gaggeler, H. W., Schotterer, U., Tobler, L., Van De Velde, K., Ferrari, C., Cozzi, G., Turetta, A., Rosman, K., Bolshov, M., Capodaglio, G., Cescon, P., Boutron, C., 2004. Historical record of European emissions of heavy metals to the atmosphere since 1650's from Alpine snow/ice cores drilled near Monte Rosa. Environmental Sciences and Technology 38, 4085–4090.

Barling, J., Goldstein, S. L., 1990. Extreme isotopic variations in Heard island lavas and the nature of mantle reservoirs. Nature 348, 59–62.

Becker, J., Dietze, H., 2000. Precise and accurate isotope ratio measurements by ICP-MS. Fresenius Journal of Analytical Chemistry 368, 23–30.

Becker, J. S., Zoriy, M., Becker, J. S., Pickardt, C., Przybylski, M., 2004. Determination of phosphorus and metals in human brain proteins after isolation by gel electrophoresis by laser ablation inductively coupled plasma source mass spectrometry. Journal of Analytical Atomic Spectrometry 19, 149–152.

BenOthman, D., White, W., Patchett, J., 1989. The geochemistry of marine sediments, island arc magma genesis, and crust-mantle recycling. Earth and Planetary Science Letters 94, 1–21.

Beske, H. E., Gijbels, R., Hurrle, A., Jochum, K. P., 1981. Review and evaluation of spark source-mass spectrometry as an analytical method. Fresenius Zeitschrift für Analytische Chemie 309, 329–341.

Blichert-Toft, J., Frey, F. A., Albarede, F., 1999. Hf isotope evidence for pelagic sediments in the source of Hawaiian basalts. Science 285, 879–882.

Bowring, S. A., Williams, I. S., Compston, W., 1989. 3.96 Ga gneisses from the Slave province, Northwest Territories, Canada. Geology 17, 971–975.

Breeding, C., Ague, J., Bröcker, M., Bolton, E., 2003. Blueschist preservation in a retrograded, high-pressure, low-temperature metamorphic terrane, Tinos, Greece: implications for fluid flow paths in subduction zones. Geochemistry, Geophysics, Geosystems 4, Paper number 2002GC000380.

Brenan, J., Shaw, H., Phinney, D., Ryerson, F., 1994. Rutile-aqueous fluid partitioning of Nb, Ta, Hf, Zr, U and Th: implications for high-field strength element depletions in island-arc basalts. Earth and Planetary Science Letters 128, 327–339.

Brenner, I., Zander, A., 1996. Geoanalysis using plasma spectrochemistry - Milestones and future prospects. Fresenius Journal of Analytical Chemistry 355, 559–570.

Chauvel, C., Hofmann, A., Vidal, P., 1992. HIMU-EM: The French Polynesian connection. Earth and Planetary Science Letters 110, 99–119.

Chauvel, C., McDonough, W., Guille, G., Maury, R., Duncan, R., 1997. Contrasting old and young volcanism in Rurutu Island, Austral chain. Chemical Geology 139, 125–143.

Cheatham, M., Sangrey, W., White, W., 1993. Sources of error in external calibration ICP-MS analysis of geological samples and an improved nonlinear drift correction procedure. Spectrochimica Acta Part B-Atomic Spectroscopy 48, 487–506.

Clift, P., Vannucchi, P., 2004. Controls on the tectonic accretion versus erosion in subduction zones: implications for the origin and recycling of the continental crust. Review of Geophysics 42, Paper number 2003RG000127.

Cohen, R., O'Nions, R., 1982. Identification of recycled continental material in the mantle from Sr, Nd, and Pb isotope investigations. Earth and Planetary Science Letters 61, 73–84.

David, K., Birck, J., Telouk, P., Allegré, C., 1999. Application of isotope dilution for precise measurement of Zr/Hf and Hf-176/Hf-177 ratios by mass spectrometry (ID-TIMS/ID-MC-ICP-MS). Chemical Geology 157, 1–12.

D'Orazio, M., Tonarini, S., 1997. Simultaneous determination of neodymium and samarium in silicate rocks and minerals by isotope dilution inductively coupled plasma mass spectrometry: Results on twenty geochemical reference samples. Analytica Chimica Acta 351, 325–335.

Dulski, P., 1994. Interferences of oxide, hydroxide and chloride analyte species in the determination of rare-earth elements in geological samples by Inductively-Coupled Plasma-Mass Spectrometry. Fresenius Journal of Analytical Chemistry 350, 194–203.

Dulski, P., 2001. Reference materials for geochemical studies: New analytical data by ICP-MS and critical discussion of reference values. Geostandards Newsletter: The Journal of Geostandards and Geoanalysis 25, 87–125.

Eggins, S., Woodhead, J., Kinsley, L., Mortimer, G., Sylvester, P., McCulloch, M., Hergt, J., Handler, M., 1997. A simple method for the precise determination of ≥ 40 trace elements in geological samples by ICPMS using enriched isotope internal standardisation. Chemical Geology 134, 311–326.

Eisele, J., Sharma, M., Galer, S., Blichert-Toft, J., Devey, C., Hofmann, A., 2002. The role of sediment recycling in EM-1 inferred from Os, Pb, Hf, Nd, Sr isotope and trace element systematics of the Pitcairn hotspot. Earth and Planetary Science Letters 196, 197–212.

Elliot, T., Plank, T., Zindler, A., White, W., Bourdon, B., 1997. Element transport from slab to volcanic front at the Mariana arc. Journal of Geophysical Research 102, 14991–15019.

Ellison, S. L. R., Rosslein, M., Williams, A., 2000. Quantifying uncertainty in analytical measurement. Tech. Rep. Guide CG4, Eurachem/CITAC.

Escrig, S., Campas, F., Dupré, B., Allegré, C., 2004. Osmium isotopic constraints on the nature of the DUPAL anomaly from Insian mid-ocean-ridge basalts. Nature 431, 59–63.

Field, M., Sherrell, R., 1998. Magnetic sector ICPMS with desolvating micronebulization: Interference-free subpicogram determination of rare earth elements in natural samples. Analytical Chemistry 70, 4480–4486.

Gäbler, H.-E., 2002. Applications of magnetic sector ICP-MS in geochemistry. Journal of Geochemical Exploration 75, 1–15.

Galer, S. J. G., O'Nions, R. K., 1985. Residence time of thorium, uranium and lead in the mantle with implications for mantle convection. Nature 316, 778–782.

Goldstein, S. L., O'Nions, R. K., Hamilton, P. J., 1984. A Sm-Nd isotopic study of atmospheric dusts and particulates from major river systems. Earth and Planetary Science Letters 70, 221–236.

Govindaraju, K., 1994. 1994 Compilation of Working Values and Sample Description for 383 Geostandards. Geostandards Newsletter: The Journal of Geostandards and Geoanalysis 18, 1–158.

Griselin, M., Pearson, D., Ottley, C., Davies, G., 1999. A low-blank, low detection limit method for REE analysis of geological samples by isotope dilution ICP-MS. In: Holland, J., Tanner, S. (Eds.), Plasma Source Mass Spectrometry - New Developments and Applications, 234. Royal Society of Chemistry Special Publication, 246–252.

Halliday, A. N., Dickin, A. P., Fallick, A. E., Fitton, F. G., 1988. Mantle dynamics: a Nd, Sr, Pb, and O isotopic study of the Cammeroon Line Volcanic Chain. Journal of Petrology 29, 181–211.

Hanan, B., Blichert-Toft, J., Pyle, D., Christie, D., 2004. Contrasting origins of the upper mantle revealed by hafnium and lead isotopes from the Southeast Indian Ridge. Nature 432, 91–94.

Hart, S., 1988. Heterogeneous mantle domains: signatures, genesis and mixing chronologies. Earth and Planetary Science Letters 90, 273–296.

Hart, S., Blusztajn, J., Dick, H., Meyer, P., Muehlenbachs, K., 1999. The fingerprint of seawater circulation in a 500-m section of ocean crust gabbros. Geochimica et Cosmochimica Acta 63, 4059–4080.

Hauri, E., Hart, S., 1993. Re-Os isotope systematics of HIMU and EMII oceanic island basalts from the south Pacific Ocean. Earth and Planetary Science Letters 114, 353–371.

Hauri, E. H., Lassiter, J. C., DePaolo, D. J., 1996. Osmium isotope systematics of drilled lavas from Mauna Loa, Hawaii. Journal of Geophysical Research 101, 11793–11806.

Hemond, C., Devey, C. W., Chauvel, C., 1994. Source compositions and melting processes in the Society and Austral plumes (South Pacific Ocean): Element and isotope (Sr, Nd, Pb, Th) geochemistry. Chemical Geology 115, 7–45.

Heumann, K., 1986. Isotope-dilution mass-spectrometry of inorganic and organic substances. Fresenius Zeitschrift für Analytische Chemie 325, 661–666.

Heumann, K., Gallus, S., Radlinger, G., Vogl, J., 1998. Precision and accuracy in isotope ratio measurements by plasma source mass spectrometry. Journal of Analytical Atomic Spectrometry 13, 1001–1008.

Hill, S. J. (Ed.), 1999. Inductively Coupled Plasma Spectrometry and Its Application. Sheffield Academic Press, Sheffield.

Hofmann, A., 1997. Mantle geochemistry: the message from ocanic volcanism. Nature 385, 219–229.

Hofmann, A., 2004. Sampling mantle heterogeneity through oceanic basalts: isotopes and trace elements. In: Carlson, R. (Ed.), Treatise on Geochemistry, vol. 2, The Mantle and Core. Elsevier - Pergamon, Oxford, 61–101.

Hofmann, A., Feigenson, M., Raczek, I., 1984. Case studies on the origin of basalt: III. Petrogenesis of the Mauna Ulu eruption, 1969-1971. Contributions to Mineralogy and Petrology, 88, 24–55.

Hofmann, A., Jochum, K., Seufert, H., White, W., 1986. Nb and Pb in oceanic basalts: new constraints on mantle evolution. Earth and Planetary Science Letters 79, 33–45.

Hofmann, A., White, W., 1982. Mantle plumes from acient oceanic crust. Earth and Planetary Science Letters 57, 421–436.

Hoogewerf, J., van Bergen, M., Vroon, P., Hertogen, J., Wordel, R., Sneyers, A., Nasution, A., Varekamp, J., Moens, H., Mouchel, D., 1997. U-series, Sr-Nd-Pb isotope and trace-element systematics across an active island arc-continent collision zone: implications for element trabsfer at the slab-wedge interface. Geochimica et Cosmochimica Acta 61, 1057–1072.

Ionov, D., Hofmann, A., 1995. Nb-Ta-rich mantle amphiboles and micas: implications for subduction-related metasomatic trace elmenet fractionations. Earth and Planetary Science Letters 131, 341–356.

Irvine, T. N., Baragar, W. R. A., 1971. A guide to the chemical classification of the common volcanic rocks. Canadian Journal of Earth Science 8, 523–548.

Jenner, G., Longerich, H., Jackson, S., Fryer, B., 1990. ICP-MS - A powerful tool for high-precision trace-element analysis in Earth sciences - Evidence from analysis of selected USGS reference samples. Chemical Geology 83, 133–148.

Joannon, S., Telouk, P., Pin, C., 1997. Determination of U and Th at ultra-trace levels by isotope dilution inductively coupled plasma mass spectrometry using a geyser-type ultrasonic nebulizer: application to geological samples. Spectrochimica Acta Part B-Atomic Spectroscopy 52, 1783–1789.

Jochum, K., Dingwell, D., Rocholl, A., Stoll, B., Hofmann, A., and 32 co-authors, 2000. The preparation and preliminary characterisation of eight geological MPI-DING reference glasses for in-site microanalysis. Geostandards Newsletter: The Journal of Geostandards and Geoanalysis 24, 87–133.

Jochum, K., Hofmann, A., 1995. Contrasting Th/U in historical Mauna Loa and Kilauea lavas. In: Rhodes, J., Lockwood, J. (Eds.), Mauna Loa revealed: structure, composition, and hazards, vol. 92 of Geophysical Monograph. AGU, Washington, D. C, 307–314.

Jochum, K., Seufert, H., Midinet-Best, S., Rettmann, E., Schönberger, K., Zimmer, M., 1988. Multi-element analysis by isotope dilution-spark source-mass spectrometry (ID-SSMS). Fresenius Zeitschrift für Analytische Chemie 331, 104–110.

Jochum, K., Stoll, B., Herwig, K., Amini, M., 2004. Trace element and isotope analyses of geo- and cosmological samples by laser ablation-sector field-ICPMS. In: Douthitt, C. (Ed.), High Resolution ICPMS. ThermoElectron, submitted.

Jochum, K., Stoll, B., Pfänder, J., Seufert, M., Flanz, M., Maissenbacher, P., Hofmann, M., Hofmann, A., 2001. Progress in multi-ion counting spark-source mass spectrometry (MIC-SSMS) for the analysis of geological samples. Fresenius Journal of Analytical Chemistry 370, 647–653.

Johnson, M., Plank, T., 1999. Dehydration and melting experiments constrain the fate of subducted sediments. Geochemistry, Geophysics, Geosystems 1, Paper number 1999GC000014.

Kane, J., Potts, P., 2002. Traceability in geochemical analysis. Geostandards Newsletter: The Journal of Geostandards and Geoanalysis 26, 171–180.

Kay, R., Kay, S., 1993. Delamination and delamination magmatism. Tectonophysics 219, 177–189.

Kelemen, P. B., Yogodzinski, Scholl, D. W., 2003. Along-strike variation in the Aleutian island-arc: Genesis of high Mg# andesite and implication for the continental crust. In: Eiler, J. (Ed.), Inside the subduction factory, vol. 139 of Geophysical Monograph Series. AGU, Washington D.C., 223–276.

Kerl, W., Becker, J., Dietze, H., Dannecker, W., 1997. Isotopic and ultratrace analysis of uranium by double-focusing sector field ICP mass spectrometry. Fresenius Journal of Analytical Chemistry 359, 407–409.

Kogiso, T., Tatsumi, Y., Nakano, S., 1997. Trace element transport during dehydration processes in the subducted crust: 1. Experiments and implications for the origin of ocean island basalts. Earth and Planetary Science Letters 148, 193–205.

Lassiter, J., Hauri, E., 1998. Osmium-isotope variations in Hawaiian lavas: evidence for recycled oceanic lithosphere in the Hawaiian plume. Earth and Planetary Science Letters 164, 483–496.

Le Roex, A. P., Clift, P., Adair, B. J. I., 1990. Tristan da Cunha South Atlantic: geochemistry and petrogenesis of a Basanite-Phonolite lava series. Journal of Petrology 31, 779–812.

LeFevre, B., Pin, C., 2002. Determination of Zr, Hf, Th and U by isotope dilution and inductively coupled plasma-quadrupole mass spectrometry after concomitant separation using extraction chromatography. Geostandards Newsletter: The Journal of Geostandards and Geoanalysis 26, 161–170.

Lichte, F., Meier, A., Crock, J., 1987. Determination of the rare-earth elements in geological materials by inductively coupled plasma mass-spectrometry. Analytical Chemistry 59, 1150–1157.

Longerich, H., 1989. The application of isotope-dilution to inductively coupled plasma-mass spectrometry. Atomic Spectroscopy 10, 112–115.

Longerich, H., Jenner, G., Fryer, B., Jackson, S., 1990. Inductively coupled plasma-mass spectrometric analysis of geological samples - a critical evaluation based on case-studies. Chemical Geology 83, 105–118.

Loss, R., 2003. Atomic weights of the elements 2001 - (IUPAC Technical Report). Pure and Applied Chemistry 75, 1107–1122.

McCulloch, M., Gamble, J., 1991. Geochemical and geodynamical constraints on subduction zone magmatism. Earth and Planetary Science Letters 102, 358–374.

McKenzie, D., O'Nions, R., 1983. Mantle reservoirs and ocean island basalts. Nature 301, 229–231.

Meisel, T., Fellner, N., Moser, J., 2003. A simple procedure for the determination of platinum group elememts and rhenium (Ru, Rh, Pd, Re, Os, Ir, and Pt) using ID-ICP-MS with an inexpensive on-line matrix seperation in geological and environmental materials. Journal of Analytical Atomic Spectrometry 18, 720–726.

Miller, J., Miller, J., 1984. Statistics for analytical chemistry. Ellis Horwood Series in Analytical Chemistry. Ellis Horeood Limited, Chichester.

Moens, L., Jakubowski, N., 1998. Double-focusing mass spectrometers in ICPMS. Analytical Chemistry 70, 251A–256A.

Morris, J. D., Leeman, W. P., Tera, F., 1990. The subducted component in island arc lavas: constraints from Be isotopes and B-Be systematics. Nature 344, 31–36.

Nakamura, Y., Tatsumoto, M., 1988. Pb, Nd, and Sr isotopic evidence for a multicomponent source for rocks of Cook-Austral Islands and heterogeneities of mantle planes. Geochimica et Cosmochimica Acta 52, 2909–2924.

Nichols, G., Wyllie, P., Stern, C., 1994. Subduction zone melting of pelagic sediments constrained by melting experiments. Nature 371, 785–788.

Niu, Y., O'Hara, M., 2003. Origin of ocean island basalts: A new perspective from petrology, geochemistry, and mineral physics consideration. Journal of Geophysical Research 108, Paper number 2002JB002048.

Palacz, Z. A., Saunders, A. D., 1986. Coupled trace element and isotope enrichment in the Cook-Austral-Samoa islands, southwest Pacific. Earth and Planetary Science Letters 79, 270–280.

Pearce, J., Baker, P., Harvey, P., Luff, I., 1995. Geochemical evidence for subduction fluxes, mantle melting and fractional crystallization beneath the South Sandwich island arc. Journal of Petrology 36, 1073–1109.

Pearce, J., Peate, D., 1995. Tectonic implications of the composition of volcanic arc magma. Annual Reviews of Earth and Planetary Science 23, 251–285.

Pearce, N., Perkins, W., Westgate, J., Gorton, M., Jackson, S., Neal, C., Chenery, S., 1997. A compilation of new and published major and trace element data for NIST SRM 610 and NIST SRM 612 glass reference materials. Geostandards Newsletter: The Journal of Geostandards and Geoanalysis 21, 115–144.

Pearson, D. G., Irvine, G. J., Ionov, D. A., Boyd, F. R., Dreibus, G. E., 2004. Re-Os isotope systematics and platinum group element fractionation during mantle melt extraction: a study of massif and xenolith peridotite suites. Chemical Geology 208, 29–59.

Pin, C., LeFevre, B., 2002. Isotope dilution with matrix element removal: A key for high-precision, high-accuracy trace analysis of geological samples using inductively coupled plasma-mass spectrometry. Geostandards Newsletter: The Journal of Geostandards and Geoanalysis 26, 135–148.

Plank, T., Langmuir, C., 1998. The chemical composition of subducting sediment and its consequences for the crust and mantle. Chemical Geology 145, 325–394.

Platzner, I., Becker, J., Dietze, H., 1999. Stability study of isotope ratio measurements for uranium and thorium by ICP-QMS. Atomic Spectroscopy 20, 6–12.

Potts, P., 1997. Geoanalysis: Past, present and future. The Analyst 122, 1179–1186.

Prohaska, T., Hann, S., Latkoczy, C., Stingeder, G., 1999. Determination of rare earth elements U and Th in environmental samples by inductively coupled plasma double focusing sectorfield mass spectrometry (ICP-MS). Journal of Analytical Atomic Spectrometry 14, 1–8.

Raczek, I., Stoll, B., Hofmann, A., Jochum, K., 2001. High-precision trace element data for the USGS reference materials BCR-1, BCR-2, BHVO-1, BHVO-2, AGV-1, AGV-2, DTS-1, DTS-2, GSP-1 and GSP-2 by ID-TIMS and MIC-SSMS. Geostandards Newsletter: The Journal of Geostandards and Geoanalysis 25, 77–86.

Rehkämper, M., Hofmann, A., 1997. Recycled ocean crust and sediment in Indian Ocean MORB. Earth and Planetary Science Letters 147, 93–106.

Reisberg, L., Zindler, A., Marcantonio, F., White, W., Wyman, D., Weaver, B., 1993. Os isotope systematics in ocean island basalts. Earth and Planetary Science Letters 120, 149–167.

Riepe, W., Kaiser, H., 1966. Massenspektrometrische Spurenanalyse von Calcium, Strontium und Barium in Natriumazid durch Isotopenverdünnungstechnik. Fresenius Zeitschrift für Analytische Chemie 223, 321–335.

Robinson, P., Townsend, A., Yu, Z., Münker, C., 1999. Determination of scandium, yttrium and rare earth elements in rocks by high resolution inductively coupled plasma-mass spectrometry. Geostandards Newsletter: The Journal of Geostandards and Geoanalysis 23, 31–46.

Roelandts, I., 1999. GeostandarRef Corner - Geochemical reference sample bibliography for 1999. Geostandards Newsletter: The Journal of Geostandards and Geoanalysis 23, 261–281.

Rosman, K., Taylor, P., 1998. Isotopic compositions of the elements 1997. Pure and Applied Chemistry 70, 217–236.

Roy-Barman, M., Allegre, C. J., 1995. $^{187}Os/^{186}Os$ in oceanic basalts: tracing ocanic crust recycling in the mantle. Earth and Planetary Science Letters 129, 145–161.

Rudnick, R., 1995. Making continental crust. Nature 378, 571–578.

Rudnick, R., Fountain, D., 1995. Nature and composition of the continental crust: a lower crustal perspective. Reviews of Geophysics 33, 267–309.

Rudnick, R., Gao, S., 2004. Composition of the continental crust. In: Rudnick, R. (Ed.), Treatise on Geochemistry, vol. 3, The Crust. Elsevier-Pergamon, Oxford, 1–64.

Salters, V., Stracke, A., 2004. Composition of the depleted mantle. Geochemistry Geophysics Geosystems 5, Paper number 2003GC000597.

Salters, V. J. M., White, W. M., 1998. Hf isotope constraints on mantle evolution. Chemical Geology 145, 447–460.

Shaw, D., Dickin, A., L. H., R. M., Schwarz, H., Truscott, M., 1994. Crustal geochemistry in the Wawa-Foyelet region, Ontario. Canadian Journal of Earth Science 31, 1104–1121.

Stalder, R., Foley, S., Brey, G., Horn, I., 1998. Mineral-aqueous fluid partitioning of trace elements at 900-1200¡C and 3.0-5.7 GPa: New experimental dta for garnet, clinopyroxene, and rutile, and implications for mantle metasomatism. Geochimica et Cosmochimica Acta 62, 1781–1801.

Stanley, S., 1989. Earth and life through time. Freeman and Company, New York.

Staudigel, H., Plank, T., White, W., Schmincke, H., 1996. Geochemical fluxes during seafloor alteration of the basaltic upper crust: DSDP sites 417 and 418. In: Bebout, G., Scholl, D., Kirby, S., Platt, J. (Eds.), Subduction: Top to the Bottom, vol. 96 of Geophysical Monograph Series. AGU, Washington D.C., 19–38.

Stern, C., Kilian, R., 1996. Role of the subducted slab, mantle wedge and continental crust in the generation of adakites from the Andean Austral Volcanic Zone. Contributions to Mineralogy and Petrology 123, 263–281.

Stoll, B., Jochum, K., 1999. MIC-SSMS analyses of eight new geological standard glasses. Fresenius Journal of Analytical Chemistry 364, 380–384.

Stracke, A., Bizimis, M., Salters, V., 2003. Recycling oceanic crust: Quantitative constraints. Geochemistry Geophysics Geosystems 4, Paper number 2001GC000223.

Stracke, A., Hofmann, A., Hart, S., 2005. FOZO, HIMU and the rest of the mantle zoo. Geochemistry, Geophysics, Geosystems , in press.

Stracke, A., Salters, V. J. M., Sims, K. W. W., 1999. Assessing the prescence of garnet-pyroxenite in the mantle sources of basalts through combined hafnium-neodymium-thorium isotope systematics. Geochemistry Geophysics Geosystems 1, Paper number 1999GC000013.

Stracke, A., Willbold, M., Hemond, C., 2004. The origin of EM1 signatures in baslats from Tristan da Cunha and Gough. EOS Transactions AGU 85, Fall Meeting Supplement, Abstract V51B–0565.

Sun, S., McDonough, W., 1989. Chemical and isotopic systematics of oceanic basalts: implications for mantle composition and processes. In: Saunders, A., Norry, M. (Eds.), Magmatism in the Ocean basins, vol. 42 of Special Publication. Geological Society, 313–345.

Tatsumi, Y., 2000. Continental crust formation by crustal delamination in subduction zones and complementary accumulation of the enriched mantle I component in the mantle. Geochemistry, Geophysics, Geosystems 1, Paper number 2000GC000094.

Tatsumi, Y., Kogiso, T., 1997. Trace element transport during dehydration processes in the subducted crust: 2. Origin of chemical and physical characteristics in arc magmatism. Earth and Planetary Science Letters 148, 207–221.

Tatsumoto, M., Nakamura, Y., 1991. DUPAL anomaly in the Sea of Japan: Pb, Nd, and Sr isotope variations at the eastern Eurasian continental margin. Geochimica et Cosmochimica Acta 55, 3697–3708.

Taylor, D., Bievre, P. D., Walder, A., Entwistle, A., 1995. Validation of the analytical linearity and mass discrimination correction model exhibited by a multiple collector inductively coupled plasma mass spectrometer by means of a set of synthetic uranium iostope mixtures. Journal of Analytical Atomic Spectrometry 10, 395–398.

Taylor, R., McLennan, S., 1985. The continental crust: its composition and evlution. Blackwell, Oxford.

Tibi, M., Heumann, K. G., 2003. Muti-element trace determinations in pure alkaline earth fluoride powders by high-resolution ICP-MS using wet-chemical sample preparation and laser ablation. Analytical and Bioanalytical Chemistry 377, 126–131.

Tiepolo, M., Vannucci, R., Oberti, R., Foley, S., Bottazzi, P., Zanetti, A., 2000. Nb and Ta incorporation and fractionation in titanian pargasite and kaersutite: crystal-chemical constraints and implications for natural systems. Earth and Planetary Science Letters 176, 185–201.

Toyoda, K., Tokonami, M., 1990. Diffusion of rare-earth elements in fish teeth from deep-sea sediments. Nature 345, 607–609.

Trueman, C., Tuross, N., 2002. Trace elements in recent and fossil bone apatite. In: M.J. Kohn, J. R., Hughes, J. (Eds.), Phosphates - geochemical, geobiological, and materials importance, vol. 48 of Reviews in Mineralogy and Geochemistry. Mineralogical Society of America, Washington D.C., 489– 521.

Uyeda, S., 1982. Subduction zones: an introduction to comparative subductology. Tectonophysics 81, 133–159.

Vanhaecke, F., Moens, L., Dams, R., Taylor, P., 1996. Precise measurement of isotope ratios with a double-focusing magnetic sector ICP mass spectrometer. Analytical Chemistry 68, 567–569.

Vannucchi, P., Galeotti, S., Clift, P., Ranero, C., von Huene, R., 2004. Long-term subductio-erosion along the Guatemalan margin of the Middle America Trench. Geology 32, 617–620.

Vidal, P., Chauvel, C., Brousse, R., 1984. Large mantle heterogenity beneath french Polynesia. Nature 307, 536–538.

Villaseca, C., Downes, H., Pin, C., Barbero, L., 1999. Nature and composition of the lower continenatl crust in central Spain and the granulite-granite linkage: inferences from granulitic xenoliths. Journal of Petrology 40, 1465–1496.

von Huene, R., Ranero, C., Vannucchi, P., 2004. Generic model of subduction erosion. Geology 32, 913–916.

Weaver, B., 1991a. The origin of oceanic island basalt end-member compositions: trace element and isotopic constraints. Earth and Planetary Science Letters 104, 381–397.

Weaver, B., 1991b. Trace element evidence for the origin of ocean-island basalts. Geology 19, 123–126.

Weaver, B., Tarney, J., 1984. Empirical approach to estimating the composition of the continental crust. Nature 310, 575–577.

Weis, D., Frey, F. A., Leyrit, H., Gautier, I., 1993. Kerguelen Archipelago revisited: geochemical and isotopic study of the Southeast Province lavas. Earth and Planetary Science Letters 118, 101–119.

Weyer, S., Münker, C., Rehkämper, M., Mezger, K., 2002. Determination of ultra-low Nb, Ta. Zr and Hf concentrations and the chondritic Zr/Hf and Nb/Ta ratios by isotope dilution analyses with multiple collector ICP-MS. Chemical Geology 187, 295–313.

White, W., 1985. Sources of oceanic basalts: radiogenic isotopic evidence. Geology 13, 115–118.

White, W., Duncan, R., 1996. Geochemistry and geochronology of the Society islands: new evidence for deep mantle recycling. In: Basu, A., Hart, S. (Eds.), Earth processes: reading the isotopic code, vol. 95 of Geophysical Monograph. AGU, Washington, D. C, 183–206.

White, W., Dupré, B., 1986. Sediment subduction and magma genesis in the Lesser Antilles: isotopic and trace element constraints. Journal of Geophysical Research 91, 5927–5941.

White, W., Hofmann, A., 1982. Sr and Nd isotope geochemistry of oceanic basalts and mantle evolution. Nature 296, 821–825.

Wilson, S., 2005. *http* : *//minerals.cr.usgs.gov/geo_chem_stand.*

Woodhead, J., Hergt, J., 2000. Pb-isotope analyses of USGS reference materials. Geostandards Newsletter: The Journal of Geostandards and Geoanalysis 24, 33–38.

Woodhead, J. D., Devey, C., 1993. Geochemistry of the Pitcairn seamount, I: source character and temporal trends. Earth and Planetary Science Letters 116, 81–99.

Woodhead, J. D., McCulloch, M. T., 1989. Ancient seafloor signals in Pitcairn island lavas and evidence for large amplitude, small length-scale mantle heterogeneities. Earth and Planetary Science Letters 94, 257–273.

Workman, R., Hart, S., Jackson, M., Regelous, M., Farley, K., Blusztajn, J., Kurz, M., Staudigel, H., 2004. Recycled metasomatized lithosphere as the origin of the Enriched Mantle II (EM2) end-member: Evidence from the Samoan Volcanic Chain. Geochemistry Geophysics Geosystems 5, Paper number 2003GC000623.

Wright, E., White, W. M., 1987. The origin of Samoa: new evidence from Sr, Nd, and Pb isotopes. Earth and Planetary Science Letters 81, 151–162.

Xie, Q., Kerrich, R., 1995. Application of isotope-dilution for precise measurement of Zr and Hf in low-abundance samples and international reference materials by inductively-coupled plasma-mass Spectrometry - Implications for Zr (Hf) REE fractionations in komatiites. Chemical Geology 123, 17–27.

Zindler, A., Hart, S., 1986. Chemical geodynamics. Annual review of Earth and Planetary Science 14, 493–571.

A Trace element data for reference material BHVO-1

Trace element concentrations [$\mu g\ g^{-1}$] obtained from five independent measurements (spiking and digestion) in the basaltic USGS reference material BHVO-1. The mean and RSD (in %) of triplicate analysis as well as overall mean and RSD are shown. Europium concentration in parenthesis has been excluded from calculation of mean and RSD. Reference values from Raczek et al. [2001], Jochum et al. [2001], and Govindaraju [1994]. Continued.

El.	BHVO-1 (1)					BHVO-1 (2)				
	1	2	3	Mean	RSD	1	2	3	Mean	RSD
Rb	8.44	8.43	8.44	**8.44**	0.1	8.22	8.23	8.25	**8.23**	0.2
Sr	393	393	392	**393**	0.2	393	395	396	**395**	0.3
Y	26.4	26.3	26.4	**26.3**	0.2	26.4	26.4	26.2	**26.4**	0.4
Zr	173	173	173	**173**	0.1	175	176	175	**176**	0.3
Nb	17.7	17.7	17.7	**17.7**	0.1	17.9	18.1	17.9	**17.9**	0.5
Cs	0.101	0.102	0.102	**0.102**	0.4	0.134	0.135	0.133	**0.134**	0.8
Ba	131	131	132	**131**	0.4	133	133	132	**133**	0.4
La	15.3	15.4	15.3	**15.3**	0.4	15.6	15.5	15.5	**15.5**	0.4
Ce	37.7	37.8	37.6	**37.7**	0.3	38.0	37.8	37.8	**37.9**	0.3
Pr	5.27	5.27	5.28	**5.27**	0.1	5.35	5.31	5.33	**5.33**	0.3
Nd	24.6	24.6	24.5	**24.6**	0.4	24.9	24.8	24.8	**24.8**	0.2
Sm	6.12	6.05	6.09	**6.09**	0.6	6.20	6.21	6.18	**6.20**	0.3
Eu	(2.78)	2.10	2.03	**2.07**	2.3	2.13	2.08	2.06	**2.09**	1.8
Gd	6.50	6.54	6.52	**6.52**	0.3	6.17	6.18	6.07	**6.14**	1.0
Tb	0.945	0.978	0.968	**0.964**	1.8	0.951	0.951	0.933	**0.945**	1.1
Dy	5.55	5.59	5.51	**5.55**	0.8	5.26	5.37	5.24	**5.29**	1.3
Ho	0.949	0.946	0.945	**0.947**	0.3	0.980	0.951	0.958	**0.963**	1.6
Er	2.56	2.51	2.55	**2.54**	1.0	2.52	2.49	2.55	**2.52**	1.2
Tm	0.336	0.333	0.334	**0.334**	0.4	0.330	0.327	0.326	**0.328**	0.7
Yb	2.00	2.02	2.04	**2.02**	1.1	1.95	1.94	1.91	**1.93**	1.2
Lu	0.277	0.268	0.278	**0.274**	1.9	0.261	0.265	0.257	**0.261**	1.5
Hf	4.28	4.21	4.21	**4.23**	0.9	4.25	4.23	4.26	**4.25**	0.3
Ta	1.19	1.17	1.18	**1.18**	0.8	1.16	1.12	1.13	**1.14**	1.6
Pb	2.09	2.11	2.10	**2.10**	0.4	2.10	2.11	2.10	**2.10**	0.2
Th	1.21	1.21	1.21	**1.21**	0.2	1.21	1.21	1.22	**1.21**	0.4
U	0.406	0.406	0.404	**0.406**	0.3	0.412	0.413	0.412	**0.412**	0.2

El.	BHVO-1 (3)					BHVO-1 (4)					BHVO-1 (5)					BHVO-1		
	1	2	3	Mean	RSD	1	2	3	Mean	RSD	1	2	3	Mean	RSD	Mean	RSD	Ref
Rb	8.07	8.20	8.31	**8.19**	1.5	7.91	7.93	7.93	**7.92**	0.2	8.50	8.56	8.52	**8.52**	0.3	**8.26**	2.9	9.31
Sr	397	398	396	**397**	0.2	394	395	394	**394**	0.2	398	399	398	**398**	0.1	**395**	0.5	396
Y	26.6	26.4	26.6	**26.5**	0.5	26.4	26.4	26.4	**26.4**	0.1	26.4	26.6	26.7	**26.5**	0.5	**26.4**	0.4	27.6
Zr	174	174	174	**174**	0.2	175	175	175	**175**	0.1	173	175	175	**174**	0.6	**174**	0.6	175
Nb	17.7	17.8	17.9	**17.8**	0.5	17.9	17.9	17.9	**17.9**	0.1	17.8	17.9	17.9	**17.9**	0.3	**17.8**	0.6	18.2
Cs	0.090	0.091	0.093	**0.091**	1.9	0.089	0.088	0.089	**0.089**	0.4	0.097	0.097	0.095	**0.096**	1.1	**0.102**	18	-
Ba	132	132	133	**132**	0.2	133	133	133	**133**	0.2	134	133	131	**133**	1.1	**132**	0.6	133
La	15.3	15.4	15.2	**15.3**	0.7	15.3	15.4	15.4	**15.4**	0.3	15.3	15.4	15.5	**15.4**	0.5	**15.4**	0.5	15.5
Ce	37.7	38.0	37.6	**37.8**	0.6	37.9	38.0	38.2	**38.0**	0.3	37.9	38.0	38.4	**38.1**	0.7	**37.9**	0.4	38.0
Pr	5.25	5.33	5.28	**5.29**	0.8	5.28	5.33	5.33	**5.31**	0.5	5.31	5.30	5.37	**5.32**	0.8	**5.30**	0.5	5.33
Nd	24.5	24.8	24.7	**24.7**	0.6	24.6	24.6	24.8	**24.7**	0.5	24.8	24.8	25.0	**24.9**	0.5	**24.7**	0.6	24.8
Sm	6.11	6.09	6.12	**6.11**	0.2	6.09	6.09	6.12	**6.10**	0.2	6.16	6.20	6.17	**6.18**	0.3	**6.13**	0.8	6.12
Eu	2.11	2.11	2.14	**2.12**	0.9	2.17	2.13	2.17	**2.15**	1.2	2.12	2.05	2.10	**2.09**	1.7	**2.10**	1.6	2.10
Gd	6.50	6.38	6.35	**6.41**	1.2	6.47	6.43	6.47	**6.46**	0.4	6.41	6.36	6.50	**6.42**	1.1	**6.39**	2.3	6.26
Tb	0.956	0.973	0.957	**0.962**	1.0	0.980	0.964	0.949	**0.964**	1.6	0.964	0.954	0.958	0.959	0.5	**0.959**	0.8	0.954
Dy	5.29	5.41	5.36	**5.35**	1.1	5.45	5.35	5.35	**5.38**	1.0	5.32	5.37	5.33	**5.34**	0.6	**5.38**	1.8	5.30
Ho	0.966	0.973	0.960	**0.967**	0.7	0.977	0.977	0.971	**0.975**	0.4	0.993	0.995	0.990	**0.993**	0.2	**0.969**	1.7	0.99
Er	2.54	2.55	2.50	**2.53**	1.1	2.60	2.54	2.58	**2.58**	1.2	2.56	2.56	2.53	**2.55**	0.7	**2.54**	0.9	2.56
Tm	0.312	0.313	0.316	**0.314**	0.7	0.317	0.320	0.323	**0.320**	1.0	0.338	0.342	0.340	**0.340**	0.5	**0.327**	3.2	0.33
Yb	2.00	2.04	2.01	**2.02**	0.9	2.00	1.99	1.99	**1.99**	0.4	2.01	2.00	2.01	**2.01**	0.2	**1.99**	1.8	2.04
Lu	0.273	0.278	0.273	**0.275**	0.9	0.274	0.275	0.270	**0.273**	1.0	0.268	0.271	0.272	**0.270**	0.8	**0.271**	2.1	0.271
Hf	4.30	4.30	4.28	**4.29**	0.2	4.25	4.24	4.21	**4.23**	0.5	4.30	4.28	4.26	**4.28**	0.5	**4.26**	0.7	4.3
Ta	1.20	1.19	1.19	**1.19**	0.3	1.17	1.18	1.17	**1.17**	0.5	1.19	1.19	1.18	**1.19**	0.7	**1.17**	1.9	1.18
Pb	2.15	2.17	2.17	**2.16**	0.6	2.14	2.12	2.13	**2.13**	0.5	2.15	2.17	2.15	**2.16**	0.6	**2.13**	1.4	2.1
Th	1.25	1.25	1.25	**1.25**	0.3	1.22	1.22	1.22	**1.22**	0.3	1.25	1.24	1.25	**1.24**	0.6	**1.23**	1.5	1.22
U	0.412	0.407	0.412	**0.410**	0.7	0.408	0.405	0.409	**0.407**	0.5	0.406	0.410	0.409	**0.408**	0.6	**0.409**	0.6	0.410

B Trace element data for geological reference materials

Trace element concentrations [$\mu g\ g^{-1}$] in geological reference materials. The mean and RSD (%) of three to four independent measurements (spiking and digestion) as well as the overall mean and RSD are shown. One digestion of the new USGS reference glasses BCR-2G, BHVO-2G and BIR-1G and the NIST SRM 612 has been prepared and measured three to four times. Continued.

El.	**AGV-1** [a,b]						**AGV-2** [a]					
	1	**2**	**3**	**mean**	**RSD**	**Ref**	**1**	**2**	**3**	**mean**	**RSD**	**Ref**
Rb	69.8	66.1	65.8	**67.2**	3.3	66.6	67.1	63.4	65.5	**65.4**	2.8	66.3
Sr	654	649	654	**652**	0.4	660	659	657	655	**657**	0.4	661
Y	18.4	18.4	18.2	**18.3**	0.5	20	20.7	20.1	20.8	**20.5**	1.8	-
Zr	234	231	234	**233**	0.7	227	239	241	240	**240**	0.5	-
Nb	14.8	14.5	14.8	**14.7**	1.2	15	14.5	14.7	14.5	**14.6**	0.9	-
Cs	1.31	1.27	1.30	**1.29**	1.6	1.28	1.32	1.31	1.3	**1.31**	0.5	-
Ba	1233	1252	1238	**1241**	0.8	1200	1163	1140	1159	**1154**	1.1	1130
La	38.0	39.4	37.9	**38.4**	2.2	38.2	37.5	38.1	37.8	**37.8**	0.9	37.9
Ce	66.3	66.5	65.6	**66.1**	0.7	67.6	66.9	68.1	67.3	**67.4**	0.9	68.6
Pr	7.62	7.72	7.66	**7.67**	0.7	7.80	7.55	7.59	7.56	**7.57**	0.3	7.68
Nd	32.1	32.6	32.2	**32.3**	0.8	31.7	30.1	30.5	30.1	**30.2**	0.7	30.5
Sm	5.76	5.77	5.80	**5.78**	0.4	5.72	5.31	5.46	5.31	**5.36**	1.6	5.49
Eu	1.57	1.60	1.61	**1.59**	1.5	1.58	1.49	1.49	1.49	**1.49**	0.1	1.53
Gd	4.68	4.72	4.68	**4.70**	0.4	4.70	4.49	4.54	4.49	**4.51**	0.7	4.52
Tb	0.712	0.713	0.713	**0.712**	0.1	0.708	0.637	0.629	0.642	**0.636**	1.1	0.641
Dy	3.58	3.60	3.59	**3.59**	0.3	3.55	3.47	3.38	3.45	**3.43**	1.4	3.47
Ho	0.664	0.680	0.674	**0.673**	1.2	0.685	0.648	0.644	0.662	**0.651**	1.4	0.653
Er	1.80	1.85	1.83	**1.83**	1.5	1.82	1.82	1.80	1.84	**1.82**	1.3	1.81
Tm	0.269	0.264	0.27	**0.266**	1.0	0.282	0.265	0.270	0.265	**0.267**	1.1	0.259
Yb	1.65	1.66	1.68	**1.66**	0.7	1.63	1.62	1.64	1.59	**1.62**	1.4	1.62
Lu	0.254	0.261	0.261	**0.259**	1.5	0.244	0.248	0.260	0.245	**0.251**	3.1	0.247
Hf	4.94	4.89	4.97	**4.94**	0.9	5.1	5.04	5.02	5.05	**5.04**	0.3	-
Ta	0.833	0.817	0.838	**0.829**	1.4	0.90	0.832	(1.01)	0.830	**0.831**	0.2	-
Pb	34.7	32.8	33.8	**33.8**	2.8	36	14.2	14.2	14.3	**14.2**	0.4	-
Th	6.31	6.39	6.26	**6.32**	1.0	6.5	6.18	6.10	6.19	**6.16**	0.8	-
U	1.85	1.85	1.85	**1.85**	0.1	1.92	1.82	1.80	1.81	**1.81**	0.6	-

Reference values from [a] Raczek et al. [2001], [b] Govindaraju [1994]

El.	BCR-1 [a,b,c]						BCR-2 [a,c]						BHVO-2 [a,b,c]					
	1	**2**	**3**	**Mean**	**RSD**	**Ref**	**1**	**2**	**3**	**Mean**	**RSD**	**Ref**	**1**	**2**	**3**	**Mean**	**RSD**	**Ref**
Rb	50.4	50.3	48.0	**49.6**	2.8	47	47.2	46.8	47.9	**47.3**	1.2	46.9	8.84	8.54	8.31	**8.56**	3.1	9.08
Sr	334	332	336	**334**	0.6	332	340	339	339	**339**	0.2	340	396	396	390	**394**	0.9	396
Y	37.9	37.3	36.2	**37.1**	2.3	37.9	33.8	36.0	36.1	**35.3**	3.8	-	29.3	28.9	29.1	**29**	0.7	29
Zr	186	186	187	**186**	0.5	189	174	188	190	**184**	4.6	-	172	172	171	**172**	0.2	170
Nb	13.3	13.0	12.9	**13.0**	1.6	13.5	12.0	12.8	12.7	**12.5**	3.2	-	18.6	18.4	19.6	**8.9**	3.2	18.0
Cs	0.989	0.949	0.951	**0.963**	2.4	0.96	1.06	1.04	1.11	**1.07**	3.3	-	-	-	-	-	-	-
Ba	697	698	705	**700**	0.6	682	688	687	686	**687**	0.1	677	131	131	131	**131**	0.0	131
La	24.9	25.1	25.6	**25.2**	1.4	25.1	25.4	25.4	26.0	**25.6**	1.2	24.9	15.3	15.3	15.3	**15.3**	0.3	15.2
Ce	54.2	54.6	55.7	**54.8**	1.5	53.3	55.2	55.0	55.6	**55.3**	0.5	52.9	37.3	37.8	37.6	**37.6**	0.6	37.5
Pr	6.85	6.80	6.90	**6.85**	0.7	6.79	6.76	6.73	6.80	**6.76**	0.5	6.57	5.34	5.33	5.26	**5.31**	0.8	5.29
Nd	28.7	28.6	29.0	**28.8**	0.7	29.0	28.5	28.4	28.7	**28.6**	0.5	28.7	24.6	24.6	24.3	**24.5**	0.8	24.5
Sm	6.51	6.52	6.59	**6.54**	0.6	6.61	6.43	6.40	6.41	**6.41**	0.2	6.57	6.05	6.02	6.06	**6.04**	0.3	6.07
Eu	2.10	1.98	2.10	**2.06**	3.5	1.97	2.10	2.06	2.01	**2.06**	2.3	1.96	2.08	2.04	2.01	**2.05**	1.7	2.07
Gd	6.72	6.80	6.63	**6.71**	1.2	6.7	6.63	6.67	6.73	**6.68**	0.8	6.75	6.19	6.29	6.21	**6.23**	0.8	6.24
Tb	1.08	1.08	1.05	**1.07**	1.6	1.07	1.05	1.06	1.06	**1.06**	0.4	1.07	0.937	0.941	0.921	**0.933**	1.1	0.936
Dy	6.53	6.64	6.26	**6.48**	3.0	6.43	6.33	6.37	6.28	**6.33**	0.7	6.41	5.23	5.30	5.35	**5.29**	1.2	5.31
Ho	1.32	1.25	1.28	**1.29**	2.9	1.27	1.29	1.25	1.23	**1.26**	2.4	1.3	0.953	0.967	0.971	**0.964**	1.0	0.972
Er	3.80	3.64	3.68	**3.71**	2.3	3.68	3.65	3.66	3.56	**3.62**	1.6	3.66	2.50	2.46	2.50	**2.49**	0.8	2.54
Tm	0.529	0.521	0.524	**0.525**	0.8	0.542	0.516	0.515	0.506	**0.512**	1.1	0.564	0.312	0.322	0.329	**0.321**	2.7	0.341
Yb	3.25	3.36	3.30	**3.30**	1.6	3.4	3.27	3.38	3.42	**3.36**	2.4	3.38	1.92	1.92	2.00	**1.95**	2.4	2.00
Lu	0.481	0.508	0.495	**0.495**	2.7	0.501	0.508	0.505	0.498	**0.504**	1.0	0.519	0.264	0.271	0.273	**0.269**	1.8	0.274
Hf	4.62	4.67	4.67	**4.65**	0.7	4.9	4.69	4.66	4.85	**4.74**	2.1	4.9	4.20	4.20	4.19	**4.20**	0.1	4.2
Ta	0.740	0.731	0.735	**0.735**	0.6	0.79	0.733	0.725	0.760	**0.740**	2.5	-	1.05	1.05	1.15	**1.08**	5.4	1.14
Pb	15.0	14.9	14.9	**15.0**	0.1	13.6	10.9	11.0	11.0	**12.0**	0.5	13	1.80	1.79	1.81	**1.80**	0.6	2.09
Th	5.30	5.31	5.25	**5.28**	0.6	5.8	5.22	5.29	5.19	**5.23**	1.0	5.7	1.12	1.13	1.15	**1.13**	1.3	1.16
U	1.63	1.63	1.65	**1.64**	0.9	1.76	1.63	1.62	1.64	**1.63**	0.5	1.64	0.404	0.403	0.403	**0.403**	0.2	0.404

Reference values from [a] Raczek et al. [2001], [b] Govindaraju [1994], [c] Jochum et al. [2001]

El.	G-2 [b]						JR-1 [b]						KL2-G [d]					
	1	**2**	**3**	**Mean**	**RSD**	**Ref**	**1**	**2**	**3**	**Mean**	**RSD**	**Ref**	**1**	**2**	**3**	**Mean**	**RSD**	**Ref**
Rb	171	173	171	**172**	0.8	170	257	256	264	**259**	1.6	257	8.67	9.02	8.38	**8.69**	3.7	8.9
Sr	467	482	482	**477**	1.8	478	28.6	28.4	28.6	**28.5**	0.4	30	369	367	381	**372**	2.0	364
Y	9.31	9.29	9.18	**9.24**	0.8	11	42.3	42.1	41.4	**41.9**	1.1	45.4	27.0	27.9	27.4	**27.4**	1.6	26.8
Zr	342	302	301	**315**	7.3	309	98.8	99.0	98.6	**98.8**	0.2	101	161	161	159	**160**	0.7	159
Nb	12.3	10.7	10.6	**11.2**	8.4	12	15.8	15.7	15.4	**15.6**	1.4	15.5	15.6	15.2	14.6	**15.2**	3.3	15.8
Cs	1.31	1.33	1.33	**1.32**	0.9	1.34	20.1	20.7	20.8	**20.6**	1.8	20.2	0.128	0.126	0.125	**0.126**	1.1	0.12
Ba	1907	1927	1918	**1917**	0.5	1882	47.6	47.4	47.5	**47.5**	0.2	40	125	125	126	**125**	0.5	123
La	-	88	88	**88**	-	89	18.9	18.8	18.8	**18.8**	0.3	19.7	13.1	13.1	13.2	**13.1**	0.5	13.2
Ce	-	178	176	**177**	-	160	45.8	45.7	45.5	**45.7**	0.3	47.1	33.0	32.9	33.3	**33.1**	0.6	32.9
Pr	17.4	16.8	16.7	**17.0**	2.3	18	5.92	5.87	5.85	**5.88**	0.7	5.62	4.64	4.63	4.73	**4.67**	1.1	4.71
Nd	53.0	54.7	54.5	**54.0**	1.7	55	23.8	23.5	23.6	**23.6**	0.5	23.5	22.1	22.2	21.9	**22.1**	0.6	21.7
Sm	7.07	7.19	7.13	**7.13**	0.8	7.2	5.74	5.75	5.72	**5.74**	0.3	6.07	5.59	5.62	5.67	**5.63**	0.7	5.55
Eu	1.33	1.32	1.38	**1.34**	2.2	1.4	0.271	0.263	0.269	**0.267**	1.5	0.3	1.95	1.93	2.04	**1.97**	3.1	1.95
Gd	4.08	4.03	4.12	**4.08**	1.1	4.3	5.95	5.84	5.77	**5.85**	1.5	5.24	6.07	6.12	6.00	**6.06**	1.0	6.1
Tb	0.514	0.512	0.510	**0.512**	0.4	0.48	1.12	1.15	1.13	**1.13**	1.5	1.02	0.945	0.947	0.933	**0.942**	0.8	0.93
Dy	2.23	2.20	2.28	**2.24**	1.7	2.4	6.42	6.60	6.39	**6.47**	1.7	5.78	5.46	5.40	5.34	**5.40**	1.1	5.35
Ho	0.359	0.357	0.353	**0.356**	0.9	0.4	1.30	1.30	1.30	**1.30**	0.0	1.1	0.978	0.932	0.973	**0.961**	2.6	0.99
Er	0.910	0.903	0.899	**0.904**	0.6	0.92	4.14	4.08	4.12	**4.11**	0.7	3.78	2.57	2.59	2.63	**2.60**	1.2	2.64
Tm	0.127	0.125	0.122	**0.125**	2.2	0.18	0.641	0.632	0.645	**0.639**	1.1	0.67	0.332	0.329	0.340	**0.334**	1.6	0.336
Yb	0.713	0.713	0.709	**0.712**	0.3	0.8	4.75	4.84	4.63	**4.74**	2.2	4.49	2.06	2.08	2.12	**2.09**	1.6	2.13
Lu	0.102	0.099	0.096	**0.099**	3.1	0.11	0.728	0.730	0.705	**0.721**	1.9	0.71	0.287	0.272	0.281	**0.280**	2.7	0.296
Hf	7.79	6.83	6.93	**7.18**	7.3	7.9	4.67	4.72	4.68	**4.69**	0.6	4.67	3.95	3.96	4.02	**3.98**	1.0	4.14
Ta	0.921	0.791	0.785	**0.833**	9.2	0.88	1.76	1.75	1.74	**1.75**	0.6	1.9	0.926	0.926	0.956	**0.936**	1.9	0.97
Pb	34.6	31.9	34.2	**33.1**	5.0	30	19.8	20.0	20.5	**20.1**	1.6	19.1	2.09	2.08	2.08	**2.08**	0.2	2.2
Th	23.1	21.9	23.2	**22.6**	4.1	24.7	23.8	23.6	23.7	**23.7**	0.5	26.5	1.00	1.02	1.03	**1.02**	1.3	1.03
U	-	2.21	2.18	**1.92**	-	2.07	8.48	8.40	8.50	**8.46**	0.7	9	0.537	0.538	0.540	**0.538**	0.2	0.55

Reference values from [b] Govindaraju [1994], [d] Jochum et al. [2000]

El.	ML3B-G [d]						NIST SRM 612 [e]						BIR-1 [b,c,f]						
	1	2	3	Mean	RSD	Ref	1	2	3	Mean	RSD	Ref	1	2	3	4	Mean	RSD	Ref
Rb	5.78	5.88	5.50	**5.72**	3.5	5.8	-	-	-	-	-	-	-	-	-	-	-	-	-
Sr	315	324	317	**318**	1.5	315	78.8	77.9	78.5	**78.4**	0.5	76.15	110	111	108	108	**109**	1.3	108
Y	24.1	24.1	24.8	**24.3**	1.7	24.3	38.2	38.2	36.1	**38.2**	3.3	38.25	15.4	15.5	14.8	15.1	**15.2**	2.0	16
Zr	131	131	132	**131**	0.3	126	-	-	-	-	-	-	17.9	17.9	18.7	18.7	**18.3**	2.4	15.5
Nb	7.85	7.84	8.21	**7.97**	2.7	9.0	-	-	-	-	-	-	0.536	0.533	0.527	0.557	**0.538**	2.4	0.6
Cs	0.163	0.162	0.161	**0.162**	0.8	0.14	41.6	40.2	41.8	**40.9**	2.1	41.64	-	-	-	-	-	-	-
Ba	82.3	82.1	80.1	**81.5**	1.5	80	38.2	37.6	37.8	**37.9**	0.7	37.74	6.81	6.76	6.67	6.66	**6.73**	1.1	7
La	9.16	9.00	8.91	**9.02**	1.4	8.96	35.7	35.4	35.7	**35.5**	0.4	35.77	0.615	0.613	0.593	0.594	**0.604**	2.0	0.609
Ce	23.6	23.4	23.3	**23.4**	0.5	23.3	35.2	34.9	35.2	**35.1**	0.5	38.35	1.92	1.91	1.85	1.86	**1.89**	1.9	1.897
Pr	3.45	3.51	3.37	**3.44**	2.0	3.47	36.8	36.5	36.8	**36.6**	0.4	37.16	0.380	0.379	0.368	0.368	**0.374**	1.8	0.368
Nd	17.1	17.3	17.3	**17.2**	0.6	16.8	35.8	35.5	35.8	**35.6**	0.5	35.24	2.39	2.38	2.34	2.34	**2.37**	1.1	2.380
Sm	4.77	4.78	4.82	**4.79**	0.5	4.79	37.0	37.1	37.1	**37.1**	0.2	36.72	1.10	1.11	1.08	1.08	**1.09**	1.4	1.100
Eu	1.66	1.65	1.63	**1.65**	1.0	1.68	34.9	35.7	34.5	**35.3**	1.7	34.44	0.503	0.498	0.513	0.519	**0.508**	1.9	0.518
Gd	5.23	5.24	5.36	**5.28**	1.4	5.23	39.2	39.4	38.3	**39.3**	1.4	36.95	1.77	1.78	1.80	1.80	**1.79**	0.9	1.874
Tb	0.813	0.854	0.781	**0.816**	4.5	0.82	-	-	-	-	-	-	0.397	0.399	0.405	0.397	**0.399**	0.9	0.36
Dy	4.77	4.88	4.89	**4.85**	1.3	4.81	35.8	35.9	36.1	**35.8**	0.4	35.97	2.52	2.49	2.53	2.52	2.52	0.7	2.562
Ho	0.915	0.906	0.927	**0.916**	1.2	0.91	37.6	37.8	38.1	**37.7**	0.7	37.87	0.555	0.561	0.560	0.563	**0.559**	0.6	0.57
Er	2.43	2.40	2.43	**2.42**	0.7	2.46	36.9	37.9	37.6	**37.4**	1.3	37.43	1.66	1.68	1.68	1.68	**1.68**	0.6	1.742
Tm	0.324	0.320	0.324	**0.323**	0.7	0.326	36.4	37.4	36.9	**36.9**	1.2	37.55	0.234	0.241	0.243	0.244	**0.240**	1.8	0.26
Yb	2.05	2.00	2.06	**2.04**	1.6	2.05	39.7	38.9	40.2	**39.3**	1.7	39.95	1.61	1.59	1.63	1.63	**1.62**	1.1	1.651
Lu	0.265	0.281	0.280	**0.275**	3.2	0.286	37.2	36.7	38.0	**36.9**	1.8	37.71	0.240	0.242	0.245	0.240	**0.241**	1.0	0.2461
Hf	3.22	3.23	3.25	**3.23**	0.4	3.32	-	-	-	-	-	-	0.567	0.570	0.562	0.570	**0.567**	0.6	0.6
Ta	0.546	0.546	0.577	**0.556**	3.2	0.55	-	-	-	-	-	-	0.090	0.090	0.091	0.098	**0.092**	4.3	0.04
Pb	1.40	1.40	1.39	**1.40**	0.5	1.45	-	-	-	-	-	-	3.28	3.28	3.27	3.23	**3.26**	0.7	3.4
Th	0.535	0.536	0.531	**0.534**	0.5	0.54	-	-	-	-	-	-	0.032	0.031	0.031	0.030	**0.031**	2.2	0.03
U	0.431	0.433	0.427	**0.430**	0.7	0.44	-	-	-	-	-	-	0.010	0.010	0.010	0.009	**0.010**	4.4	0.01

Reference values from [b] Govindaraju [1994], [c] Jochum et al. [2001], [d] Jochum et al. [2000], [e] Pearce et al. [1997], [f] Baker et al. [2002]

El.	OU-6					BCR-2						BHVO-2					
	1	2	3	Mean	RSD	1	2	3	4	Mean	RSD	1	2	3	4	Mean	RSD
Rb	126	125	119	**123**	3.1	45.6	45.8	45.9	45.8	**45.8**	0.3	8.30	8.74	8.77	8.77	**8.60**	3.0
Sr	140	140	136	**139**	1.4	339	337	339	337	**338**	0.3	394	395	394	394	**394**	0.1
Y	30.1	30.0	29.5	**29.9**	1.1	36.2	35.9	36.3	36.1	**36.1**	0.5	29.3	29.2	29.1	29.1	**29.2**	0.4
Zr	182	183	178	181	1.5	187	189	187	188	**188**	0.4	172	172	171	172	**172**	0.1
Nb	15.2	15.1	14.6	**15.0**	2.2	12.3	12.3	12.2	12.2	**12.3**	0.3	18.2	18.2	18.1	18.1	**18.2**	0.5
Cs	9.32	9.22	9.50	**9.35**	1.5	1.19	1.18	1.18	1.18	**1.18**	0.5	0.102	0.102	0.102	0.102	**0.102**	0.1
Ba	500	499	494	**498**	0.7	687	682	686	681	**684**	0.4	132	131	132	132	**132**	0.5
La	33.1	33.3	33.4	**33.3**	0.4	24.9	24.8	24.9	24.6	**24.8**	0.5	15.1	15.0	15.1	15.1	**15.1**	0.1
Ce	80.0	80.4	79.6	**80.0**	0.5	52.2	52.2	52.1	52.0	**52.1**	0.2	36.7	36.8	36.7	36.9	**36.8**	0.1
Pr	8.32	8.31	8.23	**8.29**	0.6	6.79	6.77	6.77	6.75	**6.77**	0.3	5.27	5.31	5.26	5.28	**5.28**	0.4
Nd	31.8	31.8	31.6	**31.7**	0.4	28.6	28.4	28.7	28.4	**28.5**	0.6	24.4	24.4	24.4	24.4	**24.4**	0.1
Sm	6.26	6.21	6.14	**6.20**	0.9	6.48	6.47	6.47	6.45	**6.47**	0.2	5.98	6.00	6.00	5.96	**5.99**	0.2
Eu	1.40	1.41	1.41	**1.40**	0.4	1.97	1.99	1.99	1.94	**1.97**	1.2	2.12	2.09	2.10	2.05	**2.11**	0.6
Gd	5.65	5.49	5.41	**5.52**	2.2	6.49	6.74	6.74	6.49	**6.62**	2.2	5.92	6.03	5.94	5.92	**5.96**	1.0
Tb	0.938	0.957	0.941	**0.945**	1.1	1.10	1.11	1.09	1.10	**1.10**	0.7	0.945	0.939	0.940	0.948	**0.941**	0.3
Dy	5.34	5.24	5.12	**5.23**	2.1	6.35	6.36	6.36	6.51	**6.40**	1.2	5.19	5.15	5.24	5.07	**5.19**	0.9
Ho	1.01	1.04	1.04	**1.03**	1.3	1.27	1.28	1.28	1.28	**1.28**	0.5	0.952	1.007	0.990	0.973	**0.983**	2.9
Er	2.97	3.05	3.03	**3.02**	1.4	3.65	3.73	3.73	3.66	**3.69**	1.1	2.54	2.60	2.56	2.46	**2.57**	1.3
Tm	0.455	0.477	0.468	**0.467**	2.3	0.514	0.508	0.508	0.517	**0.51**	0.9	0.322	0.339	0.322	0.311	**0.328**	3.1
Yb	3.11	3.03	3.09	**3.07**	1.3	3.33	3.53	3.53	3.34	**3.43**	3.3	1.92	1.88	1.94	1.93	**1.91**	1.6
Lu	0.471	0.474	0.474	**0.473**	0.3	0.496	0.500	0.500	0.492	**0.497**	0.7	0.268	0.260	0.265	0.260	**0.264**	1.6
Hf	4.68	4.68	4.63	**4.66**	0.7	4.70	4.72	4.70	4.72	**4.71**	0.2	4.20	4.26	4.20	4.27	**4.22**	0.9
Ta	1.07	1.07	1.04	**1.06**	1.7	0.745	0.742	0.744	0.747	**0.744**	0.2	1.08	1.09	1.08	1.09	**1.08**	0.3
Pb	32.7	31.6	30.7	**31.6**	3.2	10.8	10.9	10.9	11.1	**10.9**	0.8	1.76	1.77	1.76	1.77	**1.76**	0.2
Th	11.3	11.5	12.0	**11.6**	3.1	5.55	5.61	5.57	5.59	**5.58**	0.5	1.14	1.13	1.14	1.14	**1.14**	0.6
U	1.88	1.89	1.87	**1.88**	0.5	1.61	1.63	1.63	1.64	**1.63**	0.7	0.402	0.400	0.406	0.406	**0.403**	0.8

El.	BIR-1G						PCC-1 [b]					
	1	**2**	**3**	**4**	**Mean**	**RSD**	**1**	**2**	**3**	**Mean**	**RSD**	**Ref**
Rb	-	-	-	-	-	-	-	-	-	-	-	-
Sr	110	109	110	110	**110**	0.1	0.388	0.392	0.385	**0.388**	0.9	0.4
Y	15.9	15.9	16.0	15.9	**15.9**	0.3	0.078	0.079	0.076	**0.077**	2.3	0.1
Zr	17.7	17.8	17.8	17.7	**18**	0.2	2.57	2.58	2.56	**2.57**	0.4	10
Nb	0.534	0.533	0.531	0.533	**0.533**	0.3	0.0169	0.0169	-	**0.0169**	-	1
Cs	-	-	-	-	-	-	-	-	-	-	-	-
Ba	6.81	6.81	6.80	6.80	**6.81**	0.1	0.877	0.885	0.914	**0.892**	2.2	1.2
La	0.601	0.603	0.601	0.601	**0.602**	0.2	0.0311	0.0313	0.0304	**0.0309**	1.5	0.052
Ce	1.87	1.87	1.87	1.87	**1.87**	0.1	0.0602	0.0594	0.0599	**0.0598**	0.6	0.1
Pr	0.371	0.372	0.373	0.373	**0.372**	0.3	0.0082	0.0083	0.0077	**0.0081**	4.4	0.013
Nd	2.36	2.39	2.37	2.38	**2.38**	0.4	0.0260	0.0254	0.0254	**0.0256**	1.5	0.042
Sm	1.10	1.09	1.09	1.09	**1.09**	0.2	0.0083	0.0084	0.0071	**0.0079**	8.8	0.0066
Eu	0.526	0.513	0.528	0.530	**0.524**	1.5	0.0006	0.0006	0.0006	**0.0006**	4.3	0.0018
Gd	1.85	1.83	1.84	1.88	**1.85**	1.1	0.0089	0.0088	0.0090	**0.0089**	1.1	0.0140
Tb	0.418	0.413	0.413	0.413	**0.414**	0.7	0.0016	0.0015	0.0014	**0.0015**	5.6	0.0015
Dy	2.62	2.60	2.66	2.68	**2.64**	1.3	0.0114	0.0112	0.0102	**0.0109**	5.8	0.01
Ho	0.586	0.574	0.580	0.577	**0.579**	0.9	0.0031	0.0030	0.0031	**0.0031**	1.3	0.0025
Er	1.74	1.73	1.75	1.75	**1.74**	0.6	0.0110	0.0110	0.0110	**0.0110**	0.1	0.012
Tm	0.249	0.243	0.252	0.251	**0.249**	1.5	0.0025	0.0024	0.0024	**0.0024**	2.2	0.0027
Yb	1.66	1.71	1.66	1.64	**1.67**	1.7	0.0256	0.0257	0.0253	**0.0255**	0.8	0.024
Lu	0.239	0.251	0.248	0.252	**0.248**	2.3	0.0050	0.0048	0.0049	**0.0049**	1.2	0.0057
Hf	0.576	0.572	0.575	0.577	**0.575**	0.4	0.0054	0.0050	0.0053	**0.0052**	3.8	0.04
Ta	0.088	0.087	0.088	0.087	**0.087**	0.4	0.113	0.111	0.100	**0.108**	6.7	0.02
Pb	3.47	3.54	3.53	3.54	**3.52**	1.0	9.38	9.30	9.87	**9.52**	3.2	10
Th	0.029	0.030	0.029	0.030	**0.030**	1.0	0.0088	0.0087	0.0093	**0.0090**	3.4	0.013
U	0.028	0.028	0.028	0.028	**0.028**	1.1	0.0039	0.0040	0.0036	**0.0038**	5.9	0.0045

Reference values from [b] Govindaraju [1994]

C Major and trace element data for ocean island basalts

Major [% wt.] and trace element [$\mu g\ g^{-1}$] data for basaltic samples from St. Helena, Gough, and Tristan da Cunha determined by XRF and ID-LA-ICP-MS, respectively (following pages).

	St. Helena											
Sample	**H 8**	**H 13**	**H 28**	**H 38**	**H 64**	**H 68**	**H 69**	**H 74**	**H 75**	**H 86**	**H 125**	**H 146**
SiO_2	44.9	44.2	45.5	43.4	44.3	43.9	45.2	45.0	43.7	46.8	44.0	47.1
Al_2O_3	17.2	11.3	15.1	9.42	12.6	11.1	13.9	15.1	14.3	15.6	13.2	16.3
FeO* [a]	10.5	11.7	12.5	11.1	11.4	11.6	11.3	12.0	11.8	11.8	11.9	11.6
Fe_2O_3	1.75	1.96	2.09	1.85	1.90	1.93	1.88	2.00	1.97	1.96	1.98	1.94
FeO	8.93	9.97	10.7	9.45	9.71	9.82	9.61	10.2	10.0	10.0	10.1	9.90
MnO	0.160	0.170	0.190	0.170	0.170	0.180	0.170	0.180	0.190	0.190	0.180	0.240
MgO	4.43	13.5	6.64	15.9	11.0	14.3	9.09	6.57	7.81	5.61	10.0	3.09
CaO	9.81	10.78	9.37	12.7	12.55	10.78	10.93	9.88	10.19	9.2	11.21	7.73
Na_2O	3.49	1.73	3.89	1.16	2.08	1.68	2.26	2.94	2.21	3.76	2.37	3.88
K_2O	1.31	0.72	1.25	0.44	0.74	0.67	0.85	1.12	1.03	1.36	0.98	1.67
TiO_2	3.16	2.29	3.22	1.92	2.6	2.27	2.6	3.28	3.05	2.82	2.8	2.53
P_2O_5	0.760	0.380	0.690	0.220	0.380	0.340	0.440	0.570	0.550	0.690	0.460	1.210
LOI	2.62	2.00	0.13	2.88	0.72	1.84	2.1	1.83	3.38	0.7	1.58	2.69
Mg# [b]	47	71	53	75	67	72	63	53	58	50	64	36
Rb	24.9	11.7	24.1	9.81	15.6	13.9	17.4	22.3	18.8	28.1	19.0	35.8
Sr	892	427	742	327	468	397	526	619	587	684	556	869
Y	31.8	21.8	31.6	18.4	25.3	22.1	26.4	30.7	29.4	31.6	26.5	39.1
Zr	292	183	297	130	197	180	219	267	261	314	224	408
Nb	65.6	38.3	66.3	24.9	39.6	37.0	44.5	56.9	57.9	69.5	46.7	88.7
Cs	0.340	0.275	0.386	0.212	0.142	0.090	0.146	0.168	0.123	0.203	0.304	0.270
Ba	363	206	359	130	208	183	237	326	313	375	273	464
La	46.8	27.2	44.4	17.7	27.4	24.6	30.1	40.8	40.1	47.1	32.2	70.9
Ce	101	58	98	40	62	55	66	87	86	100	70.9	145
Pr	11.9	7.06	11.7	4.96	7.55	6.70	8.01	10.3	10.1	11.6	8.51	16.9
Nd	47.5	29.0	47.6	21.0	31.6	28.0	33.5	41.9	40.8	46.2	35.2	65.8
Sm	9.12	5.98	9.28	4.55	6.67	5.84	6.92	8.41	8.13	8.83	7.23	11.7
Eu	2.93	1.91	2.94	1.46	2.17	1.95	2.26	2.75	2.54	2.82	2.31	3.54
Gd	8.13	5.59	8.34	4.38	6.30	5.61	6.49	7.91	7.26	7.93	6.86	10.1
Tb	1.10	0.780	1.12	0.610	0.873	0.780	0.900	1.08	1.00	1.08	0.940	1.35
Dy	5.82	4.21	6.02	3.35	4.82	4.34	4.98	5.91	5.36	5.84	5.18	7.28
Ho	1.10	0.808	1.15	0.660	0.926	0.838	0.963	1.16	1.04	1.14	1.00	1.42
Er	2.75	2.00	2.81	1.63	2.31	2.09	2.44	2.82	2.59	2.89	2.49	3.65
Tm	0.361	0.258	0.366	0.218	0.302	0.267	0.320	0.361	0.337	0.388	0.318	0.489
Yb	2.26	1.60	2.29	1.38	1.91	1.70	2.06	2.28	2.17	2.46	2.02	3.10
Lu	0.298	0.207	0.294	0.178	0.247	0.220	0.266	0.300	0.286	0.320	0.258	0.417
Hf	6.15	4.15	6.39	3.15	4.60	4.11	4.91	5.80	5.64	6.57	4.98	8.38
Ta	3.93	2.28	3.94	1.49	2.43	2.30	2.75	3.48	3.49	4.23	2.86	5.40
Pb	2.76	1.66	2.90	0.99	1.52	1.38	1.84	2.48	2.51	3.26	2.11	3.98
Th	4.81	2.96	4.56	1.82	2.82	2.49	3.21	4.25	4.36	5.15	3.45	7.28
U	1.61	0.77	1.33	0.52	0.82	0.75	0.94	1.19	1.18	1.45	1.01	2.05

[a] FeO* based on Fe^{2+}/Fe^{3+}=0.85; [b] Mg# = $[Mg^{2+}/(Mg^{2+}+Fe^{2+})]\times100$

	Gough											
Sample	**G 1**	**G 6**	**G 13**	**G 14**	**G 35**	**G 38**	**G 40**	**G 93**	**G 102**	**G 110**	**G 115**	**G 116**
SiO_2	47.4	47.6	48.0	49.1	48.5	43.7	49.3	47.2	49.3	48.0	45.2	47.5
Al_2O_3	12.8	13.4	13.5	13.6	13.4	15.2	13.5	13.5	14.8	13.8	10.3	15.1
FeO*[a]	10.5	10.3	10.4	9.82	11.4	11.9	9.86	10.5	10.9	10.1	12.2	10.9
Fe_2O_3	1.75	1.72	1.73	1.64	1.90	1.99	1.64	1.75	1.82	1.69	2.03	1.82
FeO	8.93	8.76	8.83	8.34	9.70	10.1	8.38	8.93	9.30	8.62	10.3	9.26
MnO	0.140	0.120	0.130	0.130	0.140	0.120	0.130	0.140	0.150	0.130	0.160	0.150
MgO	9.81	7.94	8.37	8.01	8	6.56	7.86	8.73	5.28	7.9	15.5	4.94
CaO	8.24	7.81	8.09	7.55	7.71	6.75	7.98	7.46	5.54	7.8	7.68	8.45
Na_2O	2.62	2.69	2.84	3.12	2.64	2.48	3.03	2.74	3.57	2.9	1.81	2.79
K_2O	1.79	2.32	2.31	2.54	1.67	0.84	2.07	2.63	3.44	2.44	1.48	2.36
TiO_2	2.92	3.36	3.36	3.1	3.33	3.28	2.96	3.47	3.55	3.27	2.48	3.85
P_2O_5	0.490	0.740	0.750	0.740	0.580	0.310	0.540	0.780	0.810	0.760	0.330	0.690
LOI	0.77	2.12	0.53	0.10	0.9	6.74	0.51	1.08	0.62	0.72	1.31	1.55
Mg#[b]	66	62	63	63	60	54	63	64	50	62	73	49
Rb	35.0	48.2	46.4	51.7	43.0	16.3	41.8	47.7	71.0	40.3	31.2	42.5
Sr	684	872	892	871	676	680	720	911	715	835	472	855
Y	23.3	27.1	28.0	25.0	29.9	26.2	26.9	27.0	33.9	27.6	22.4	31.3
Zr	244	319	320	336	278	282	298	366	443	334	190	317
Nb	33.9	45.6	43.8	44.6	39.2	37.6	43.0	46.7	72.8	46.2	38.1	57.8
Cs	0.128	1.25	0.521	0.541	0.843	0.558	0.275	0.336	1.37	0.688	0.163	0.180
Ba	687	779	781	826	554	479	672	898	943	752	432	763
La	31.9	45.2	45.7	49.9	37.2	33.4	39.8	49.4	61.3	48.2	27.6	47.4
Ce	67.1	95.7	97.6	100	78.4	59.7	82.5	108	126	101	60	97
Pr	8.15	11.6	11.8	12.1	10.0	8.82	10.2	12.8	14.6	11.8	7.57	11.9
Nd	33.9	47.6	48.5	48.9	42.3	37.1	41.6	51.6	57.2	47.5	31.5	48.1
Sm	6.96	9.30	9.50	9.35	8.98	8.01	8.49	9.73	10.7	8.96	6.61	9.32
Eu	2.35	2.94	2.99	2.86	2.88	2.64	2.69	3.10	3.16	2.91	2.13	3.17
Gd	6.48	8.29	8.51	8.05	8.38	7.47	7.67	8.23	9.17	7.93	6.00	8.31
Tb	0.87	1.07	1.10	1.03	1.13	1.03	1.05	1.06	1.24	1.06	0.82	1.10
Dy	4.64	5.63	5.60	5.23	6.00	5.51	5.55	5.48	6.54	5.54	4.41	5.82
Ho	0.864	1.02	1.03	0.951	1.12	1.03	1.05	0.991	1.22	1.01	0.831	1.11
Er	2.05	2.45	2.43	2.15	2.67	2.40	2.52	2.39	3.04	2.40	2.07	2.82
Tm	0.255	0.303	0.292	0.255	0.335	0.295	0.303	0.302	0.398	0.298	0.271	0.369
Yb	1.53	1.80	1.76	1.50	1.98	1.77	1.91	1.80	2.42	1.82	1.69	2.23
Lu	0.198	0.219	0.222	0.188	0.252	0.220	0.233	0.223	0.305	0.228	0.215	0.281
Hf	5.49	7.02	7.02	7.18	6.36	6.38	6.62	8.05	9.46	7.19	4.32	7.18
Ta	2.01	2.75	2.63	2.62	2.42	2.39	2.48	2.73	4.35	2.76	2.30	3.49
W	0.4	0.7	0.6	0.6	0.5	0.5	0.5	0.5	1.1	0.6	0.5	0.7
Pb	3.73	4.23	4.64	4.48	3.95	4.71	4.67	6.86	6.05	4.88	2.58	4.43
Th	3.90	4.78	4.67	5.37	3.73	4.29	4.73	4.92	8.64	4.97	3.02	5.02
U	0.664	0.990	1.00	1.04	0.920	1.91	0.877	1.05	1.41	1.06	0.724	0.974

[a] FeO* based on Fe^{2+}/Fe^{3+}=0.85; [b] Mg# = $[Mg^{2+}/(Mg^{2+}+Fe^{2+})]\times100$

Sample	Gough G 117	G 118	G 120	G 131	G 132	G 135	G 136	G 139	G 141	G 142	B 167
SiO_2	46.7	46.7	50.5	46.5	51.2	49.6	49.7	46.2	47.0	46.1	47.5
Al_2O_3	15.8	11.4	15.3	13.3	14.2	14.8	15.1	14.6	14.4	12.1	16.2
FeO*[a]	10.6	10.9	10.4	11.0	9.06	9.20	9.56	10.0	10.7	11.5	10.1
Fe_2O_3	1.76	1.82	1.73	1.83	1.51	1.53	1.59	1.67	1.78	1.91	1.69
FeO	8.98	9.30	8.80	9.32	7.70	7.82	8.13	8.50	9.08	9.76	8.62
MnO	0.150	0.150	0.100	0.140	0.120	0.100	0.120	0.150	0.150	0.150	0.120
MgO	4.52	13.0	4.23	9.19	5.04	5.85	5.51	6.82	7.34	12.1	3.39
CaO	7.94	8.47	6.09	8.48	9.09	6.56	6.8	8.47	7.34	7.79	6.31
Na_2O	2.78	2.04	3.47	2.66	2.79	3.28	3.37	2.17	2.67	2.19	3.1
K_2O	2.31	1.76	2.85	1.98	2.41	2.57	2.65	2.7	2.77	2.16	3.29
TiO_2	3.76	2.75	3.03	3.56	3.1	2.84	2.93	3.67	3.32	3.02	3.87
P_2O_5	0.690	0.480	0.790	0.720	0.580	0.800	0.770	0.750	0.750	0.530	0.790
LOI	2.49	1.18	1.54	0.5	1.06	0.88	1.43	3.11	2.09	0.43	3.67
Mg#[b]	47	71	46	64	54	57	55	59	59	69	41
Rb	32.1	34.6	58.1	39.8	41.7	54.4	57.8	50.1	53.6	60.1	59.1
Sr	744	640	775	962	776	762	852	792	762	744	578
Y	34.4	24.9	31.6	27.3	29.2	29.2	29.2	30.0	33.3	22.6	28.1
Zr	356	232	395	269	321	335	347	345	349	247	440
Nb	53.4	40.8	49.0	41.3	40.0	49.6	50.1	57.5	53.1	45.8	58.9
Cs	0.098	0.314	0.349	0.228	0.644	0.218	0.440	3.94	1.06	0.498	0.289
Ba	712	503	825	889	644	794	832	940	861	716	879
La	47.7	35.6	61.2	44.1	42.7	50.4	51.5	52.9	59.1	38.4	47.6
Ce	103	71	125	89	89	103	102	106	110	77	106
Pr	12.9	9.15	14.5	11.0	10.9	12.2	12.3	13.0	13.8	9.19	12.5
Nd	54.1	37.4	57.6	45.9	45.9	49.6	49.5	52.9	56.1	37.7	51.5
Sm	10.7	7.26	10.8	9.06	9.02	9.47	9.44	9.96	10.7	7.16	9.92
Eu	3.39	2.28	3.31	2.86	2.78	2.95	2.94	3.14	3.33	2.34	3.17
Gd	9.51	6.47	9.47	8.06	8.18	8.54	8.27	8.80	9.51	6.45	8.53
Tb	1.26	0.850	1.23	1.04	1.09	1.14	1.09	1.14	1.24	0.856	1.14
Dy	6.67	4.52	6.29	5.43	5.80	5.95	5.69	6.00	6.48	4.56	5.95
Ho	1.26	0.86	1.15	1.01	1.09	1.11	1.06	1.11	1.22	0.864	1.09
Er	3.06	2.14	2.70	2.35	2.68	2.64	2.50	2.64	2.78	2.07	2.60
Tm	0.389	0.278	0.334	0.291	0.337	0.323	0.312	0.328	0.331	0.255	0.324
Yb	2.42	1.65	1.98	1.68	2.07	1.94	1.85	1.95	1.96	1.54	1.94
Lu	0.311	0.213	0.247	0.211	0.266	0.244	0.235	0.247	0.250	0.198	0.247
Hf	7.90	5.24	8.63	5.94	7.11	7.20	7.39	7.59	7.36	5.34	9.45
Ta	3.32	2.48	2.98	2.40	2.53	2.95	3.01	3.49	3.12	2.84	3.49
W	0.5	0.8	0.9	0.6	0.6	0.7	1.1	0.4	1.4	0.4	0.5
Pb	4.92	2.86	5.44	4.30	4.57	5.03	5.46	4.91	4.81	3.82	6.27
Th	5.18	3.61	5.44	4.57	4.30	5.82	6.03	6.02	5.89	4.75	7.01
U	0.908	0.805	1.26	0.937	0.949	1.23	1.38	1.07	1.25	0.917	0.959

[a] FeO* based on $Fe^{2+}/Fe^{3+}=0.85$; [b] Mg# = $[Mg^{2+}/(Mg^{2+}+Fe^{2+})]\times100$

	Tristan da Cunha											
Sample	**T 6**	**T 16**	**T 20**	**T 39**	**T 60**	**T 64**	**T 112**	**T 114**	**T 120**	**T 122**	**T 129**	**T 167**
SiO_2	42.2	43.9	46.0	41.5	40.6	42.1	43.3	42.5	44.0	42.9	42.4	42.4
Al_2O_3	13.9	16.4	16.4	13.6	10.5	13.2	14.6	12.4	15.4	13.4	13.7	14.1
FeO*[a]	14.0	10.9	10.8	14.3	15.4	12.9	12.8	13.7	12.3	14.4	14.3	12.8
Fe_2O_3	2.34	1.81	1.80	2.39	2.57	2.15	2.14	2.29	2.05	2.41	2.38	2.14
FeO	11.9	9.25	9.17	12.2	13.1	11.0	10.9	11.7	10.5	12.3	12.1	10.9
MnO	0.160	0.180	0.180	0.160	0.160	0.160	0.160	0.160	0.170	0.170	0.160	0.160
MgO	6.71	4.74	4.43	7.45	12.2	8.91	6.61	9.49	5.75	7.28	7.94	7.78
CaO	11.81	10.26	9.4	11.62	13.7	11.89	11.61	11.85	10.22	11.49	10.86	11.51
Na_2O	2.4	3.27	3.75	2.47	1.45	2.45	2.87	2.33	3.11	2.23	2.56	2.64
K_2O	1.9	2.92	3.05	1.04	0.83	1.62	1.9	1.53	2.41	1.74	1.96	2.08
TiO_2	3.98	3.69	3.26	4.12	3.7	3.87	3.8	3.69	3.68	3.8	3.81	3.83
P_2O_5	0.520	1.140	0.910	0.650	0.260	0.890	0.580	0.460	0.680	0.460	0.460	0.740
LOI	0.16	0.25	0.01	0.52	-0.52	-0.3	-0.36	-0.48	-0.32	-0.47	-0.23	-0.3
Mg#[b]	50	48	46	52	62	59	52	59	49	51	54	56
Rb	43.8	53.0	68.0	28.7	22.9	40.9	46.2	36.6	63.7	37.5	54.4	58.4
Sr	887	1406	1285	1070	526	1166	983	863	1122	859	855	1061
Y	25.1	30.4	31.4	25.8	19.3	26.3	26.9	22.6	27.6	24.4	24.5	26.0
Zr	243	286	350	226	161	221	269	204	291	238	260	249
Nb	54.6	74.7	90.2	47.4	26.0	52.3	61.9	42.9	70.4	51.7	51.7	56.2
Cs	0.569	0.673	0.891	0.541	0.259	0.429	0.527	0.457	0.707	0.390	0.584	0.704
Ba	576	860	890	552	270	649	593	625	724	559	562	666
La	48.3	60.4	76.6	43.3	26.4	47.7	51.4	39.7	59.5	46.4	48.5	50.8
Ce	105	130	159	97.1	59.6	105	111	89.6	124	100	103	107
Pr	13.0	16.7	19.1	12.4	7.75	13.5	13.6	11.2	15.1	12.1	12.4	13.4
Nd	53.0	68.2	74.4	52.3	33.8	56.7	54.8	46.4	60.5	49.5	49.8	55.0
Sm	9.63	11.9	12.5	9.78	6.84	10.5	9.90	8.49	10.5	8.94	9.08	9.94
Eu	2.92	3.62	3.76	2.99	2.13	3.20	3.06	2.55	3.18	2.69	2.76	2.98
Gd	7.72	9.24	9.72	8.19	6.00	8.63	8.06	7.12	8.52	7.48	7.51	8.22
Tb	0.982	1.14	1.22	1.04	0.776	1.08	1.03	0.903	1.08	0.962	0.962	1.04
Dy	5.05	5.84	6.21	5.34	4.05	5.54	5.28	4.70	5.61	4.97	5.02	5.31
Ho	0.939	1.07	1.14	0.980	0.743	1.01	0.976	0.868	1.05	0.926	0.936	0.975
Er	2.26	2.66	2.82	2.31	1.73	2.37	2.42	2.05	2.54	2.24	2.24	2.34
Tm	0.284	0.340	0.366	0.279	0.214	0.291	0.314	0.251	0.319	0.271	0.279	0.285
Yb	1.78	2.12	2.29	1.65	1.25	1.70	1.91	1.50	1.97	1.63	1.67	1.69
Lu	0.218	0.260	0.287	0.208	0.159	0.214	0.240	0.190	0.249	0.208	0.216	0.216
Hf	5.72	6.24	7.66	5.49	4.45	5.24	6.24	5.08	6.50	5.65	5.93	5.71
Ta	3.47	4.75	5.57	3.07	1.70	3.38	3.91	2.89	4.43	3.29	3.20	3.54
W	0.6	0.8	1.0	0.5	0.3	0.6	0.7	0.3	0.6	0.6	0.7	0.6
Pb	3.18	4.74	6.51	2.96	1.98	2.96	4.12	3.26	4.88	3.67	3.96	4.36
Th	6.30	7.39	9.90	5.10	3.30	5.15	6.58	4.53	8.16	5.66	6.62	6.53
U	1.44	1.75	2.23	1.06	0.734	1.20	1.53	1.04	1.82	1.30	1.53	1.49

[a] FeO* based on Fe^{2+}/Fe^{3+}=0.85; [b] Mg# = $[Mg^{2+}/(Mg^{2+}+Fe^{2+})]\times100$

	Tristan da Cunha										
Sample	**T 170**	**T 186**	**T 342**	**T 347**	**T 349**	**T 359**	**T 364**	**T 482**	**T 497**	**T 499**	**T 505**
SiO_2	43.3	41.6	45.0	45.9	40.6	45.3	45.3	43.1	43.3	46.5	43.7
Al_2O_3	15.7	13.4	16.3	16.3	14.2	16.5	16.3	14.4	14.0	16.8	15.8
FeO* [a]	12.0	14.4	10.8	10.4	13.5	10.9	10.8	12.7	12.3	10.0	11.7
Fe_2O_3	2.01	2.39	1.80	1.73	2.24	1.82	1.81	2.12	2.05	1.67	1.96
FeO	10.2	12.2	9.19	8.81	11.4	9.26	9.22	10.8	10.5	8.53	9.97
MnO	0.180	0.170	0.160	0.170	0.160	0.170	0.170	0.170	0.160	0.190	0.180
MgO	5.51	6.88	5.00	4.55	7.75	4.94	4.93	6.94	7.61	3.55	5.43
CaO	10.67	12.58	9.92	9.4	11.14	10.02	9.97	11.07	11.42	9.08	10.37
Na_2O	3.31	2.67	3.47	3.66	2.18	3.53	3.74	3	3.12	4.45	3.35
K_2O	2.56	1.65	2.59	2.99	1.55	2.76	2.97	2.13	2.24	3.39	2.58
TiO_2	3.79	4.1	3.73	3.36	4.09	3.6	3.58	3.89	3.6	2.88	3.72
P_2O_5	1.000	0.430	1.110	0.840	0.830	0.740	0.730	0.680	0.730	0.920	1.220
LOI	-0.3	-0.34	-0.12	0.01	1.84	0.44	-0.33	-0.51	-0.52	0.02	-0.08
Mg# [b]	49	50	49	48	55	49	49	53	56	43	49
Rb	55.1	46.5	60.9	76.3	54.6	72.9	69.5	47.8	52.9	99.2	62.9
Sr	1395	800	1455	1216	1659	1207	1194	1051	1125	1541	1427
Y	32.0	25.3	31.4	30.6	27.8	29.9	29.6	27.8	27.0	34.4	32.2
Zr	269	243	327	331	267	311	307	272	262	405	302
Nb	71.2	50.7	77.3	82.3	58.9	78.3	79.0	63.9	65.7	104.2	72.5
Cs	0.686	0.586	0.713	0.927	0.661	1.052	0.901	0.545	0.728	1.47	0.887
Ba	898	535	845	865	800	875	868	641	683	1014	847
La	64.7	45.0	67.9	72.4	55.3	67.5	66.9	55.3	60.3	92.7	66.3
Ce	140	98.0	142	149	120	139	138	117	128	190	146
Pr	17.7	12.0	17.9	18.0	14.8	16.9	16.7	14.3	15.2	22.1	18.3
Nd	71.8	49.9	72.8	70.1	60.9	66.8	65.8	58.2	61.1	83.9	74.5
Sm	12.6	9.32	12.6	11.9	11.0	11.5	11.5	10.4	10.4	13.6	13.1
Eu	3.76	2.80	3.75	3.61	3.29	3.42	3.43	3.12	3.10	3.96	3.90
Gd	10.2	7.97	10.1	9.40	9.28	9.17	9.06	8.64	8.64	10.5	10.5
Tb	1.27	1.03	1.26	1.20	1.17	1.16	1.16	1.10	1.09	1.32	1.30
Dy	6.57	5.33	6.36	6.16	5.99	5.96	5.95	5.66	5.66	6.82	6.60
Ho	1.21	0.990	1.17	1.15	1.10	1.11	1.11	1.05	1.06	1.28	1.21
Er	2.89	2.32	2.80	2.78	2.57	2.67	2.70	2.49	2.48	3.09	2.85
Tm	0.354	0.282	0.355	0.356	0.310	0.336	0.346	0.307	0.307	0.385	0.348
Yb	2.10	1.68	2.11	2.18	1.83	2.03	2.08	1.84	1.81	2.44	2.10
Lu	0.265	0.214	0.266	0.280	0.232	0.261	0.263	0.236	0.231	0.316	0.268
Hf	6.09	5.93	7.13	7.00	6.35	6.78	6.86	6.20	5.98	8.50	6.86
Ta	4.56	3.22	4.98	5.08	3.77	4.84	4.99	3.98	4.09	6.52	4.53
W	0.8	0.5	0.9	0.6	0.5	0.5	0.7	0.6	0.6	1.4	0.6
Pb	4.66	3.78	5.45	5.94	4.61	2.72	6.33	14.9	4.39	9.82	5.99
Th	7.21	5.70	8.88	9.59	6.45	9.45	9.27	6.93	7.43	12.06	7.49
U	1.62	1.27	2.05	2.24	1.31	2.13	2.10	1.51	1.64	2.87	2.30

[a] FeO* based on Fe^{2+}/Fe^{3+}=0.85; [b] Mg# = $[Mg^{2+}/(Mg^{2+}+Fe^{2+})]\times100$

	Tristan da Cunha							
Sample	**T 526**	**T 529**	**T 555**	**T 557**	**T 562**	**T 564**	**T 568**	**T 619**
SiO_2	41.6	44.0	41.3	42.1	42.0	44.4	44.1	46.0
Al_2O_3	15.9	16.3	14.1	13.5	15.0	15.5	15.5	17.1
FeO*[a]	12.6	11.6	13.6	13.4	13.0	12.2	12.2	9.6
Fe_2O_3	2.10	1.94	2.27	2.23	2.16	2.03	2.03	1.60
FeO	10.7	9.88	11.6	11.4	11.0	10.4	10.4	8.14
MnO	0.180	0.180	0.170	0.170	0.170	0.170	0.170	0.170
MgO	5.45	4.88	7.67	8.00	6.30	5.60	5.62	4.28
CaO	10.66	10.12	11.94	11.96	11.56	10.22	10.18	9
Na_2O	2.69	3.37	2.22	2.56	3.02	3.51	3.41	4.15
K_2O	2.03	2.58	1.7	1.63	2.53	2.39	2.26	3.24
TiO_2	3.94	3.69	4.05	3.93	4.12	3.65	3.66	3.15
P_2O_5	0.910	1.000	0.610	0.570	0.610	0.700	0.710	1.110
LOI	1.18	0.36	0.77	-0.37	-0.36	-0.31	-0.33	0.05
Mg#[b]	48	47	54	56	50	49	49	48
Rb	40.1	73.7	35.1	38.3	60.9	52.9	53.5	61.5
Sr	1397	1397	970	954	1152	1126	1159	1567
Y	30.2	32.7	27.1	25.1	27.6	27.1	27.5	31.8
Zr	267	284	247	228	241	298	294	339
Nb	78.2	75.1	58.5	51.5	61.7	85.6	78.9	109
Cs	0.529	0.847	0.426	0.420	0.790	0.633	0.656	0.842
Ba	966	941	585	579	807	731	738	1003
La	62.6	65.5	50.4	47.1	49.9	60.6	61.6	83.7
Ce	137	144	110	103	109	132	130	177
Pr	17.8	17.8	13.6	12.8	13.7	16.1	16.2	21.3
Nd	70.9	72.2	55.6	53.2	56.9	62.3	62.9	80.3
Sm	12.3	12.4	10.3	9.84	10.4	10.8	11.0	13.0
Eu	3.85	3.66	3.12	2.97	3.11	3.43	3.44	4.00
Gd	9.20	9.95	8.60	8.28	8.55	8.04	8.48	9.51
Tb	1.16	1.24	1.08	1.06	1.06	1.02	1.08	1.19
Dy	5.87	6.31	5.53	5.44	5.40	5.21	5.50	6.04
Ho	1.07	1.17	1.02	1.01	1.00	0.951	1.02	1.11
Er	2.65	2.78	2.40	2.33	2.42	2.35	2.43	2.74
Tm	0.341	0.345	0.298	0.278	0.304	0.308	0.311	0.353
Yb	2.19	2.10	1.80	1.68	1.80	2.04	2.00	2.30
Lu	0.266	0.268	0.231	0.214	0.229	0.249	0.248	0.284
Hf	6.12	6.26	5.91	5.50	5.59	6.58	6.51	6.99
Ta	5.12	4.73	3.71	3.37	3.91	5.21	4.87	6.61
W	0.6	0.7	0.6	0.5	0.6	0.9	0.8	1.2
Pb	4.65	4.95	3.33	3.10	3.67	4.93	4.79	6.81
Th	7.03	7.60	5.76	5.58	6.36	7.57	7.82	10.2
U	1.55	1.74	1.32	1.24	1.48	1.88	1.91	2.35

[a]FeO* based on Fe^{2+}/Fe^{3+}=0.85; [b]Mg# = $[Mg^{2+}/(Mg^{2+}+Fe^{2+})]\times100$

D Transition element data for ocean island basalts

Concentrations of transition metals [$\mu g\ g^{-1}$] in basaltic samples from St. Helena, Gough, and Tristan da Cunha determined by ID-LA-ICP-MS using ^{43}Ca as internal standard.

Sample	Sc	V	Cr	Co	Ni	Sample	Sc	V	Cr	Co	Ni
H 8	18	160	36	27	26	**G 142**	23	190	317	55	324
H 13	38	241	735	72	316	**B 167**	23	230	82	29	64
H 28	25	199	166	42	97	**T 6**	33	424	101	56	42
H 38	46	205	878	60	369	**T 16**	14	247		27	2
H 64	45	246	514	52	221	**T 20**	15	228	5	28	6
H 68	38	208	795	57	289	**T 39**	26	281	36	36	23
H 69	34	210	336	42	150	**T 60**	52	307	138	50	79
H 74	25	229	146	38	76	**T 64**	29	250	107	40	73
H 75	29	231	224	42	97	**T 112**					
H 86	27	208	157	41	80	**T 114**	39	400	172	57	74
H 125	34	228	337	47	177	**T 120**	22	294	18	39	24
H 146	13	115	38	34	23	**T 122**	34	405	122	52	44
G 1	25	176	363	43	256	**T 129**	31	361	127	52	67
G 6	24	204	312	46	225	**T 167**	29	338	98	43	48
G 13	24	188	317	44	237	**T 170**	19	280	26	32	15
G 14	22	171	271	39	191	**T 186**	35	430	52	50	42
G 35	23	199	284	46	201	**T 342**	18	229	2	26	7
G 38	24	136	218	38	180	**T 347**	15	270	23	29	10
G 40	25	194	327	43	181	**T 349**	30	339	97	51	83
G 93	23	188	251	50	245	**T 359**	18	296	2	30	6
G 102	17	197	121	38	127	**T 364**	17	280	2	31	6
G 110	21	168	166	33	163	**T 482**	28	304	78	40	46
G 115	28	194	764	80	512	**T 497**	25	330	129	47	69
G 116	27	253	81	35	64	**T 499**	11	199	3	21	4
G 117	26	220	39	30	41	**T 505**	19	268	9	32	9
G 118	29	192	619	63	416	**T 526**	19	352	21	39	15
G 120	19	150	117	26	102	**T 529**	17	253	20	30	16
G 131	24	191	315	45	230	**T 555**	29	290	69	39	39
G 132	27	208	139	32	73	**T 557**	32	352	95	42	53
G 135	18	179	180	34	104	**T 562**					
G 136	19	158	163	32	123	**T 564**	23	333	23	41	25
G 139	26	238	234	39	129	**T 568**	24	349	16	42	25
G 141	23	190	242	42	190	**T 619**	14	255	7	28	9

E Accuracy and reproducibility of ID-LA-ICP-MS

Trace element concentrations [$\mu g\ g^{-1}$] in reference materials determined by ID-LA-ICP-MS

Sample	BHVO-1 (n=12)		KL2-G (n=7)		ML3B-G (n=7)	
	Average	1σ	Average	1σ	Average	1σ
Rb	9.42	0.33	8.54	0.27	5.85	0.06
Sr	401	8	372	7	318	6
Y	27.1	0.4	27.9	0.3	26.8	0.0
Zr	173	3	160	3	131	1
Nb	17.6	0.5	14.7	0.8	8.18	0.10
Cs	0.096	0.004	0.122	0.005	0.141	0.005
Ba	135	2	125	2	81.5	1.0
La	15.8	0.1	13.6	0.2	9.54	0.04
Ce	37.5	0.4	32.3	0.3	23.3	0.2
Pr	5.33	0.03	4.65	0.04	3.45	0.01
Nd	24.9	0.2	22.1	0.20	17.2	0.3
Sm	6.08	0.12	5.63	0.11	4.79	0.05
Eu	2.09	0.02	1.97	0.03	1.72	0.01
Gd	6.32	0.09	6.09	0.19	5.59	0.03
Tb	0.915	0.014	0.905	0.024	0.847	0.012
Dy	5.54	0.10	5.57	0.20	5.35	0.07
Ho	1.01	0.02	1.03	0.04	1.01	0.01
Er	2.60	0.06	2.67	0.11	2.66	0.02
Tm	0.323	0.005	0.344	0.007	0.326	0.002
Yb	2.02	0.02	2.15	0.06	2.07	0.03
Lu	0.265	0.003	0.283	0.001	0.277	0.002
Hf	4.24	0.08	3.98	0.08	3.23	0.06
Ta	1.14	0.02	0.962	0.048	0.530	0.003
W	0.204	0.044	0.406	0.015	0.303	0.016
Pb	2.10	0.04	2.08	0.04	1.40	0.03
Th	1.21	0.04	0.924	0.023	0.576	0.021
U	0.409	0.004	0.538	0.005	0.430	0.004

F Primitive upper mantle normalized trace element data for ocean island basalts

Primitive upper mantle (PUM; Sun and McDonough [1989]) normalized trace element patterns of investigated sample suites. Note that all suites are enriched in Nb, Ta and depleted in Pb. HIMU-type suites (a to e) are strongly depleted in very incompatible elements (VICE), whereas EM-type suites (f to r) are less depleted but more heterogeneous in VICE compared to HIMU-type OIB. See text for discussion.

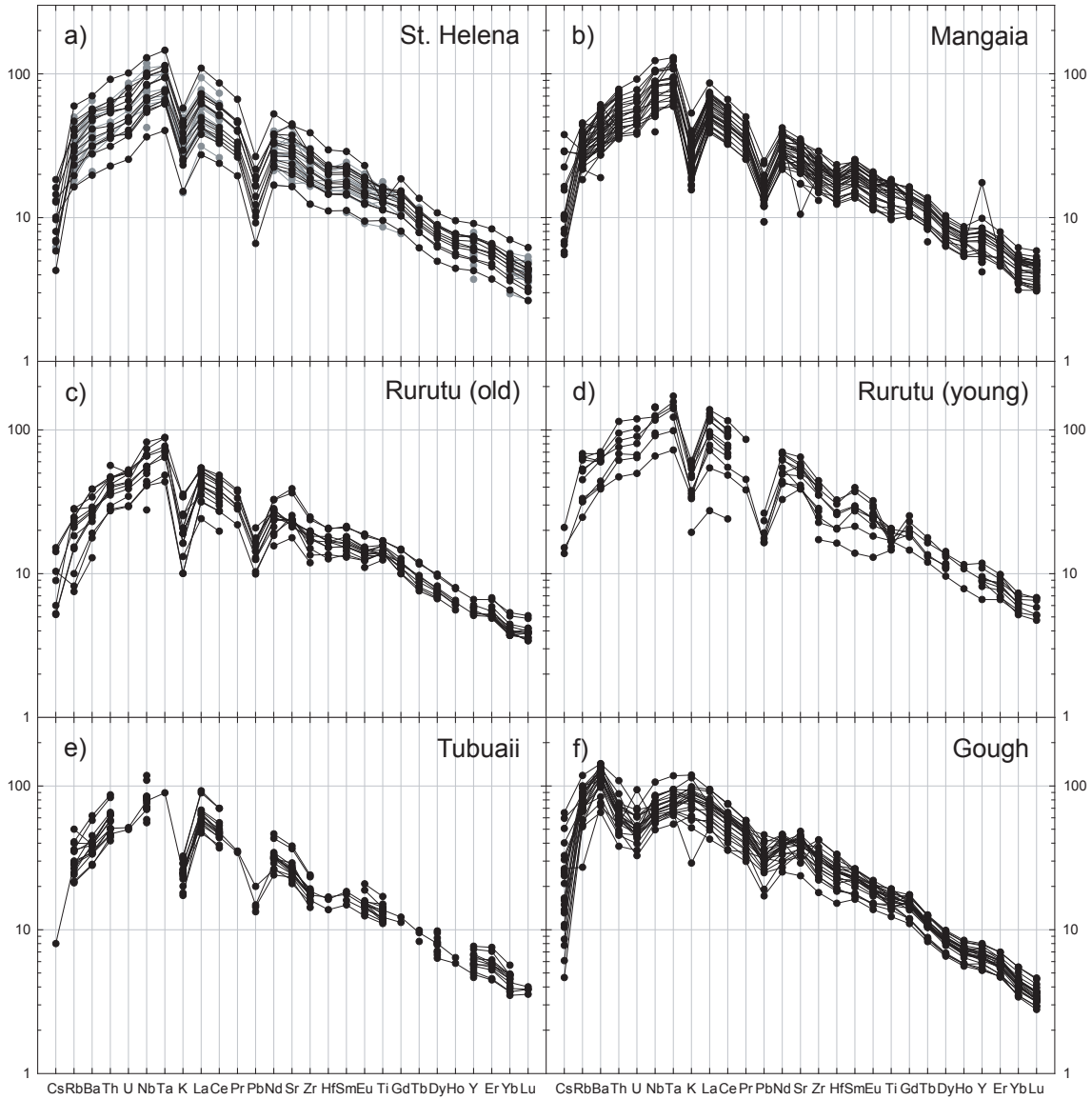
a)
St. Helena
b)
Mangaia
c)
Rurutu (old)
d)
Rurutu (young)
e)
Tubuaii
f)
Gough
100
10
1
Cs Rb Ba Th U Nb Ta K La Ce Pr Pb Nd Sr Zr Hf Sm Eu Ti Gd Tb Dy Ho Y Er Yb Lu

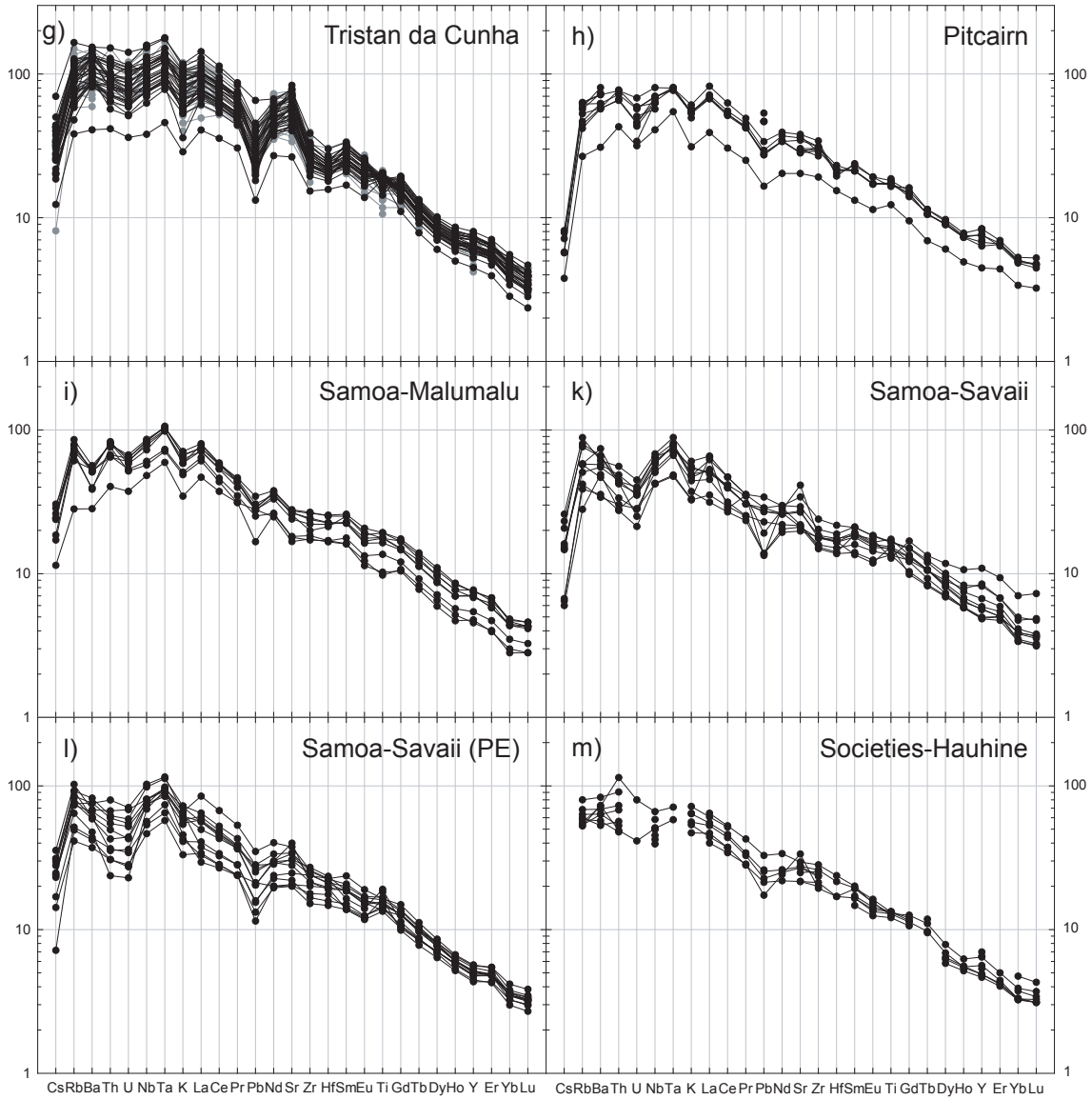
g)
Tristan da Cunha
h)
Pitcairn
i)
Samoa-Malumalu
k)
Samoa-Savaii
l)
Samoa-Savaii (PE)
m)
Societies-Hauhine
100
10
1
Cs Rb Ba Th U Nb Ta K La Ce Pr Pb Nd Sr Zr Hf Sm Eu Ti Gd Tb Dy Ho Y Er Yb Lu

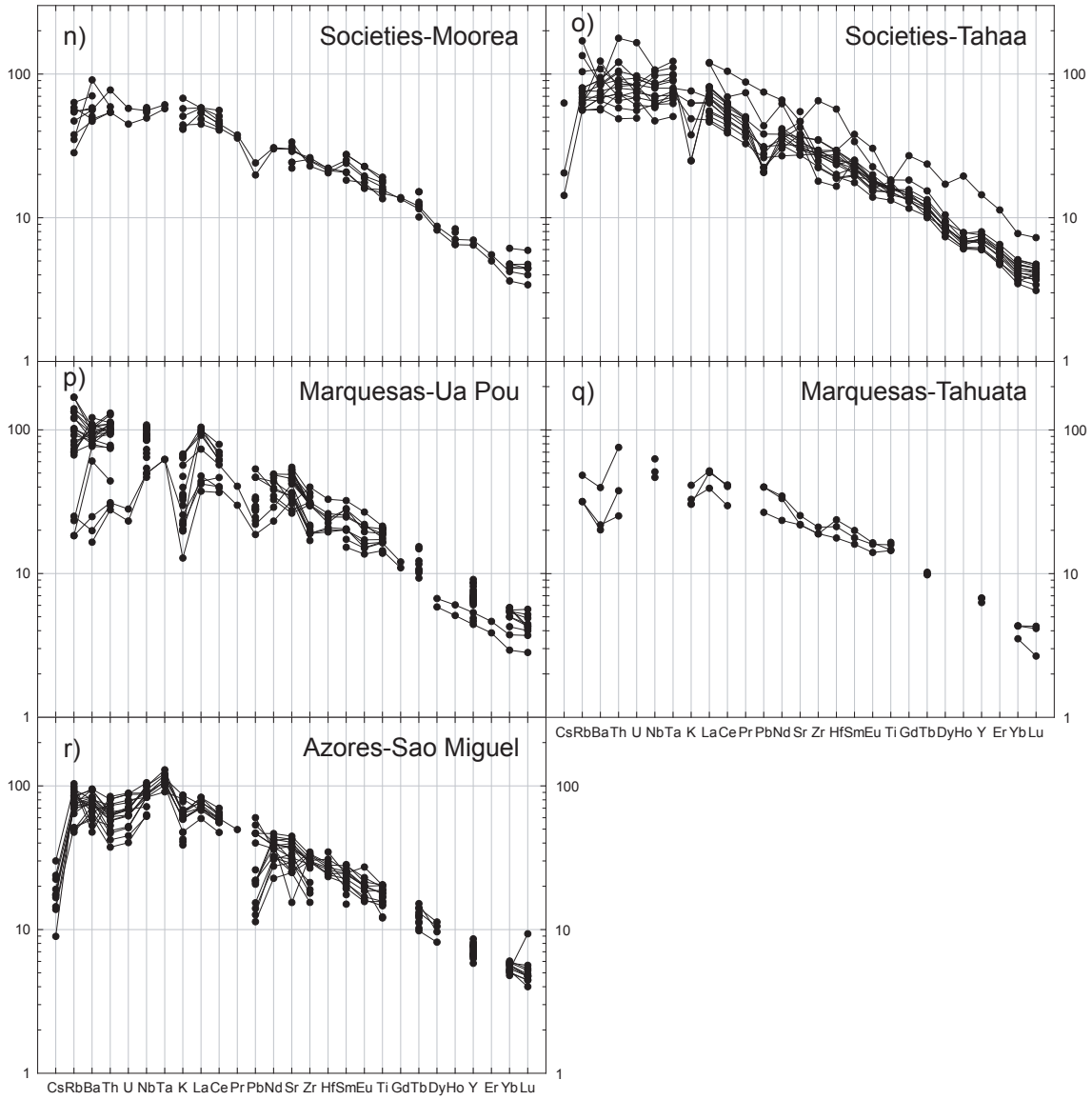
n)
Societies-Moorea
o)
Societies-Tahaa
p)
Marquesas-Ua Pou
q)
Marquesas-Tahuata
r)
Azores-Sao Miguel
100
10
1
Cs Rb Ba Th U Nb Ta K La Ce Pr Pb Nd Sr Zr Hf Sm Eu Ti Gd Tb Dy Ho Y Er Yb Lu

G Quantitative modeling of OIB melts

G.1 Model parameters

The calculations and parameters used in this model (partition coefficients, fluid-mobility factors, mineral and melting modes) are published in Stracke et al. [2003]. For the generation of the trace element characteristics of the EM sources, it is assumed that a mixture of 40% MORB [Sun and McDonough, 1989], 50% gabbro [Hart et al., 1999], 10% MORB [Staudigel et al., 1996] together with fragments of eroded lower continental crust and sediments (upper continental crust) are recycled into the mantle. Subducted sediments, in contrast to the lower continental crust are water-barren and we therefore assume that the sediment component is modified by partial melting during subduction (e.g., Hoogewerf et al. [1997]; Nichols et al. [1994]). Dehydration of the altered oceanic crust and/or sediments may provide water to the overlying lower crustal material. Owing to the erosional process, the lower continental crust is likely to be fractured [von Huene et al., 2004] thus promoting canalization of fluids. In this case, the quantitative fluid-rock interaction (leading to large scale metasomatism and/or partial melting) is limited [Breeding et al., 2003; Ague, 2004]. Therefore, the bulk chemical composition of the eroded lower crustal material is likely to be unaffected by subduction zone alteration processes.

After storage in the mantle, partial melting (F = 0.01 to 0.05) of this mixture gives rise to the observed EM-type OIB. The compositions of the oceanic crust components are given in Table G1.

G.2 Composition of the recycled continental components

The compositional variation of the lower continental crust is hart to constrain because of the great heterogeneity at small as well as at large scale. Additional uncertainty may be introduced by the methods that are used to estimate the composition of the lower continental crust (see Rudnick and Gao [2004] for a recent review). However, different sections of the continental crust from worldwide locations have been used to estimate the average lower crust composition (see Rudnick and Gao [2004]). Taking these different compositions as averaged estimates for different parts of the lower continental crust we propose that they are, at present, the best estimates of the large-scale compositional variations within the lower continental crust.

We have therefore used estimated average values from the literature (Table G1). These estimates are based on different analytical approaches (geochemical data, seismic data, heat flow data, etc.) and on different materials from the continental crust (global sediment

data, granulites and xenoliths from Scotland, Central Spain, etc.) and therefore should yield weighted averages of different sections of the upper and lower continental crust. Some modifications of the literature data have been made to account for the isotope and element compositions of the EM-type OIB and will be discussed in the following. Most modifications were done for parent-daughter elements of isotope decay systems to obtain the present day Sr, Nd, Pb, and Hf isotopic compositions of EM-type OIB. Is has to be noted that, as pointed out earlier, the present day isotopic composition is not only a function of the abundance of parent and daughter elements, but also of time. Thus, all modifications done for the parent-daughter concentrations are arbitrarily (although kept as small as possible) since the exact age of the recycled components is unknown. This topic will be fully treated in a companion paper. Table G1 also shows the median, maximum and minimum value of estimated literature element concentration in the lower crust using the data compilation given in Rudnick and Gao [2004].

G.3 Average lower continental crust

The average chemical composition of the lower continental crust is taken from Rudnick and Gao [2004] and was used to model the average trace element composition of EM-1 basalts (Gough, Pitcairn, Tristan) shown in Fig. 30a as well as the variation in Ba/Rb versus Th/Rb and Ba-Nb versus Rb/Nb spaces (Fig. 31). Modifications exclusively affect the parent/daughter ratios of isotope decay systems to achieve the required isotopic composition of the EM-1-type OIB and range between 5 and 40% (Pb 50%).

G.4 Average upper continental crust

The average chemical composition of the lower continental crust is taken from Taylor and McLennan [1985] and was used to model the average trace element composition of EM-2-type OIB (Samoa-Malumalu, -Savaii, Society-Tahaa) shown in Fig. 30b as well as the variation in Ba/Rb versus Th/Rb, and Ba/Nb versus Rb/Nb spaces (Fig. 31). The modifications are only minor and include U, Nd, Sr, Sm concentrations (less than 20%) and Cs that has been reduced from 4.6 to 1 $\mu g\ g^{-1}$ to obtain the low Cs concentration in EM2-type OIB.

G.5 'Mature' lower continental crust

The lower crustal composition by Weaver and Tarney [1984] is used for modeling the variation of EM-type OIB in Ba/Rb versus Th/Rb and Ba/Nb versus Rb/Nb space (Fig. 31). This composition is used as an estimate for an evolved composition of the lower continental

crust, as it may be representative for stabilized, mature continents. This estimate is based on granulite data from the Lewisian complex, Scotland and has a composition similar to tonalite-trondhjemite-granodiorite assemblages [Rudnick and Gao, 2004]. Modifications of the literature data include Rb and Sr that have been increased by 20% and reduced by 40%, respectively to achieve the necessary $^{87}Sr/^{86}Sr$ composition of the EM-1 basalts. Lead has been reduced from 13 to 5 $\mu g\ g^{-1}$. The Pb value by Weaver and Tarney [1984] is unrealistically high especially if these parts of the lower crust have experienced long term magmatic and metamorphic modification. We therefore attribute the high Pb value to analytical problems because of the analytical capabilities of the early 1980's. Assuming a Pb value of 5 $\mu g\ g^{-1}$ the resulting Ce/Pb (8.8) is in better accordance with the value by Shaw et al. [1994] (7.5) which has also been derived from granulites.

G.6 'Young' lower continental crust

The lower crustal composition by Villaseca et al. [1999] is used for modeling the variation of EM-type OIB in Ba/Rb versus Th/Rb, and Ba/Nb versus Rb/Nb space (Fig. 31). This composition is used as an estimate for an extremely felsic composition of the lower continental crust. It has high SiO_2 and K_2O content similar to that of the upper continental crust as well as a high heat flow and may be representative for young lower crust [Rudnick and Gao, 2004]. The modifications of this estimate are the highest of all assumed compositions. The Rb, Ba, and Th concentrations are the highest of all lower crustal estimates given in Rudnick and Gao [2004] and have been lowered by 80%, 90%, 113%, respectively (Rb from 90 to 50 $\mu g\ g^{-1}$, Ba from 994 to 500 $\mu g\ g^{-1}$, and Th from 5.8 to 2.7 $\mu g\ g^{-1}$). Nevertheless, the modified concentrations are still among the highest of all estimates and thus may be representative of an extreme end-member of the lower crustal composition. Since Villaseca et al. [1999] do not give a Pb concentration, we assumed an U/Pb ratio of 0.1 (that is similar to most other estimates) to infer the Pb concentration. The Nd and Sm concentrations have been increase by 25 and reduced by 10% respectively to obtain the $^{143}Nd/^{144}Nd$ isotopic composition of the EM-1-type OIB.

Table G1: Trace element concentrations [$\mu g\ g^{-1}$] of components used for modeling the composition of EM-type ocean island basalts. Also given are the minimum, median, and maximum concentrations of different estimates of the lower continental crust given in Rudnick and Gao [2004].

	N-MORB	Altered MORB	Gabbro	Average upper continental crust		Average lower continental crust		'Mature' lower continental crust		'Young' lower continental crust		Lower continental crust estimates		
Ref.	Sun and McDonough [1989]	Staudigel et al. [1996]	Hart et al. [1999]	Used value	Taylor and McLennan [1985]	Used value	Rudnick and Gao [2004]	Used value	Weaver and Tarney [1984]	Used value	Villaseca et al. [1999]	Rudnick and Gao [2004] Min.	Med.	Max.
Ti	7600	7074	8045	3837	3837	4916	4916	2997	2997	6234	6234	2997	5396	7973
Rb	0.56	9.6	0.56	112	112	17	11	14	11	50	90	7.0	25	90
Sr	90	115	158	450	350	348	348	400	569	286	286	196	350	712
Zr	74	67	78	190	190	86	86	202	202	206	206	68	121	206
Y	28	27	27	22	22	16	16	7.0	7.0	40	40	7.0	18	40
Nb	2.3	1.2	1.7	12	12	5.0	5.0	5.0	5.0	15	15	5.0	6.6	15
Cs	0.007	0.15	0.019	1.0	4.6	0.30	0.30	0.07	0.07	0.07	0.07	0.07	0.30	2.6
Ba	6.3	22.6	9.5	550	550	259	259	757	757	500	994	150	516	1434
La	2.5	1.8	4.8	30	30	8.0	8.0	22	22	38	38	8.0	20	38
Ce	7.5	6.0	15	64	64	20	20	44	44	73	73	20	40	73
Nd	7.3	6.6	10	35	26	12	11	19	19	40	30	2.8	18	30
Sm	2.6	2.5	3.1	4.3	4.5	2.0	2.8	3.3	3.3	6.0	6.6	1.1	3.7	6.6
Eu	1.0	0.91	1.1	0.88	0.88	1.1	1.1	1.2	1.2	1.8	1.8	1.0	1.3	3.6
Gd	3.7	3.7	4.1	3.8	3.8	3.1	3.1	3.1	3.1	6.8	6.8	0.48	3.7	6.8
Dy	4.6	4.4	5.0	3.5	3.5	3.1	3.1	2.5	2.5	6.7	6.7	0.60	3.6	6.7
Er	3.0	2.8	2.8	2.3	2.3	1.9	1.9	1.3	1.3	4.2	4.2	1.3	2.2	4.2
Yb	3.1	2.7	2.8	2.2	2.2	1.5	1.5	1.2	1.2	4.0	4.0	0.79	1.9	4.0
Lu	0.46	0.43	0.40	0.32	0.32	0.25	0.25	0.18	0.18	0.65	0.65	0.12	0.29	0.65
Hf	2.1	1.9	2.1	5.8	5.8	1.9	1.9	3.6	3.6	6.0	6.0	1.9	2.8	6.0
Ta	0.13	0.10	0.11	2.0	2.0	0.60	0.60	0.70	0.70	0.70	0.70	0.21	0.60	1.3
Pb	0.30	0.24	0.60	18.0	17.0	3.0	4.0	5.0	13.0	5.0	(-)	3.0	5.0	13.0
Th	0.12	0.07	0.16	10.7	10.7	1.3	1.2	0.42	0.42	2.7	5.7	0.42	1.4	6.6
U	0.047	0.30	0.044	2.5	2.8	0.27	0.20	0.050	0.05	0.47	0.47	0.050	0.34	1.4

H Curriculum Vitae

30. Oktober 1974 Geboren in Ulm/Donau als Kind von Maria und Bernhard Willbold

September 1981 Einschulung in die Grundschule in Lauingen

September 1985 Übertritt in das St.-Bonaventura-Gymnasium in Dillingen

Juni 1994 Erwerb der allgemeinen Hochschulreife

1994 bis 1995 Zivildienst im Kreiskrankenhaus Lauingen

November 1995 Beginn des Studiums der Geophysik an der Ludwig-Maximilians-Universität München

Mai 1996 Wechsel auf das Fach Geologie/Paläontologie am Institut für Allgemeine und Angewandte Geologie der LMU München

Januar 1998 Erwerb des Vordiploms in Geologie/Paläontologie

Dezember 2001 Erwerb des Diploms in Geologie/Paläontolgie an der LMU München. Titel der Diplomkartierung: Pyroclastic rocks of the Bolsena volcanic province (central Italy): geological map of a section between M. Segnale and Bagnoregio (1:10000). Titel der Diplomarbeit: Chemical composition of the Neoproterozoic mafic Kandy complex in Sri Lanka: implications for the assembly of Gondwana.

März 2002 Anstellung als wissenschaftlicher Mitarbeiter am Max-Planck-Institut für Chemie Mainz

Juni 2004 Anstellung als wissenschaftlicher Mitarbeiter am Department für Geo- und Umweltwissenschften, Sektion Mineralogie, Petrologie und Geochemie über eine Drittmittelstelle der Deutschen Forschungsgemeinschaft (DFG). Thema: Fraktionierung von "high-field strength" Elementen in Rhyodaziten von Island und Entstehung von "subduktionsbezogenen" Spurenelementcharakteristika in Ozeaninseln (Antragsteller: E. Hegner und A. Rocholl)